FINAL TECHNICAL REPORT

LOW LOSS SUBSTRATES FOR MICROWAVE APPLICATIONS AND SOL-GEL PROCESSING OF SUPERCONDUCTORS

April 1, 1994, to September 25, 1996

Advanced Research Projects Agency
and The Office of Naval Research

Order No. N00014-94-1-0641

L. Eric Cross

Rustum Roy

19970227 026   Amar S. Bhalla

Materials Research Laboratory

The Pennsylvania State University

University Park, PA 16802

DISCLAIMER NOTICE
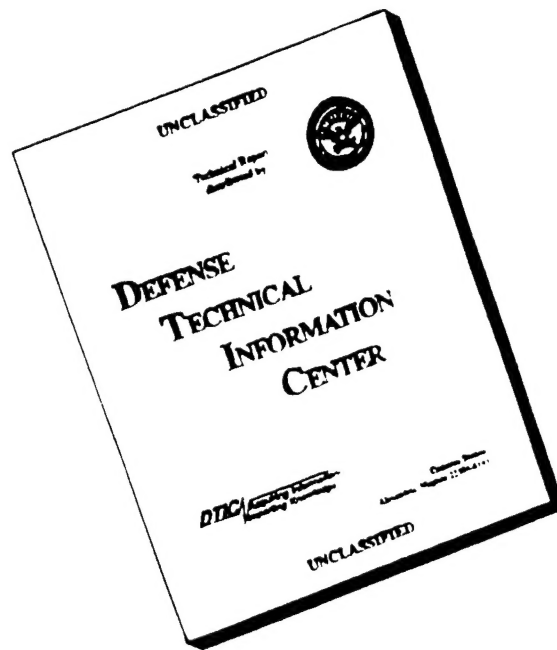
THIS DOCUMENT IS BEST QUALITY AVAILABLE. THE COPY FURNISHED TO DTIC CONTAINED A SIGNIFICANT NUMBER OF PAGES WHICH DO NOT REPRODUCE LEGIBLY.

ABSTRACT

This document is a final technical report of the research program entitled "Low Loss Substrates for Microwave Applications and Sol-Gel Processing of Superconductors." This program was funded through the Advanced Research Projects Agency and The Office of Naval Research under grant No.: N00014-94-1-0641. The grant was for the period April 1, 1994, to September 25, 1996.

Systematic studies on low κ oxide substrate materials suitable for epitaxial deposition of high Tc superconducting (HTSC) yttrium barium cuprate (YBCO) films and their microwave applications have been extended to oxide materials with magnetoplumbite structure, such as $LaMgAl_{11}O_{19}$, $NdGaMgAl_{10}O_{19}$, $CaGa_6Al_6O_{19}$, and $CaGa_{12}O_{19}$. The unique capabilities of a laser heated pedestal growth (LHPG) system have been utilized for test-growth of candidate materials in single crystal fiber form to determine structure, thermal, and dielectric properties and to make positive identification of twin free systems. Dielectric properties, thermal expansion coefficients, melting temperatures and growth feasibility were tested.

Through successful collaboration among MRL/Penn State and other DARPA/ONR supported projects thorough tests on the compatibility of the SAT films as buffer layer in MgO/YBCO system have been performed. Excellent epitaxial YBCO films with J_c of 10^6 A/cm^2 were reproducibly obtained.

Mechanisms relating the bonding nature and the order-disorder in complex perovskite niobates and tantalates that governing the characteristics of their dielectric properties were studied through collaboration with the microprobe Raman spectroscopy groups.

Work on the Shannon ion polarizability model for predicting dielectric permittivity in solids is being continued. Newly compiled normalized ion polarizabilities which take into consideration apparent bonding strengths improve the predictive capability considerably.

Solution sol-gel routes to form the phase pure powder of SAT and BMT were carried out. The atomic scale homogeneity, low temperature processing, higher sinterability and high reproducibility, were shown to be the major advantages of the method. We have demonstrated in this program that it is possible to grow oriented films of several materials on suitable substrates by this method at very modest temperature and therefore prepared ourselves for a new program that couples PSU to the cryogenic group, Science and Technology Center, Northrop Grumman.

TABLE OF CONTENTS

LIST OF APPENDICES

1. INTRODUCTION

This document is a final technical report of a research program entitled "Low Loss Substrates for Microwave Applications and Sol-Gel Processing of Superconductors." This program was funded through the Advanced Research Projects Agency and The Office of Naval Research under grant No.: N00014-94-1-0641. The grant was for the period April 1, 1994 through September 25,1996.

The program of studies at the Pennsylvania State University Materials Research Laboratory focused upon generating new substrate materials for the deposition of superconducting yttrium barium cuprate (YBCO) during the initial contract period (9/1/90-3/31/94) has yielded already several exciting new hosts in complex oxide perovskites family (e.g., BMT, SAT, and SAN, etc. see Appendices 1 and 2). New requirements which emerged during the initial contract period were concerned with the potential application of YBCO superconductor to the development of ultra high density interconnect systems for a new generation of high speed high density multichip modules. This application dictates new requirements for the substrate design. An essential feature is the geometry of the X and Y layers of HTSC lines that must have geometry in cross section of order 2 x 1 μ meters thus necessitating a current carrying capability for the HTSC of ~10^6 A/cm². For this current capability clearly the YBCO must be highly grain oriented very near to single crystal, so that the whole multilayer structure is in the form of very highly oriented overgrowths on a single crystal substrate. Impedance characteristics for the interconnect structure dictate that the dielectrics used must be of low permittivity (ideally <10) if the geometry is to be preserved. Highly oriented thin films (2 μm or above) will be needed for the separation of strip line and ground plane structures. Dielectric loss requirements are a little less stringent than those required for the microwave applications; however, tanδ < 0.001 is highly desirable at the 77K working temperature.

This current program has been focused on the combination of two aspects: (1) an extension to the initial program as to explore and utilize the suitable candidate

materials in HTC film processing and applications; and (2) to address impedance characteristics for the interconnect structure that requires highly oriented thin films, low permittivity and suitable dielectric loss level. Renewed emphasis on the application of YBCO in microwave structures returns the program closer to the original objectives.

2. SCIENTIFIC RESEARCH GOALS

This program was to continue exploring a wide range of materials, mostly of oxide compounds and solid solutions where the atomic/ionic arrangement in the lattice can be directly related to that of the preferred 'c' face of the YBCO superconductor. The phenomenological correlation of Shannon will be used to predict new low permittivity compositions. Correlation with measured dielectric properties will be used to improve and extend Shannon's tables of polarizabilities and to further explore optimum expressions for the oxygen polarizability.

High density ceramics were to be fabricated to explore thermal expansion behavior and to test chemical compatibility with YBCO.

Bulk single crystal and monocrystal fibers of the most promising compositions were to be grown to determine thermal, chemical and dielectric properties and make positive identification of twin free systems. The laser heated pedestal growth apparatus in MRL was to be used in the growth of crystals of new substrate materials.

Sol-Gel method was to be used to study the fabrication of the oxide films and to permit the close control of the chemistry and microorderness that are essential to compare dielectric loss performance in film and in bulk crystal. Effort was to be pushed to grow thicker films preserving orientation, so that the constraint upon permittivity may be partially relieved.

3. MATERIALS PROCESSING AND CHARACTERIZATION

3.1 MATERIALS PROCESSING

3.1.1 Solid State Ceramic Synthesis

Ceramic samples were prepared by solid state reaction, using conventional techniques. Calcining and sintering conditions were optimized through the study. Differential thermal analysis (DTA) was used to determine the minimum calcining temperature to achieve the desired phases and to select sintering temperatures. X-ray diffraction was used extensively to characterize the crystallographic phases and to adjust the processing conditions.

3.1.2 Single Crystal Growth by LHPG Technique

The LHPG technique has several unique features that were of special importance for this program. These advantages include containerless crystal growth and therefore the capability of growing refractory materials (that have low dielectric losses in general); capability of growing both incongruently and congruently melting compositions; and rapid growth rates. Fiber geometry also provides one dimensional dielectric material that may by itself meet microwave antenna requirements for some special device applications.[1]

The laser heated pedestal growth (LHPG) method has been shown to be a powerful method for rapidly growing small diameter single crystals, particularly oxides of high melting temperature, for both property studies and fiber devices.[2,3] The LHPG equipment used in this investigation consisted of a power source (water cooled, tunable flowing gas CO_2 55W laser), an optical layout, and a growth section. The molten zone temperature during a stable growth was monitored using an optical pyrometer with a linear dimension resolution of 0.1mm.

3.1.3 Solution Sol-Gel Powder and Thick Film Processing

The solution-sol-gel (SSG) method, which was pioneered at Penn State more than 40 years ago,[4] consists three parts: (i) mixing various components in solution, often with the use of metal organic precursors; (ii) forming a sol and causing it to gel as the key step in the process to retain chemical homogeneity during desiccation; and (iii) shaping during or after gelation into essentially final shape before firing. The atomic scale homogeneity and low temperature processing, besides simplicity and low cost are the major advantages of the SSG method.

Compared to the extensive work on a wide variety of deposition methods employed for oxide superconductors, only a small effort has so far gone into the SSG method for superconducting films.[5,6,7,8] The preliminary results obtained so far are encouraging and further effort is justified.

We have demonstrated in this program that it is possible to grow oriented films of several materials on suitable substrates by this method at very modest temperature. High sinterability and high reproducibility are important for these low κ substrate materials. Wet chemical methods are effective for attaining these characteristics.

By using modified solution sol-gel process SAT, SAN, and BMT thin films and high density ceramics were made and the properties are shown to be very good as suitable material for substrates application.

3.2 MATERIALS CHARACTERIZATION

3.2.1 Crystal Structures and Chemical Composition

Crystallographic structures of new candidate materials were studied extensively by x-ray diffraction.

Crystal quality and twinning were studied using polarized optical microscope and Laue back reflection photography. Scanning electron microscopy was also used for microstructure studies.

Chemical compositions of ceramic and crystal materials were analyzed quantitatively using electron probe micro-analysis (EPMA, CAMECA, SX-50) with spatial resolution of $2\mu m$ on the surface area and $0.2\mu m$ in depth. Relative analytic accuracy was $\pm 2\%$.

3.2.2 Dielectric Properties: at Microwave and Radio Frequency

Radio frequency dielectric constants and the tangent loss were measured using a General Radio 1621 Capacitance Measurement System. Dielectric properties at microwave frequency were measured using resonance techniques equipped with an HP8510A network analyzer. Post resonance technique (the Hakki and Coleman technique) was used to measure the dielectric constants of the ceramic samples.

Cavity perturbation technique was used for the measurements on samples of thin rod (e.g., single crystal fiber samples) or bar-shaped. The Q factors (of microwave frequency) at liquid nitrogen temperature were measured by a transmission resonance technique.

3.2.3 Thermal Properties

Thermal property compatibility of the substrates with HTSC films is critical for epitaxial film growth, in terms of determining the deposition and annealing temperatures, possibility of producing thick films, and reducing the degradation process in films and devices under working conditions.

Thermal expansion coefficients of new substrate materials were measured and compared to the thermal properties of the YBCO superconductor. The measurements were carried out from room temperature up to about 800°C by using a vertical push-rod dilatometer equipped with a high sensitivity linear variable differential transformer (LVDT). The heating and the cooling rates for thermal expansion measurements were regulated at 1 or 1.5°C/min using a microprocessor based temperature controller.

3.2.4 Growth Behavior and Melting Temperatures

The melting point was determined rather simply using a strip furnace, with two operators using two separate optical pyrometers and averaging several readings per sample.

The heating element consisted of a V-shaped ribbon of iridium metal clamped between two water-cooled brass electrical contacts. The current through the strip as controlled by two variable AC transformers connected in a vernier arrangement for better temperature control. The notch of the V acts as a black body cavity.

The samples, after determined to be a single phase by x-ray diffraction, were placed in the notch of the strip in form of small amount of granular powder. The onset of a melting process can be directly observed using optical pyrometer

Growth behavior and the molten zone temperature of a crystal sample during a stable growth by LHPG method were monitored simultaneously using a CCD camera and using an optical pyrometer.

4. CONTINUING SEARCH FOR CANDIDATE MATERIALS: COMPOSITIONS OF MAGNETOPLUMBITE STRUCTURE

Significant extension on the material studies has been in the area of the growth of the magnetoplumbite family of crystals using the laser heated pedestal growth.

Compounds of magnetoplumbite structure with compositions such as $LaMgAl_{11}O_{19}$, $NdGaMgAl_{10}O_{19}$, $CaGa_6Al_6O_{19}$, and $CaGa_{12}O_{19}$, are studied in this work to identify whether they possess suitable properties to be used as substrates for epitaxial deposition of high T_C superconducting (HTS) yttrium barium cuprate (YBCO) thin films for microwave applications. The study is directed toward (1) to test the feasibility of single crystal fiber growth by utilizing the Laser Heated Pedestal Growth (LHPG) technique, and (2) to evaluate the various characteristics of the materials including their crystallographic structures, thermal expansion coefficients, and dielectric properties (dielectric constant and loss tangent) to judge the potential of these materials as substrates for HTS thin films.

Ceramic synthesis and single crystal fiber growth by LHPG

Magnetoplumbite aluminates $LaMgAl_{11}O_{19}$ (LMA) and $NdGaMgAl_{10}O_{19}$ (NGMA) have been successfully synthesized using conventional oxide mixing process at conditions of 1650°C/6hrs and 1610°C/6hrs respectively. Single crystal fibers of LMA and NGMA have been successfully grown, using LHPG method. The growth temperatures 1922°C and 1820°C have been used for LMA and NGMA respectively and the typical growth rate used was about 8mm/hr. Gallium substitution of magnetoplumbite aluminate $CaGa_6Al_6O_{19}$ (CGA) has been used and ceramics were synthesized successfully using conventional oxide mixing process at condition of 1550°C/6hrs. The growth of single crystal fiber of CGA in the temperature range of 1750°C~1800°C by LHPG method was possible. However, the growth of CGA longer single crystal fibers was hampered by

Ga_2O_3 vaporization and bubble formation. Special care has to be taken for the growth of longer single crystal fibers. The synthesis of $CaGa_{12}O_{19}$ (CG) at temperature 1430°C apparently has not been successful. The X-ray powder diffraction pattern shows that large amount of unreacted Ga_2O_3 in monoclinic form was left in the fired ceramic. The mechanical strength of the fired ceramic was poor. The growth of CG single crystal fiber using the fired ceramic was unsuccessful. Perhaps better ceramics preparation may result the stoichiometric single crystal fibers of CG.

4.1 LATTICE MATCH BETWEEN THE SUBSTRATES OF THE MAGNETOPLUMBITE ALUMINATE STRUCTURE AND YBCO THIN FILMS

Crystal structures of LMA, NGMA, CGA are all of hexagonal symmetry with space group of $P6_3/mmc$. When the surface orientation of LMA, NGMA and CGA is ($1\bar{1}00$) the substrates will yield a good lattice match with YBCO. In this orientation the lattice mismatch between the ($1\bar{1}00$) substrate of LMA, NGMA, CGA and the (001) YBCO thin film is only about 2%~3%.

4.2 THERMAL COMPATIBILITY BETWEEN THE SUBSTRATES OF THE MAGNETOPLUMBITE ALUMINATE STRUCTURE AND YBCO THIN FILMS

In general, LMA, NGMA and CGA have good thermal expansion match with YBCO thin films.

4.3 DIELECTRIC PROPERTY

All three materials, LMA, NGMA and CGA have moderate dielectric constant in the range 11.4, 15.2 and 17 at room temperature, respectively. For LMA and NGMA, dielectric constant as function of temperature shows that the dielectric constant changes not much as the temperature was decreased from 180°C to -170C°. It is also found that dielectric constants of LMA, NGMA and CGA are frequency independent over a broad temperature region (-170C° to 180C°). The dielectric losses of the three materials are all on the order of 10^{-3} at radio frequencies. Based on the earlier results on LMA the losses of these materials at microwave frequency and liquid nitrogen temperature are expected in the range of 10^{-4}.

4.4 SUMMARY

The magnetoplumbite aluminates as a member of the alumina-rich family are good candidates as substrate materials for HTS thin films. The magnetoplumbite structure is a very flexible structure, able to accommodate large spectrum of cation substitutions, which, in turn, give rise to the potential of structure and property manipulation of the materials to meet the intricate requirements of substrates for HTS thin films. The prospective of magnetoplumbite aluminates as HTS thin film substrates is quite encouraging and these may be useful in exploiting some cross coupling effects kind of devices.

Abstract of this work is attached as Appendix 3.

5. DIELECTRIC FILMS AND INTERFACES

In preparation for a new program which couples MRL to the Westinghouse Science and Technology Center cryogenic group (now part of the Northrop Grumman Consortium) we have been exploring low temperature sol-gel routes to the deposition of highly oriented strontium aluminum tantalate (SAT) and to gain experience on increasing the film thickness with controlled crystallographic orientation and surface morphology.

5.1 THIN DIELECTRIC FILMS OF SAT BY PLD

Our experimental results on the SAT composition along with the earlier report on the congruent melting nature of the SAT and SAN compounds, have stimulated research works in the thin film area in other institutions and through collaborations with this project. SAT thin films (2000-3000Å) have been deposited on MgO (001) substrates using pulsed laser deposition (PLD). X-ray diffraction analysis shows that the SAT grows with the c-axis highly oriented normal to the substrate plane and very good in-plane epitaxy. The subsequently deposited YBCO films using PLD on SAT buffered MgO substrates exhibit excellent epitaxial growth with a narrow rocking curve width and a small f scan peak width. The critical temperature T_{co} of 90-92 K was achieved reproducibly and the critical current density over 2.7×10^6 A/cm^2 at 77K was measured.

This work not only demonstrates that high quality YBCO films can be grown on an MgO substrate with an SAT buffer layer, but also shows that SAT may be a promising buffer layer materials for making multilayer structures.

The compatibility of SAT as buffer layer on MgO with $Tl_2Ba_2CaCu_2O_8$ superconducting family was also studied and premising results were obtained. X-ray diffraction data of the $Tl_2Ba_2CaCu_2O_8$ films on SAT/MgO showed that the films were epitaxially oriented with the c-axis normal to the substrate surface and the $Tl_2Ba_2CaCu_2O_8$ [100] aligned with SAT [100] and MgO [100]. The Tc of the superconducting films ranged from 95 to 103 K and the transport Jc at 77 K in zero field was at least $3x10^5$ A/cm^2. This study shows that SAT is a suitable buffer layer material for the growth of superconducting $Tl_2Ba_2CaCu_2O_8$ films due to their good lattice match and chemical compatibility. Further details of these collaborative work can be found in Appendices 4 and 5.

5.2 SOL-GEL SYNTHESIS OF SAT AND BMT

Phase pure BMT powder was synthesized by the sol-gel technique and thin films at a significantly low temperature (~600°C), in contrast to the solid state reactions which usually requires high temperature calcining (~1400°C) with very long heating schedules. High quality, crack-free BMT films were prepared on Pt-coated Si substrates. High relative density (98.4%) BMT ceramics were formed at 1500°C in 24 hours without the addition of sintering aid. SEM analysis also showed that the films of 0.3μm in thickness were essentially crack-free.

Phase-pure SAT powder was prepared by sol-gel route including Sr metal, Al(tri-secbutoxide) and Ta(OC2H5)5 as the starting organic precursors. Sol-gel processing of SAT can lead to highly phase pure homogeneous powders , and these powders can offer significant advantages over conventionally processed powders. The SAT phase pure powder was formed at 1400°C from a transparent zero-gel (the formation temperature has been substantially reduced to 450°C by using Sr granular as precursor materials).

The sol-gel processing studies on BMT and SAT are presented in Appendix 6 and 7.

6. SYSTEMATIC SEARCH FOR CANDIDATE SUBSTRATES

6.1 DIELECTRIC MECHANISMS OF COMPLEX OXIDE PEROVSKITES BY RAMAN SPECTROSCOPY

Complex oxide perovskites SAT and SAN have been studied by microprobe Raman scattering in a temperature interval from 30 to 300K. Ceramic and single crystal forms of SAN and SAT were studied in particular to compare the difference between the O-Nb-O and O-Ta-O bonding and in relation to the order-disorder for the structure. The E_g and A_{1g} modes in SAT were found at higher frequencies, 577.7 cm^{-1} and 871.9 cm^{-1}, comparing to that of SAN, 540.28 cm^{-1} and 856.3 cm^{-1}. It is a good indication that the short range interaction constant of O-Ta-O is greater than that of O-Nb-O. This finding is in agreement with the experimental result that SAT having smaller dielectric constant and dielectric loss compared to that of SAN. The paper address this research is listed as Appendix 8.

Similar studies by the microprobe Raman spectroscopy were also carried out for sol-gel synthesized SAT and BMT powders and the details are presented in Appendix 7 and 9.

6.2 ION POLARIZABILITY ADDITIVITY MODEL: DIELECTRIC CONSTANTS PREDICTION

Recently, Shannon[9] has derived a set of 61 ion dielectric polarizabilities from a least square refinement procedure using the ion additivity rule and calculated dielectric constants for about a hundred compounds in conjunction with the Clausius-Mosotti equation. Excellent agreement between the polarizability values calculated and those experimentally measured was shown for many ternary systems including borates, aluminates, gallates, silicates, germanates, phosphates, and vanadates.

It is of great interest for us to apply the ion polarizability additivity rule to the family of substrate or potential substrate materials. We have gathered fair amount of dielectric and structural data that were previously unavailable. It is specially interesting to examine if Shannon's model and the ion polarizability data can be used to predict the dielectric constant of new materials and to identify the "abnormal" behavior in a material if present. Comparison of calculated and experimental dielectric constants

using the ion polarizability additivity rule can be found in Appendix 2. We found that good agreements are usually seen in cases of substances containing cations having high valence and small sizes, while large discrepancies are common in ternary systems that involve large cations in high coordination sites. Poor agreements are also apparent in materials containing d^0 ions (Nb, Ta) such as $Ba(Mg_{1/3}Ta_{2/3})O_3$, $Sr(Al_{0.5}Ta_{0.5})O_3$, and $Sr(Al_{0.5}Nb_{0.5})O_3$ and cations of rare-earth family such as $LaAlO_3$ and $LaGaO_3$.

Following the work of O'Keeffe[10] and Brown and Altermatt[11] on the apparent bond valences and their relations to bond lengths, we have reformulated the ion polarizability additivity rule by normalizing each ion polarizability to its electrostatic valence status. In order to narrow down the differences between the calculated and measured values, we considered several new factors in Shannon's approach. One of the new approach defines the normalized ion polarizability which is applicable for estimation of the dielectric constants with higher precision once the refined crystal structure is known. The work has been undertaken to improve the fit to experimental values by taking account of the apparent bonding valence and its correlation to bonding distance in providing a normalized ionic polarizability in a given structural configuration. The method is applicable to oxides, fluorides and oxyfluorides and has improved the accuracy of dielectric constant prediction particularly for compounds containing d^0 elements, alkali earth elements and rare-earth elements.

7. SUMMARY

Under continuous support of DARPA/ONR and through successful combination of our effort and collaboration with other element of the DARPA project, we have been able to meet the challenge of devising new alternative compositions and twin free perovskites with low congruent melting temperatures, matching thermal expansion from the YBCO processing temperatures down to the liquid nitrogen working temperature and excellent chemical compatibility. New substrates developed and the technology base built in the program have stimulated collaborations among Penn State and other elements in DARPA superconductor programs. To summarize:

Systematic studies on low κ oxide substrate materials suitable for epitaxial deposition of high Tc superconducting (HTSC) yttrium barium cuprate (YBCO) films and their microwave applications have been carried out. Several promising new hosts such as $Sr(Al_{1/2}Ta_{1/2})O_3$, $Sr(Al_{1/2}Nb_{1/2})O_3$, and $Ba(Mg_{1/3}Ta_{2/3})O_3$ in complex oxide perovskite family have been developed. The crystals of these compositions and their associated solid solutions provide new options for ultra low loss, low permittivity substrates with close structural and thermal properties matching to the YBCO. Studies were extended to the twin free perovskites (e.g., modified complex perovskites) with low congruent melting temperatures and alternative compositions with lower dielectric constants (e.g., in spinel, magnetoplumbite, and fluorite structures).

The unique capabilities of a laser heated pedestal growth (LHPG) system have been utilized for test-growth of candidate materials in single crystal fiber form to determine structure, thermal, and dielectric properties and to make positive identification of twin free systems.

Dielectric properties, thermal expansion coefficients, melting temperatures and growth feasibility were tested for a wide range of substrate materials and solid solutions. This knowledge base is important for the projected work and for the fundamental materials research.

Systematic study on the surface crystallographic compatibility and epitaxial relations with the YBCO provided further guidelines for substrates selection and film deposition design.

Development on the predictive capability of the dielectric constant of ionic solids, by improving ion polarizability additivity model (Shannon's approach), may provide a base for the selection of new compositions for further study.

Material studies has been extended in the area of the growth of the magnetoplumbite family of crystals using the laser heated pedestal growth.

Successful collaboration between MRL/Penn State and other ONR supported projects have yielded thorough test on the realization of the SAT films in YBCO bilayer and trilayer structures and as buffer layer in MgO\YBCO system.

Mechanisms relate to distinguish the niobates and the tantalates in their dielectric properties were studied, through collaboration, by microprobe Raman spectroscopy.

Work on the Shannon ion polarizability model for predicting dielectric permittivity in solids is being continued. Newly compiled normalized ion polarizabilities which take into consideration apparent bonding strengths improve the predictive capability considerably.

We intend to keep active interaction and close collaboration with other elements of DARPA/ONR programs and continue to maintain strong standing as a knowledge base in substrate materials science and technology.

8. REFERENCES

PUBLICATIONS FROM THE ORIGINAL DARPA/ONR SUPPORTED PROGRAM PRECEDING THE CURRENT REPORT PERIOD:

(1)   Jyh Sheen, Ruyan Guo, A.S. Bhalla, and L.E. Cross, "Measurements of Dielectric Constant and Quality Factor of $Ba(Mg_{1/3}Ta_{2/3})O_3$ at X Band Frequencies," *Ferroelectrics Letters* **16** (1/2), 33-41 (1993).

(2)   Jyh Sheen, Ruyan Guo, A.S. Bhalla, and L.E. Cross, "Microwave Dielectric Properties Measurements of Potential HTSC Substrate Materials," *Ferroelectrics*, **145**, 15-22 (1993).

(3)   Jyh Sheen, "Microwave Dielectric Properties Measurements by Various Resonance Techniques on the Potential Substrate Materials for High Tc Superconductor Thin Films," Ph.D. Thesis, Penn State University (Dec. 1993).

(4)   Ruyan Guo, A. S. Bhalla, and L.E. Cross, "$Ba(Mg_{1/3}Ta_{2/3})O_3$ Single Crystal Fiber Grown by Laser Heated Pedestal Growth Technique," *J. Appl. Phys.* **75**(9) 4704-4708 (1994).

(5)   Rustum Roy, Ruyan Guo, A.S. Bhalla, and L.E. Cross, "'Oriented Film Growth", Not 'Epitaxy' in HTSC Film Growth," *J. Vac. Sci. Technol. A* **12**(2) 269-273 (1994).

(6)   Jyn Sheen, A.S. Bhalla, and L.E. Cross, "A Modification to a Simple Field Model to the $TE_{01\delta}$ Mode of the Parallel-Plate Open Dielectric Resonator," *Microwave and Optical Technology Letters*, **7**(5), 226 (1994).

(7) Ruyan Guo, A.S. Bhalla, L.E. Cross, and Rustum Roy, "Surface Crystallographic Structure Compatibility between Substrates and High Tc (YBCO) Thin Films," *J. Mater. Res.* **9**(7), 1644-1656 (1994).

(8) G. Harshe, A.S. Bhalla, and L.E. Cross, "Synthesis and Dielectric Properties of a Cubic Perovskite Material: $La(Mg_{1/2}Ti_{1/2})O_3$," *Materials Letter* **18**(4), 173 (1994).

(9) Ruyan Guo, P. Ravindranathan, U. Selvaraj, A.S. Bhalla, L.E. Cross, and R. Roy, "Modified Mixed Oxide Perovskite for High Tc Superconductor Substrate Applications," *J. Materials Science* **29**(19) (Oct. 1, 1994).

(10) Ruyan Guo, A.S. Bhalla, R. Roy, and L.E. Cross, "Ion Polarizability Additivity Rule and Its Application on HTSC Substrate Materials," *Ferroelectrics* **155** (1-4) (Proceedings of the Eighth International Meeting on Ferroelectrics), 43-48, (1994).

(11) S. Erdei, L.E. Cross, F.W. Ainger, and A. Bhalla, "Ca-Sr-Ga-Nb Mixed System for HTSC Substrate Applications," *J. Crystal Growth* **139**, 54-66 (1994).

(12) Ruyan Guo, A.S. Bhalla, Rustum Roy and L.E. Cross, "Candidate HTSC Film Substrates of Complex Oxide Perovskite Compositions," *Epitaxial Oxide Thin Films and Heterostructures, Proceedings of the MRS Spring Meeting* SPIE 1994 (Sept. 1994).

REFERENCES CITED IN THIS REPORT:

1   R.J. Dinger and D.J. White, *IEEE Trans. Antennas Propagat.* **38**(8), 1313 (1990).

2   J.S. Haggerty, W.P. Menashi and J.F. Wenckus, *Method for Forming Refractory Fibers by Laser Energy*, U.S. Patent 3,944,640, March 16, 1976 and *Apparatus for Forming Refractory Fibers*, U.S. Patent 4,012,213, March 15, 1977.

3   R.S. Feigelson, *MRS Bull.* **13**, 47 (1988).

4   R. Roy, Science, 238, 1664 (1987).

5   S.A. Kremer, G. Kordas, J. McMillan, G.C. Hilton, and D.S. Van Harligen, *Appl. Phys. Lett.,* **53**, 156 (1988).

6   S.A. Khan, P. Barboux, B.G. Bagley, and J.M. Tarascan, *Appl. Phys. Lett.,* **53**, 700 (1988).

7   P. Barboux, J.M. Tarascan, L.H. Coreene, G.W. Hull, and B.G. Bagley, *J. Appl. Phys.,* **63**, 2725 (1988).

8   P. Ravindranathan, S. Komarneni, A.S. Bhalla, and R. Roy, Presented at the MRS Meeting, Boston, MA (November 1989).

9   R. D. Shannon, *J. Appl. Phys.* **73**(1), 348 (1993).

10 M. O'Keeffe, *Structure and Bonding,* **71** (Springer-Verlag, Berlin Heidelberg, 1989) p.163-190.

11 I.D. Brown and D. Altermatt, *Acta Cryst.* **B41**, 244 (1985).

9. PUBLICATIONS

(1).   R. Guo, J. Sheen, A.S. Bhalla, F.W. Ainger, S. Erdei, E.C. Subbarao, and L.E. Cross, "Strontium Aluminum Tantalum Oxide and Strontium Aluminum Niobium Oxide as Potential Substrates for HTSC Thin Films," *J. Materials Research*, 10(1), 18-25 (1995).

(2).   A.S. Bhalla and Ruyan Guo, "Oxide Perovskite Crystals for HTSC Film Substrates Microwave Applications," *Proceedings of the Fourth International Conference and Exhibition: World Congress on Superconductivity, Vol. I, NASA Conference Publication 3290*, 188-197 (1994).

(3).   K.Y. Chen, S. Afonso, R.C. Wang, Y.Q. Tang, G. Salamo, F.T. Chan, R. Guo, A. Bhalla, "Epitaxial $Sr_2(AlTa)O_6$ Films as Buffer Layers on MgO for $YBa_2Cu_3O_{7-x}$ Thin Film Growth," *J. Appl. Phys.*, 78(3):2138-40 (1995).

(4).   K.Y. Chen, S. Afonso, R.C. Wang, Y.Q. Tang, G. Salamo, F.T. Chan, R. Guo, A. Bhalla, "Epitaxial Growth of Superconducting $YBa_2Cu_3O_{7-x}$ Films on $Sr_2(Al_{0.5}Ta_{0.5})O_3$ Buffered MgO Substrates," *The Electrochemical Society Proceedings: Low Temperature Electronics and High Temperature Superconductivity*, ed. Claeys, Raider, Kirschman, and Brown, 95-9, 121-126 (1995).

(5).   Y.Q. Tang, K.Y. Chen, S. Afonso, X.L. Xu, Q. Xiong, G. Salamo, F.T. Chan, R. Guo, A. Bhalla, "Epitaxial $Tl_2Ba_2CaCu_2O_8$ Superconducting Thin Film on $Sr_2(AlTa)O_6$ Buffer Layer," *J. Appl. Phys*, 78(11):6846-6848 (1995).

(6).   A.S. Bhalla and Ruyan Guo, "Substrates for Microwave Applications of High Tc Superconductors," *Ceramic Transactions,* Vol. 68, 119-130, *Amer. Ceram. Soc., Westerville, OH* (1996).

(7).   D. Ravichandran, R. Meyer, Jr., R. Guo, A.S. Bhalla, L.E. Cross, and R. Roy, "Sol-Gel Synthesis of $Ba(Mg_{1/3}Ta_{2/3})O_3$: Phase Pure Powder and Thin Films," *Mat. Res. Bull.*, 31(7), 817-825 (1996).

(8).   R. Tao, A.R. Guo, C.-S. Tu, I. Siny, R.S. Katiyar, Ruyan Guo, and A.S. Bhalla, "Temperature Dependent Raman Spectroscopic Studies on Microwave Dielectrics $Sr(Al_{1/2}Ta_{1/2})O_3$ and $Sr(Al_{1/2}Nb_{1/2})O_3$," *Ferroelectric Letters*, 21 (3/4) 79-85 (1996).

(9).   Amar Bhalla and Ruyan Guo, "Design of Dielectric Substrates for HTS Films," *World Congress on Superconductivity, Poland* (in printing, 1996).

(10).   D. Ravichandran, R. Toy, B. Jin A.S. Bhalla, "A Study of Sol-Gel Derived $Sr_2(AlTa)O_6$ by Raman Spectroscopy," *J. Materials Science Letters* 15, 805-806 (1996).

(11).   D. Ravichandran, B. Jin, R. Roy, A.S. Bhalla, "Raman Spectroscopy of Sol-Gel Derived $BaMg_{1/3}Ta_{2/3}$ Perovskites," *Materials Letters*, 25, 257-259 (1995).

10. PRESENTATION AT NATIONAL AND INTERNATIONAL MEETINGS

(1)   (invited) A. S. Bhalla and R. Guo, "Structure and Property of Substrate Materials for HTSC Films," World Congress on Superconductivity, June 27-July 1, 1994, Orlando, Florida.

(2) (invited) Amar S. Bhalla and Ruyan Guo, "Oxide Perovskite Crystals for HTSC Film Substrates in Microwave Applications," International Conference on Substrate Crystals and HTSC Films (ICSCS-F '96), September 16-20, 1996, Jaszowiec, Poland.

(3) (Keynote Lecture) A. Bhalla, "Microwave Dielectric Substrates for HTSC Devices," Meeting on Functional Materials, India (march 1996).

(4) (invited) Ruyan Guo, "Low Loss and Low Permittivity Dielectric Substrate Materials for Microwave Applications, (invited)" First Asian Meetings on ferroelectrics, Oct. 3-7, Xi'an, China.

(5) S. Afonso, Y.Q. Tang, K.Y. Chen, G.J. Salamo, F.T. Chan and R. Guo, "$Sr(Al_5Ta_5)O_3$ as a New Dielectric Material for YBCO/Dielectric/YBCO Trilayer Thin Films," The American Physical Society Annual Meeting (1994).

(6) Ruyan Guo, A.S. Bhalla, Rustum Roy and L.E. Cross, "Modified Ionic Polarizability Additivity Model and Its Application in Dielectric Property Studies of Ionic Materials," The Ninth IEEE International Symposium on the Applications of Ferroelectrics, Aug. 7-10, 1994, University Park, Pennsylvania.

(7) Ruyan Guo, A.S. Bhalla, Rustum Roy and L.E. Cross, "Studies of Oxide Crystals for HTSC Film Substrates Microwave Applications," The Ninth IEEE International Symposium on the Applications of Ferroelectrics, Aug. 7-10, 1994, University Park, Pennsylvania.

(8) D. Ravichandran, Ruyan Guo, A. Bhalla, L.E. Cross, and R. Roy, "Formation of $Sr_2(AlTa)O_6$ Perovskites via Organic Precursors," MRS 1995 Spring Meeting, April 17-21, 1995, San Francisco, California.

(9) K.Y. Chen, S. Afonso, R.C. Wang, Y.Q. Tang, G. Salamo, F.T. Chan, R. Guo and A. Bhalla, "High Quality YBCO Films on MgO Substrates with $Sr(Al_{0.5}Ta_{0.5})O_3$ Buffer Layer," MRS 1995 Spring Meeting, April 17-21, 1995, San Francisco, California.

(10) Ruyan Guo, A.S. Bhalla, Rustum Roy and L.E. Cross, "Modified Ionic Polarizability Additivity Model and Its Application in Dielectric Property Studies of Substrate Materials," MRS 1995 Spring Meeting, April 17-21, 1995, San Francisco, California.

(11) D. Ravichandran, Ruyan Guo, A. Bhalla, L.E. Cross, and R. Roy, "Sol-Gel Derived Ba(Mg1/3Ta2/3)O3 for HTSC Thin Films Substrates," 1995 ACerS Annual Meeting, May 1-3, 1995, Cincinnati, Ohio.

(12) G. Salamo, F.T. Chan, R. Guo, and A. S. Bhalla, "Epitaxial Growth of YBCO Films on Sr(Al0.5Ta0.5)O3 Buffered MgO Substrates," The Electrochemical Society 187th Meeting on Interface, May 21-26 (1995) Reno, Nevada.

(13) Ruiwu Tao, A. R. Guo, C. -S. Tu, R. S. Katiyar, Ruyan Guo, and A. S. Bhalla, "Raman Studies on $Sr(Al_{1/2}Ta_{1/2})O_3$ (SAT) and $Sr(Al_{1/2}Nb_{1/2})O_3$ (SAN) Single Crystals Prepared by Laser Heated Pedestal Growth Technique," MRS 1995 Fall Meeting, Nov.27-Dec.1,1995, Boston, Massachusetts.

(14) D. Ravichandran, R. Roy, A.S. Bhalla, R. Guo, and L.E. Cross, "$Sr_2(AlTa)O_6$ Powder and Thin Films at Low Temperatures for High Tc Oxides Substrates," MRS 1995 Fall Meeting, Nov.27-Dec.1,1995, Boston, Massachusetts.

(15) Ruiwu Tao, I.G. Siny, A.R. Guo, and R.S. Katiyar, Ruyan Guo and A.S. Bhalla, "A Comparative Study of the 1:1 and 1:2 B-Site Ordering in Complex Perovskite-Type Materials $AB'_xB''_{1-x}O_3$ by Raman Scattering" American Physical Society 1996 Annual Meeting, San Diego (Feb. 25-29 1996).

(16) Ruiwu Tao, I.G. Siny, A.R. Guo, and R.S. Katiyar, Ruyan Guo and A.S. Bhalla, "Raman and Temperature Dependent Raman Studies on $Ba(Mg_{1/3}Ta_{2/3})O_3$ (BMT)," MRS 1996 Spring Meeting, San Francisco, CA (April 8-12, 1996).

(17) Manwen Yao, Ruyan Guo and A.S. Bhalla, "Dielectric Single Crystals of Magnetoplumbite Structure Grown by Laser Heated Pedestal Growth Technique," ACerS 1996 Annual meeting, Indianapolis, Indiana (April 14-17, 1996).

(18) D. Ravichandran, R. Guo, R. Roy, A.S. Bhalla, and L.E. Cross, "Sol-Gel Synthesis of $Sr_2(AlTa)O_6$ Films for HTC Microwave Device Applications," Applied Superconductivity Conference, Aug. 25-30, 1996, Pittsburgh, Pennsylvania.

(19) M. Yao, R. Guo and A.S. Bhalla, "Single Crystals of Magnetoplumbite Structure Grown by Laser Heated Pedestal Growth Technique," The Tenth IEEE International Symposium on Applications of Ferroelectrics, East Brunswick, NJ, Aug. 18-21, 1996.

11. PARTICIPANTS

Name	Status	Remarks
Amar S. Bhalla	Prof. of Solid State Science & Senior Scientist	Co-PI
L. Eric Cross	Evan Pugh Professor of Electrical Engineering	Co-PI
Rustum Roy	Evan Pugh Professor of Solid State	Co-PI
Ruyan Guo	Senior Research Associate	
Sandor Erdei	Faculty Research Associate	
D. Ravichandran	Post-Doctoral Research Associate	
Manwen Yao	Graduate Research Assistant	M.S. student
Frank W. Ainger	Senior Scientist	Visiting Faculty

12. APPENDICES

Appendix 1.

"Strontium Aluminum Tantalum Oxide and Strontium Aluminum Niobium Oxide as Potential Substrates for HTSC Thin Films"

J. Materials Research, **10**(1), 18-25 (1995)

R. Guo

J. Sheen

A.S. Bhalla

F.W. Ainger

S. Erdei

E.C. Subbarao

L.E. Cross

Strontium aluminum tantalum oxide and strontium aluminum niobium oxide as potential substrates for HTSC thin films

Ruyan Guo, A. S. Bhalla, Jyh Sheen, F. W. Ainger, S. Erdei, E. C. Subbarao, and L. E. Cross
Materials Research Laboratory, The Pennsylvania State University, University Park, Pennsylvania 16802-4800

Single crystal fibers of $A(B1_{1/2}B2_{1/2})O_3$ perovskites type with compositions $Sr(Al_{1/2}Ta_{1/2})O_3$ (SAT) and $Sr(Al_{1/2}Nb_{1/2})O_3$ (SAN) were grown successfully for the first time, using a laser-heated pedestal growth (LHPG) technique. Their crystallographic structures were found to be simple cubic perovskite with lattice parameters $a = 3.8952$ Å (SAT) and $a = 3.8995$ Å (SAN) that are close lattice matches to the YBCO superconductors. No structural phase transitions or twins have been found, and the average coefficients of the thermal expansion match well with the YBCO superconductor materials. We report that SAT is one of the most promising substrates to date for the epitaxial growth of HTSC thin films suitable for microwave device applications as it has low dielectric constants ($\kappa \sim 11-12$, at 100 Hz–10 GHz and 300 K) and low dielectric loss ($\sim 4 \times 10^{-5}$ at 10 kHz and 80 K), together with lattice parameter matching, thermal expansion matching, and chemical compatibility with the high T_c superconductors (YBCO).

I. INTRODUCTION

The rise of electronic technology utilizing high temperature oxide superconducting materials requires at the very least the mastering of processing of the epitaxial thin films of high T_c superconducting (HTSC) materials on suitable substrates and the understanding of their properties. Superconductor device applications demand that the substrate materials for HTSC meet several requirements: lattice matching (or atomic structure matching)[1] to the HTSC materials for ideal epitaxial films, thermal compatibility in terms of thermal expansion matching over the temperature range of film processing and annealing (>900 K) down to the operating temperature (90 K), low dielectric constants for integrated circuit designs (<25 or ideally less than 10), very low dielectric loss ($\leq 10^{-4}$) at microwave frequencies (~ 10 GHz) and at low temperatures (90 K) for microwave device applications, chemical inertia and compatibility with the HTSC thin film deposition, and mechanically strong and scratch resistant. As a single crystal substrate is most desirable (as large as 4 in. in diameter), it is also vital that the crystal should be available at a reasonable cost. All the currently available substrates present some compromises. $SrTiO_3$ crystals of high quality and large sizes, though they are readily available and yield the best quality epitaxial thin films (primarily due to their close interatomic structure matching to the HTSC), have high dielectric constant (>300) arising from the phase transition near the working temperature (~ 110 K). Al_2O_3 sapphire single crystal substrates, which have low dielectric constant κ and low loss at microwave frequencies, require a buffer layer to avoid chemical interactions with the YBCO. One of the substrates, probably the one most currently used, $LaAlO_3$, though good in lattice matching and of reasonable dielectric properties, is heavily twinned and goes through a ferroelastic phase transition at ~ 435 °C.[2] Table I lists some of the most commonly used substrates for comparison purposes.

The objective of our investigation was to screen various complex oxide materials to identify suitable HTSC substrate materials and to test the feasibility of single crystal growth by utilizing a laser-heated pedestal crystal growth (LHPG) technique. The LHPG technique has several unique features that are of special importance for this task. These advantages include containerless crystal growth and, therefore, the capability of growing refractory materials (that have low dielectric losses in general), capability of growing both incongruently and congruently melting compositions, and rapid growth rates. Fiber geometry also provides one-dimensional dielectric material that may by itself meet microwave antenna requirements for some special device applications.[5]

The compounds $Sr(Al_{1/2}Ta_{1/2})O_3$ (SAT) and $Sr(Al_{1/2}Nb_{1/2})O_3$ (SAN) were first prepared and tested to learn their crystallographic phases and their melting behavior by the group at AT&T Bell Labs.[6] Ceramic samples were identified to have double cell cubic perovskite structure with $a = 7.795$ Å and melting temperatures of 1900 °C and 1790 °C for SAT and SAN, respectively. On the basis of our understanding of the crystal chemistry-dielectric property relationships of various

TABLE I. Most commonly used high T_c superconductor substrates.

Substrates	Symmetry, lattice constants (Å)	Dielectric constant κ (at RT)	Thermal expansion α ($\times 10^{-6}$/°C)	Comments
$YBa_2Cu_3O_{7-\delta}$	Ortho. $a = 3.836$ $b = 3.883$ $c = 11.68$ (Ref. 3)		$\alpha_a = 14$ $\alpha_b = 9$ $\alpha_c = 19$ (Ref. 4)	
$SrTiO_3$	Cubic $a = 3.905$	> 300	10.6	Good epitaxial YBCO film: high dielectric constant
$LaAlO_3$	Rhomb. $a = 3.789$ $\alpha = 90.12°$	23	8.2 ($\parallel[110]$) 6.4 ($\parallel[001]$)	Structural phase transition at ~ 435 °C; heavy twinning
Al_2O_3	Rhomb. $a, b = 4.7586$ $c = 12.9897$ $\gamma = 120°$	$\kappa_a = 9.34$ $\kappa_c = 11.54$	6	Poor lattice matching; poor thermal expansion matching; chemical interactions with YBCO (buffer layer often required)
MgO	Cubic $a = 4.2114$	9.65	10.4	Reasonable cost: easy to cleave; large lattice mismatching
YSZ ($Zr_{0.72}Y_{0.28}O_{1.862}$)	Cubic $a = 5.16(2)$	26	4.5	Chemical interactions with YBCO; $BaZrO_3$ forms at the interface (buffer layer often required)

oxide perovskites, and the reports by the Bell Labs group that showed both the SAN and SAT melt congruently and produce a single phase of the perovskite structure after melting, we selected SAT and SAN as primary candidates in the $A(B1_{1/2}B2_{1/2})O_3$ complex oxide perovskite family for crystal growth and investigated their properties in relation to substrate applications.

This paper reports two single crystals. $Sr(Al_{1/2}Ta_{1/2})O_3$ (SAT) and $Sr(Al_{1/2}Nb_{1/2})O_3$ (SAN), both of $A(B1_{1/2}B2_{1/2})O_3$ complex oxide perovskite formula, grown by the laser-heated pedestal growth technique. Their preparation, chemical analysis, crystal structures, and dielectric and thermal expansion properties are reported. They have twin-free simple cubic perovskite structures and attractive dielectric properties. They have the potential to be used as microwave substrates for YBCO superconducting thin films.

II. EXPERIMENTAL PROCEDURE

A. Ceramic preform preparation

Ceramic samples were prepared by solid state reaction, using conventional techniques. Several batches with various calcining and sintering conditions were prepared and the procedure was somewhat optimized through the study. Differential thermal analysis (DTA) was used to determine the minimum calcining temperature to achieve the desired phases and to select sintering temperatures. X-ray diffraction was used extensively to characterize

the crystallographic phases and to adjust the processing conditions. Some of the processing parameters used are summarized in Table II.

B. Laser heated pedestal growth: The instrument

The laser-heated pedestal growth (LHPG) method has been shown to be a powerful method for rapidly growing small diameter single crystals, particularly oxides of high melting temperature, for both property studies and fiber devices.[7,8] The LHPG equipment used in this investigation consisted of a power source (water-cooled, tunable flowing gas CO_2 55 W laser), an optical layout, and a growth section. The molten zone temperature during a stable growth was monitored using an optical pyrometer with a linear dimension resolution of 0.1 mm. A schematic diagram of the LHPG station is shown in Fig. 1. Additional details can be found elsewhere.[9]

C. Dielectric measurements

Radio frequency dielectric constants and the loss tangent were measured using a General Radio 1621 Capacitance Measurement System. Three-terminal measurements were carried out using a shielded sample holder. The accuracy of the measurement was in the range of $\pm(10-50)$ ppm for capacitance measurement and $\pm(0.1 + 1$ step in the least significant decade) for conductance measurement. The stray capacitance, lead,

J. Mater. Res., Vol. 10, No. 1, Jan 1995

19

TABLE II. Ceramic processing conditions for $Sr(Al_{1/2}Nb_{1/2})O_3$ and $Sr(Al_{1/2}Ta_{1/2})O_3$.

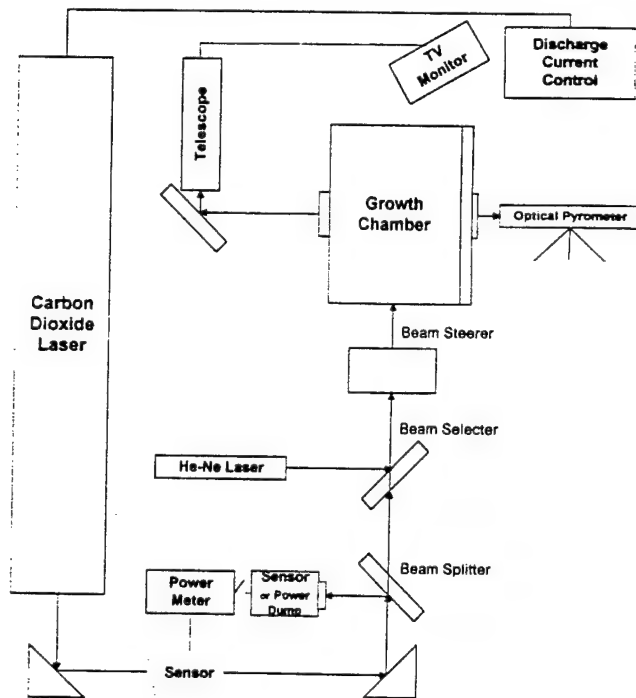| Composition	Starting chemicals (purity)		Calcination condition	Sintering condition	Density (g/cm^3)
$Sr(Al_{1/2}Nb_{1/2})O_3$	$SrCO_3$ Al_2O_3 Nb_2O_5	(4N) (3N5) (4N)	1570 °C for 3 h	1600 °C for 3 h	5.051 (91.7% theoretical)
$Sr(Al_{1/2}Ta_{1/2})O_3$	$SrCO_3$ Al_2O_3 Ta_2O_5	(4N) (3N5) (4N)	1600 °C for 3 h	1620 °C for 4 h	6.537 (96.6% theoretical)

FIG. 1. Schematic diagram of the laser-heated pedestal growth station.

and contact resistance were corrected during measurement by taking an open circuit measurement. The edge corrections of the measurement results were made using an empirical equation derived from the measurements on a family of fused silica samples:

$$C_e = \left(0.02798 \cdot \ln\left(\frac{P}{t}\right) - 0.05922\right) \cdot P \qquad (1)$$

where C_e is the edge capacitance, and P and t are the perimeter and the thickness of the sample in centimeters.

Dielectric properties at microwave frequency were measured using resonance techniques equipped with an HP8510A network analyzer. The post-resonance technique (the Hakki and Coleman technique[10]) was used to measure the dielectric constants of the ceramic samples. Cavity perturbation technique[11] was used for the measurements on samples of thin rods (e.g., single crystal fiber samples) or bar-shaped. The Q factors (in

microwave frequency) at liquid nitrogen temperature were measured by a transmission resonance technique.

III. RESULTS AND DISCUSSION

A. Crystallographic phases in ceramics

1. $Sr(Al_{1/2}Ta_{1/2})O_3$

The presence of an intermediate phase, $SrTa_2O_6$, was noticed in ceramic powders for calcining temperatures between 1250 °C and ~1550 °C, and the phase disappeared after calcination at 1550 °C. Another intermediate phase, $SrAl_2O_4$, could also form and remain in the ceramic powder until the melting point (~1960 °C)[12] when excess Al was present. This intermediate phase could be harmful for single crystal growth, and therefore repeated grinding followed by calcining was performed. A MgO crucible (instead of Al_2O_3 crucible) was used to avoid excess Al diffusion into the compound during the calcination process. The x-ray diffraction pattern for the SAT ceramics sintered at 1655 °C for 5 h is shown in Fig. 2(a). The crystallographic phase of the SAT powder is a double cell cubic perovskite as reported by Brandle and Fratello,[6] with a lattice parameter $a = 7.7767$ Å. The sharp (111), (311), (331), and (333) diffraction peaks indicate that the SAT has a strong tendency to form a B-site ordered (Al:Ta = 1:1) perovskite structure.

2. $Sr(Al_{1/2}Nb_{1/2})O_3$

As in the case of SAT, the presence of an intermediate phase, $SrNb_2O_6$, was found in the powder at a calcining temperature $T \sim 1150$ °C. This intermediate phase reacted with the remaining SrO and Al_2O_3 to form pure SAN phase at a higher temperature (~1570 °C). The SAN phase was found to be an ordered perovskite cubic phase with a lattice parameter $a = 7.7824$ Å. The x-ray diffraction pattern for the SAN ceramics sintered at 1570 °C for 24 h is shown in Fig. 2(b).

B. Single crystal fiber growth and crystallographic phases

Single crystals of SAN and SAT were grown successfully using the LHPG technique. Both the feeding rods (~0.45 mm^2 in cross section) and the pulling seeds (~0.12 mm^2 in cross section) were ceramics prepared
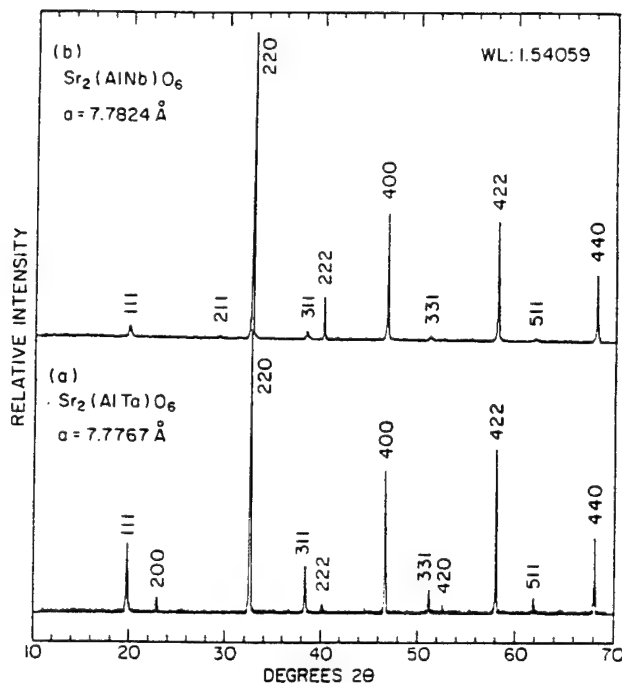
FIG. 2. X-ray diffraction patterns of (a) an SAT ceramic sintered at 1655 °C for 5 h and (b) SAN ceramic sintered at 1570 °C for 24 h.
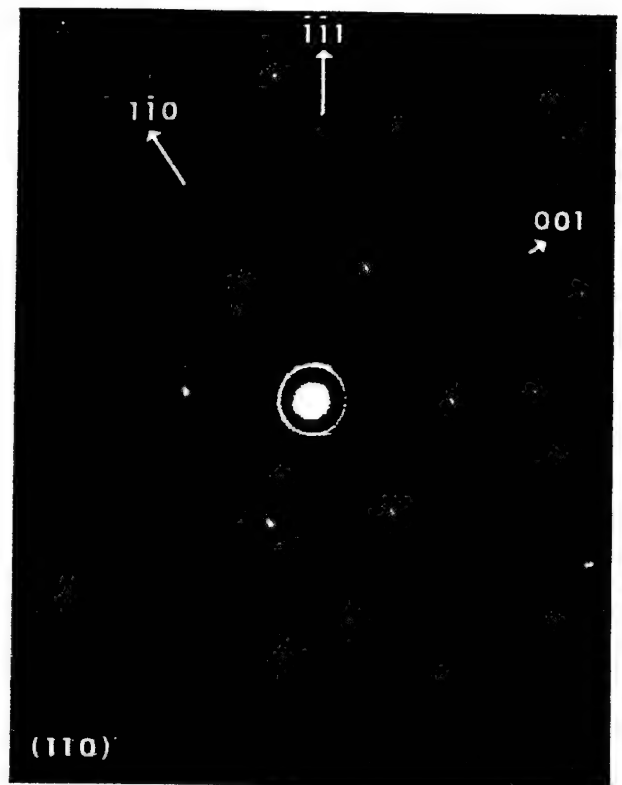

FIG. 3. Laue photograph of a single crystal SAT fiber with the x-ray beam hitting the crystal in a direction perpendicular to the growth direction at the cleavage plane.

as described in Sec. II. A. SAN and SAT single crystal fibers of ~500 μm in diameter and up to 3 cm in length (not limited) were grown using a pulling to feeding ratio of 1.5–2. All growths were performed in air. The stable molten zone temperatures during the crystal fiber growth were obtained using an optical pyrometer and were typically 1862 °C and 2030 °C for SAN and SAT, respectively, with an estimated accuracy of ±30 °C.

As-grown SAT and SAN crystals were both chemically reduced. The SAN fiber was dark gray due to the reduction of Nb^{5+} to Nb^{4+}. No clear facet was observed for SAN fibers 500 μm in diameter. As-grown SAT fiber showed a bluish color. Facets on SAT fibers ~500 μm in diameter can be seen. Figure 3 shows a Laue photograph of a single crystal SAT fiber with the x-ray beam approximately parallel to [110], normal to the cleavage plane, and hitting the crystal in the direction perpendicular to the growth direction. The crystal fiber growth direction was found to be along [$\bar{1}\,\bar{1}1$], 54° 44′ from the [001].

X-ray diffraction patterns, as shown in Fig. 4, revealed that the SAN and SAT crystal fibers grown by LHPG do not show B-site long range ordering (with only weak diffractions of the superlattice peaks), and as a result, have simple cubic symmetry. The crystallographic data for SAN and SAT single crystal fibers as determined by x-ray diffraction are a = 3.8995 Å, volume = 59.295 Å^3, Z = 1, and ρ = 5.4758 g/cm^3 (for SAN), and a = 3.8952 Å, volume = 59.109 Å^3, Z = 1,

and ρ = 6.7306 g/cm^3 (for SAT). Their cubic lattices closely match the high T_c superconductor YBCO that has an orthorhombic symmetry with lattice parameter b = 3.883 Å.[3]

The high temperature (disordered) phases existed to room temperature as the B-site orderings were inhibited during the fiber growth process because of the quenching effect produced by the high growth rates and steep axial temperature gradients employed in the LHPG growth. The high temperature disordered phases have not been reported previously in either SAN or SAT. The SAN fibers became colorless after annealing at 1630 °C for 10 h in air (no annealing effect was observed at 1000 °C for 24 h in flowing O_2). SAT became transparent after annealing in flowing O_2 at 1000 °C for 24 h. However, annealing treatments at these conditions did not cause significant or conclusive changes in the disorderedness of the structure as examined by x-ray diffraction. This observation suggested that their high temperature ideal cubic perovskite phases are stable.

C. Chemical composition analysis

Ceramic and single crystal SAN and SAT samples were analyzed quantitatively for their chemical compositions by using electron probe microscopic analysis
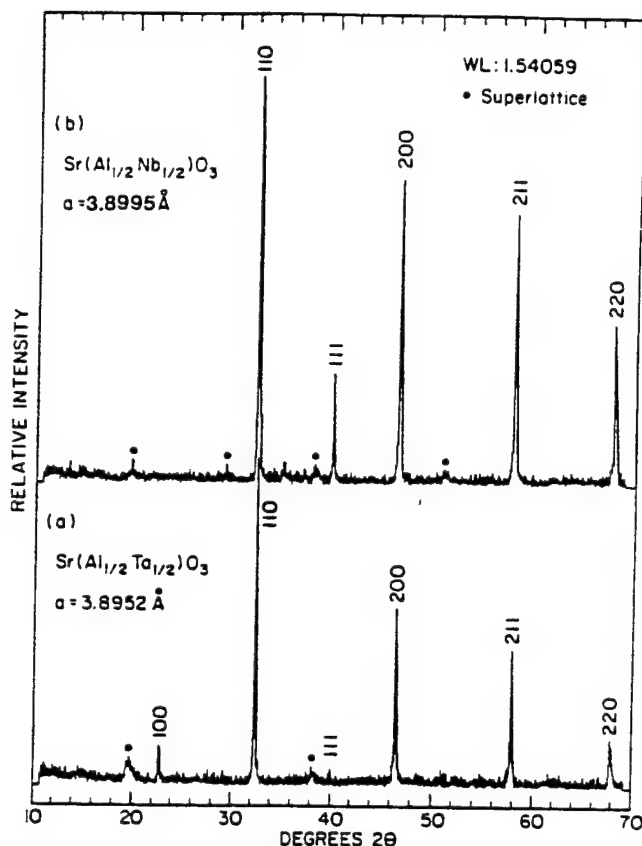
FIG. 4. X-ray (powder) diffraction patterns of single crystal: (a) SAT and (b) SAN.

(CAMECA, SX-50 with spatial resolution of 2 μm on surface area and 0.2 μm in depth). Relative analytic accuracy is $\pm 2\%$. Chemical analysis showed that the single crystals SAN and SAT grow congruently within the stoichiometric composition. The assigned composition of an as-grown SAT single crystal fiber was $Sr_{1.022 \pm 0.001} (Al_{0.496 \pm 0.001} Ta_{0.493 \pm 0.001})O_3$ and was uniform across the entire surface. As mentioned in the ceramic processing section, excess Al in the compound may cause formation of an intermediate phase $SrAl_2O_4$. Electron probe microscopic analysis detected $SrAl_2O_4$ grains in the SAT ceramic sample. It is evident from the microscope study that the $SrAl_2O_4$ phase (a hexagonal stuffed tridymite structure with $a = 5.10$ Å, $c = 8.49$ Å, mp ~ 1960 °C)[13] is formed before the densification temperature is reached as the $SrAl_2O_4$ grains are fully enclosed by SAT grains. Crystal fibers of SAT, however, are not affected by the intermediate phase as the growth zone temperature is higher than the melting temperature of the intermediate phase. Improvement in crystal quality is expected after the powder preparation process is modified to avoid the $SrAl_2O_4$ phase.

The composition of an as-grown SAN single crystal fiber was found to be $Sr_{0.931 \pm 0.006}(Al_{0.463 \pm 0.005} Nb_{0.550 \pm 0.004})O_3$, in comparison to the composition.

$Sr_{0.940}(Al_{0.477}Nb_{0.538})O_3$, found in the SAN ceramic sample. The reason for the off stoichiometry on the cation ratio for both the ceramic and single crystal samples is not yet clear; however, the congruent melting and growth behaviors were confirmed through the similarity between the ceramic sample and the crystal sample. Avoiding the formation of the intermediate $SrAl_2O_4$ phase in ceramics may be more important for improving the stoichiometry and quality of SAN single crystals than for SAT, because SAN crystals were grown at relatively lower temperatures.

D. Dielectric properties

Dielectric properties of the SAN and SAT samples were examined as functions of temperature and frequency. Table III summarizes the dielectric properties of high density SAN and SAT ceramic samples. Their dielectric constants as functions of temperature in the low frequency range and as functions of frequency at room temperature are shown in Fig. 5 and Fig. 6.

A dielectric constant as low as $11-12$ for the SAT sample is of special significance for substrate applications as, we believe, it is one of the lowest dielectric constants reported for the complex oxide perovskite family. It is the oxygen ionic polarizability that sets the baseline limitation to the dielectric polarizability in the oxide perovskite family. SAT, therefore, seems to be a special example in complex oxide perovskite compounds of cubic structure for further studies on polarization mechanisms.

More study on the effect of B-site ordering on various properties including dielectric properties is required. On the basis of our experimental results on another oxide perovskite, $Ba(Mg_{1/3}Ta_{2/3})O_3$,[14] the dielectric constant increases with the increase in the bulk density (does not strongly depend on the B-site ordering), while dielectric loss factor decreases with the enhancement in B-site ordering.

E. Thermal expansion behavior

Thermal expansion coefficients of SAN and SAT were measured and compared to the thermal properties of the YBCO superconductor. The measurement was carried out from room temperature up to about 800 °C by using a vertical push-rod dilatometer equipped with a high sensitivity linear variable differential transformer (LVDT). The heating and the cooling rates for thermal expansion measurements were regulated at 1 or 1.5 °C/min using a microprocessor-based temperature controller.

Good thermal expansion match was found in both SAT and SAN samples [the thermal expansion coefficients, $\alpha = 9.7 \times 10^{-6}/$°C (SAT) and $\alpha = 8.8 \times 10^{-6}/$°C (SAN)] compared to that of the YBCO

TABLE III. Dielectric properties of $Sr(Al_{1/2}Nb_{1/2})O_3$ and $Sr(Al_{1/2}Ta_{1/2})O_3$.

Composition	Room temperature				Low temperature, 77 K			
	10 kHz		Microwave (GHz)		10 kHz		Microwave	
	κ	$\tan \delta$ ($\times 10^{-4}$)	κ	$\tan \delta$ ($\times 10^{-4}$)	κ	$\tan \delta$ ($\times 10^{-4}$)	κ	$\tan \delta$ ($\times 10^{-4}$)
SAT (97% density)	11.8	16.8	10.7 (11.0 GHz)	3.64 (7.64 GHz)	11.8	0.42	⋯	2.09 (7.64 GHz)
SAN (92% density)	18.6	31.8	18.3 (9.61 GHz)	9.26 (6.08 GHz)	18.7	2.20	⋯	5.56 (6.08 GHz)

single crystals ($\alpha_a = 14$, $\alpha_b = 9$, and $\alpha_c = 19 \times 10^{-6}/°C$).[4] No structural phase transition was found in the measured temperature region. Figure 7 shows the average linear thermal strains of SAN, SAT, and YBCO ceramic samples as a function of temperature. Thermal property compatibility of the substrates with HTSC films is critical for epitaxial film growth, in terms of determining the deposition and annealing temperatures, possibility of producing thick films, and reducing the degradation process in films and devices under working conditions.
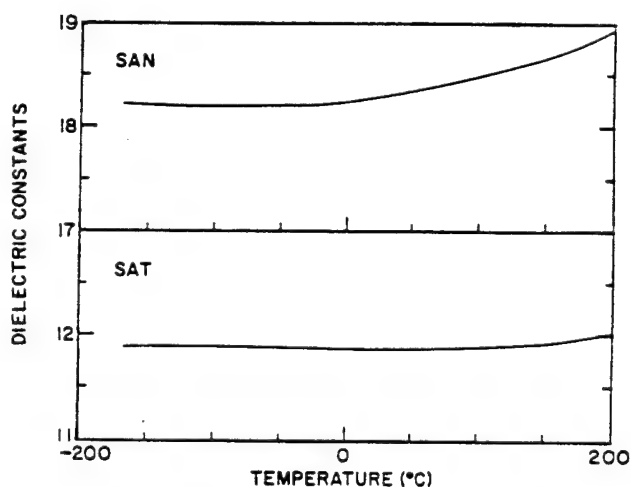

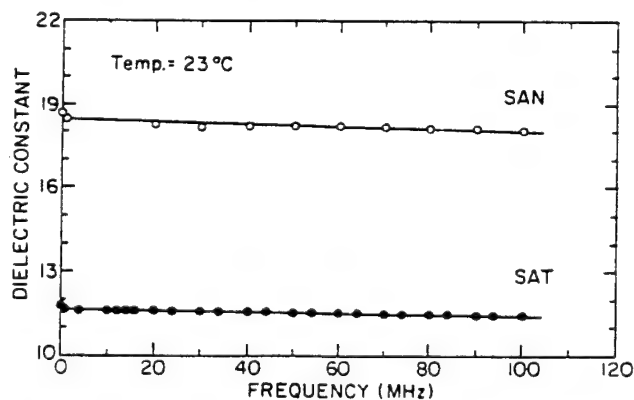FIG. 5. Dielectric constants of SAN and SAT ceramics at 10 kHz as functions of temperature.

FIG. 6. Dielectric constants of SAN and SAT ceramics as functions of frequency at room temperature.

F. Microhardness

Vickers hardness on the single crystals SAN and SAT grown by the LHPG technique was measured by using a Leitz Miniload Hardness Tester. The side of a single crystal fiber perpendicular to the fiber growth direction was ground and optically polished. The indentation diameter resulting from the diamond indenter was measured using a micrometer scale etched into the microscope eyepiece. Five indentations were measured for each different load (200 to 500 g), and the resulting values were averaged.

The Vickers hardness was calculated by a formula: $H_v(10^9 \ N/m^2) = 18.1854 \ P/d^2$, where P is the measuring force in grams and d is the mean value of the indentation diagonal in μm. Preliminary results of the microhardness measurements are given in Table IV. Comparative studies on the hardness were also performed under identical conditions on the single crystal Al_2O_3 and quartz, for those are well characterized for their high value of hardnesses. The literature values of their hardness are also given.

It is not surprising that both SAT and SAN have high values of hardness. High bonding strength in the ionic compounds and the small size of cations on both A- and B-sites may be responsible for these high values.

G. General comments

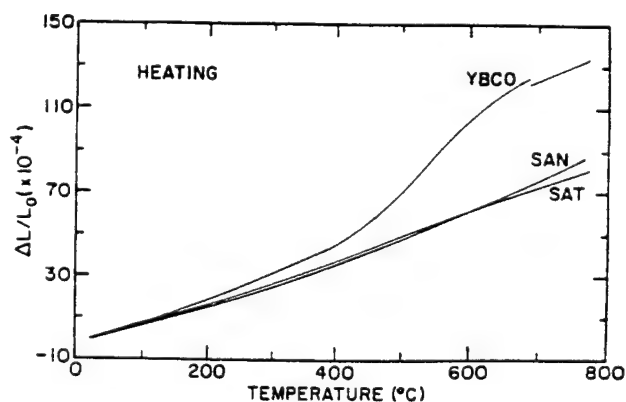Comparing SAN and SAT, it is interesting to notice the similarities and dissimilarities in the Nb- and Ta-

FIG. 7. Thermal strain measured by using a vertical push rod linear voltage differential transformer dilatometer.

J. Mater. Res., Vol. 10, No. 1, Jan 1995

23

TABLE IV. Vickers hardness data for $Sr(Al_{1/2}Nb_{1/2})O_3$ and $Sr(Al_{1/2}Ta_{1/2})O_3$ single crystals (on planes perpendicular to the growth direction).

Material	H_v (GPa) (averaged for $P = 0.2-0.5$ N)
SAT crystal fiber ($\perp$ growth direction)	15.1 ± 3.3
SAN crystal fiber ($\perp$ growth direction)	9.1 ± 1.2
Sapphire crystal fiber ($\perp c$)[20]	18.1 ± 2.1
Quartz ($\parallel c$)[20]	9.3 ± 1.2

compounds. In spite of all the similarities of SAN and SAT (e.g., identical structure type, similar lattice parameters, similar thermal expansion properties), there are a number of distinct differences between them. SAT has a higher melting temperature, higher hardness, lower dielectric constant, lower dielectric loss over broad ranges of temperature and frequency, and less reduction problem during growth. These differences between SAT and SAN are not unique to these two materials, but are common to all Nb-compounds and their analogous Ta-compounds. It is insufficient to explain the reason for those differences by, for instance, simply considering the bonding strength (as they have the same valence and coordination numbers), or on the basis of available ionic polarizability data[15] ($\alpha_i^{Ta^{5+}} = 4.73$ Å^3 and $\alpha_i^{Nb^{5+}} = 3.97$ Å^3 that would predict a lesser polarizability for SAN than SAT). It seems to us that the electronic structure differences may have caused the Ta–O bonding to be less ionic in nature and somehow enhanced the bonding strength. Detailed understandings and modeling are beyond the scope of this paper.

Considering all the suitable substrate requirements, SAT seems more desirable primarily due to its low dielectric constant. The drawbacks are the difficulty in crystal growth as SAT has higher melting temperature. The (110) cleavage plane in the SAT crystals does not seem to present a problem as cleavage is primarily determined by crystal structure and is only secondarily related to chemical composition.

Chemical compatibility of SAN and SAT substrates with YBCO was tested by spin coating YBCO films on SAN and SAT ceramic disks using the sol-gel technique.[16] No chemical interactions were observed, and the YBCO film formed was of good crystal quality with $T_c \sim 90$ K. Therefore, it is concluded that the chemical compatibility of SAN and SAT with YBCO is good.

We believe that further modification of the SAN and SAT compositions to fine tune their properties, particularly reducing their melting temperatures, will lead to easier fabrication of the crystals and better control of the reduction problem of the Nb^{5+} and Ta^{5+}. Work

following this direction will be the content of separate publications.

Using SAT polycrystalline materials as targets in a pulsed laser deposition process, Findikoglu *et al.*[17,18] have reported high quality epitaxial (c-axis orientation) growth of thin films of SAT and multilayers of YBCO/SAT on (001) $LaAlO_3$ and MgO substrates. Dielectric constants of the SAT films ($\sim100-390$ nm thick), however, were found to be $\sim23-30$, notably higher than the value ($\kappa \sim 12$) found in bulk ceramic materials. The deviations from perfect cation stoichiometry in the films may be one of the causes for the discrepancy in the value of the dielectric constants as the Al/Ta ratio in SAT films was found to be ~0.8 rather than the stoichiometric ratio of unity.[17,18] No dielectric loss data were reported for the SAT films; therefore, direct comparison between the dielectric constants of the film and the bulk SAT samples is not possible. The dielectric properties ($\kappa \sim 12$, tan $\delta \leq 10^{-3}$ at room temperature and 1 KHz) of SAT ceramic samples are reproducible. Consistent results have also been given by independent dielectric property measurements on the same SAT ceramic samples.[19]

IV. SUMMARY

We have investigated single crystals of $Sr(Al_{1/2}Nb_{1/2})O_3$ and $Sr(Al_{1/2}Ta_{1/2})O_3$ as substrate materials for epitaxial thin film fabrication of the high T_c superconductors. Single crystal fibers of SAN and SAT were grown using a laser-heated pedestal growth technique. Crystal structures, dielectric properties, thermal expansion properties, and hardness test results are reported. Both SAN and SAT are of ideal cubic perovskite structure with a lattice parameter in close match to YBCO and can be explored further for device applications. SAT currently represents one of the best potential HTSC substrate materials for microwave applications. The unique feature of this material is that it combines desired dielectric properties (dielectric $\kappa \sim 12$, loss factor tan $\delta < 10^{-4}$) at microwave frequencies with a twin-free lattice and good thermal expansion matching along with chemical compatibility.

ACKNOWLEDGMENTS

24

J. Mater. Res., Vol. 10, No. 1, Jan 1995

on Substrate Materials for High T_c Superconductors. Feb. 5–7, 1992, Williamsburg, VA.

REFERENCES

1. R. Guo, A. S. Bhalla, L. E. Cross, and R. Roy, J. Mater. Res. **9**, 1644–1656 (1994).
2. E. A. Wood, Am. Min. **36**, 768 (1951).
3. W. Wong-Ng, F. W. Gayle, D. L. Kaiser, S. F. Warkins, and F. R. Fronczek, Phys. Rev. B **41** (7), 4220 (1990).
4. H. You, U. Welp, and Y. Fang, Phys. Rev. B **43** (4), 3660 (1991).
5. R. J. Dinger and D. J. White, IEEE Trans. Antennas Propag. **38** (8), 1313 (1990).
6. C. D. Brandle and V. J. Fratello, J. Mater. Res. **5**, 2160 (1990).
7. J. S. Haggerty, W. P. Menashi, and J. F. Wenckus, *Method for Forming Refractory Fibers by Laser Energy,* U.S. Patent 3 944 640, March 16, 1976: *Apparatus for Forming Refractory Fibers,* U.S. Patent 4 012 213, March 15, 1977.
8. R. S. Feigelson, MRS Bull. **XIII**, 47 (1988).
9. J. Yamamoto and A. S. Bhalla, Mater Res. Bull. **24**, 761 (1989).
10. B. W. Hakki and P. D. Coleman, IEEE Trans. Microwave Theory Tech. **MTT-8**, 402 (1960).
11. D. C. Dube, M. T. Lanagan, J. H. Kim, and S. J. Jang, J. Appl. Phys. **63**, 2466 (1988).
12. F. Ganits, T. Yu. Chemekova, and Yu. P. Udalov, Zh. Neorg. Khim. **24** (2), 471 (1979); Russ. J. Inorg. Chem. (Engl. Transl.) **24** (2), 260 (1979).
13. F. P. Glasser and L. S. Dent Glasser, J. Am. Ceram. Soc. **46**, 377 (1963).
14. R. Guo, A. S. Bhalla, and L. E. Cross, J. Appl. Phys. **75** (9), 4704–4708 (1994).
15. R. D. Shannon, J. Appl. Phys. **73** (1), 348 (1993).
16. P. Ravindranathan *et al.,* unpublished results.
17. A. T. Findikoglu, C. Doughty, S. Bhattacharya, Qi Li, X. X. Xi, T. Venkatesan, R. E. Fahey, A. J. Stauss, and J. M. Phillips, Appl. Phys. Lett. **61**, 1718 (1992).
18. A. T. Findikoglu, S. Bhattacharya, C. Doughty, M. S. Pambianchi, Qi Li, X. X. Xi, S. M. Anlage, R. E. Fahey, A. J. Strauss, J. M. Phillips, and T. Venkatesan, IEEE Trans. Appl. Superconductivity **3** (1), 1425 (1993).
19. F. I. Mopsik, National Institute of Standards and Technology, private communication.
20. E. Breval, G. C. Dodds, and N. H. Macmillan, Mater. Res. Bull. **20**, 413 (1985).

J. Mater. Res., Vol. 10, No. 1, Jan 1995

25

Appendix 2.

"Design of Dielectric Substrates for HTS Films"

World Congress on Superconductivity, Poland (in printing, 1996)

Ruyan Guo

A.S. Bhalla

DESIGN OF DIELECTRIC SUBSTRATES FOR HTS FILMS

Amar Bhalla and Ruyan Guo

Materials Research Laboratory, The Pennsylvania State University
University Park, PA 16802 USA

ABSTRACT

Investigations on the design and engineering of candidate substrate materials suitable for HTS thin film deposition and applications have yielded several exciting new hosts such as $Ba(Mg_{1/3}Ta_{2/3})O_3$, $Sr(Al_{1/2}Ta_{1/2})O_3$, and $Sr(Al_{1/2}Nb_{1/2})O_3$. Dielectric properties, thermal expansion coefficients, melting temperatures and growth feasibility were tested for a wide range of substrate materials and solid solutions. These complex perovskite crystals and their associated solid solutions provide new options for ultra low loss, low permittivity substrates with close structural and thermal matching to the YBCO. Several new materials have been tested for HTS film depositions. A laser heated pedestal growth system (LHPG) has been used as an essential tool in producing single crystals for testing. Development on the predictive capability of the dielectric constant of ionic solids, by improving Shannon's approach, will also be discussed in this paper.

INTRODUCTION

The selection of useful substrate materials for the deposition of high Tc superconductors is of prime importance and is subjected to a number of constraints. In several microwave applications of the 'ceramic dielectric substrates,' important considerations have been given to the (a) materials' thermal properties such as thermal expansion and thermal conductivity, and (b) the electrical characteristics such as low dielectric loss, dielectric constants and dielectric coefficient with temperature, The main heart of the selection criteria are intended for the speed (in MCM devices) and the reduction of thermal effects on the signals. In case of the resonators the values of the

1

constants are adjusted with the size of the required device. If we look for HTS uses in such applications, the additional requirements from the substrates are demanded. For example additional crystallographic matching parameters are required to deposit high quality oriented (preferably epitaxial) and hence high Jc high temperature superconducting films on the single crystal substrates. These parameters are summarized in Table I.

Table I. Dielectric Property Requirements for HTS Substrates

	Multi-Chip-Modules (MCM)	Millimeter Wave Devices
Applications	Digital receivers, IR detectors, High performance computers	Oscillators; Frequency discriminators; Phase shifters; Delay lines; etc.
Requirements	High speed, $v \propto 1/(\kappa)^{1/2}$ Satisfy characteristic impedance $1/Z \propto (W/d)(\kappa)^{1/2}$; High packing density (thinner film); Low crosstalk (thinner film)	Narrow bandpass filters (high Q); Low temperature coefficient of capacitance; Compact designs (moderate κ values).
Dielectric Constant	$\kappa \sim 20$ or less is acceptable; however, for film thickness $d \sim 1\mu m$, $\kappa < 10$ is required.	κ 20~25 desirable.
Dielectric Loss	$\tan\delta < 10^{-3}$ to maintain the dielectric loss much lower than the conductor loss.	Ultra low loss, $\tan\delta < 10^{-4}$ (Q>10,000).
Type of Substrates	Single crystal films (2μm) in multi-layer integrated structure with HTSC films.	Single crystal substrates 3" or 4" in diameter.

Numerous candidate materials have been suggested for such purposes to achieve useful HTS based devices. The most widely used candidate has been the crystals of $LaAlO_3$. The serious problem of ferroelastic twinning in this material affects the quality of HTS film and the device performance.

An additional factor, i.e., thermal expansion should also be considered rather seriously in selection of the single crystal substrate materials for HTS. In this case, the films are deposited and oxidized at $\cong 500°C$ and the devices operate at liquid nitrogen temperatures. Therefore, for the less aging effects and high performance of the device point of view, thermal expansion matching over the temperature range from the deposition temperature to the operating liquid nitrogen are highly recommended.

Recently, several new materials have been suggested and are being tested. Our goal has been to design and develop new highly suitable substrates which are better than that of

LaAlO$_3$ and thus the consideration for the development was based on the approach illustrated in Figure 1. After a systematic structure-property relationship several promising new hosts such as Sr(Al$_{1/2}$Ta$_{1/2}$)O$_3$, Sr(Al$_{1/2}$Nb$_{1/2}$)O$_3$, and Ba(Mg$_{1/3}$Ta$_{2/3}$)O$_3$ in complex oxide perovskite family have been developed and summarized in this paper.

In order to broaden the family of materials from which the candidates with broad range of dielectric properties can be selected for various microwave applications, an ion polarizability additivity rule (based on R.D. Shannon's model) was applied to predict the dielectric constant of large number of suitable HTS substrates and the values are compared in some cases with the measured values (of dielectric constants).
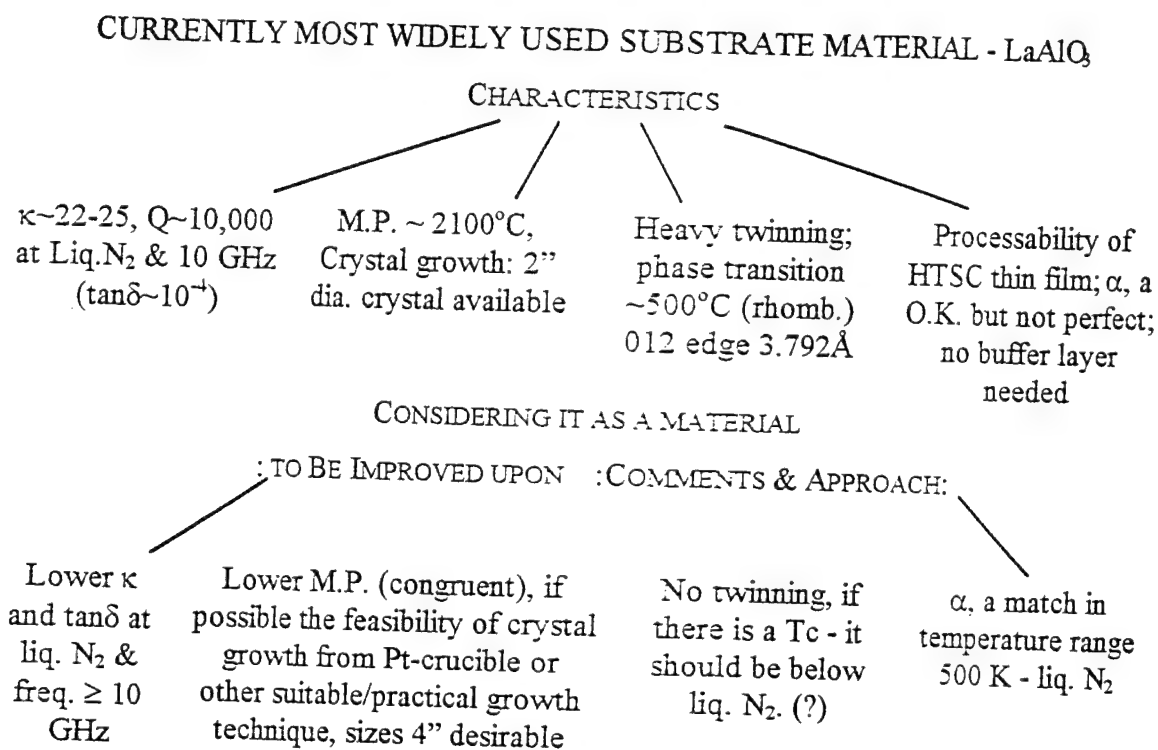
CURRENTLY MOST WIDELY USED SUBSTRATE MATERIAL - LaAlO$_3$

CHARACTERISTICS

$\kappa \sim 22-25$, Q$\sim$10,000 at Liq.N$_2$ & 10 GHz (tan$\delta \sim 10^{-4}$)

M.P. $\sim 2100°$C, Crystal growth: 2" dia. crystal available

Heavy twinning; phase transition $\sim 500°$C (rhomb.) 012 edge 3.792Å

Processability of HTSC thin film; α, a O.K. but not perfect; no buffer layer needed

CONSIDERING IT AS A MATERIAL

:TO BE IMPROVED UPON   :COMMENTS & APPROACH:

Lower κ and tanδ at liq. N$_2$ & freq. ≥ 10 GHz

Lower M.P. (congruent), if possible the feasibility of crystal growth from Pt-crucible or other suitable/practical growth technique, sizes 4" desirable

No twinning, if there is a Tc - it should be below liq. N$_2$. (?)

α, a match in temperature range 500 K - liq. N$_2$

Figure 1. The approach to replace or modify one of the most widely used substrate material - LaAlO$_3$.

EXPERIMENTAL APPROACH AND RESULTS

CRYSTALS OF COMPLEX OXIDE PEROVSKITE COMPOUNDS

Ceramic samples were prepared by solid state reaction, using conventional techniques. X-ray diffraction technique was used extensively to characterize the crystallographic phases and to adjust the processing conditions. The laser heated molten zone growth

method has been shown to be a powerful method for rapidly growing small diameter single crystals, particularly oxides of high melting temperature, for both property studies and fiber devices.[1,2,3] The LHMZ equipment used in this investigation consisted of a power source (water cooled, tunable flowing gas CO_2 55W laser), an optical layout, and a growth section. The molten zone temperature during a stable growth was monitored using an optical pyrometer.

Radio frequency dielectric constants and the loss tangent were measured using a General Radio 1621 Capacitance Measurement System. Dielectric properties at microwave frequency were measured using resonance techniques equipped with an HP8510A network analyzer. Post resonance technique (the Hakki and Coleman technique) was used to measure the dielectric constants of the ceramic samples. Cavity perturbation technique was used for the measurements on samples of thin rod (e.g., single crystal fiber samples) or bar-shaped. The Q factors (of microwave frequency) at liquid nitrogen temperature were measured by a transmission resonance technique.

$Ba(Mg_{1/3}Ta_{2/3})O_3$ (BMT)

Ceramics of complex perovskite oxides $A(B1_{1/3}B2_{2/3})O_3$ type have been explored previously as the candidate materials with excellent microwave dielectric properties.[4] $Ba(Mg_{1/3}Ta_{2/3})O_3$ (BMT), in particular, was reported to have a dielectric constant $\kappa \sim 25$ and dielectric $Q \sim 16,800$ (one of the highest in the oxide family) at 10.5 GHz, in samples with 1 mol% Mn additive as a sintering aid.[5] BMT compound is one of the most refractory oxides known thus the growth of single crystals is difficult. A single crystal of BMT was grown from a BaF_2 flux. It yielded a significantly higher dielectric constant (~ 200),[6] presumably attributable to the flux contamination.

BMT single crystal fibers were grown successfully using our LHMZ technique. It grows congruently from the melt in the temperature range of 2900-3100°C. A high temperature phase of simple cubic perovskite was obtained at room temperature, in comparison to the hexagonal ordered perovskite structure usually obtained in ceramics (see Fig. 2). Dielectric properties of both the ceramic and the single crystal BMT were studied. BMT ceramic samples have ultra low dielectric loss ($<1 \times 10^{-5}$ at 90K and 10kHz)

4

and good thermal compatibility ($\alpha \sim 9.0 \times 10^{-6}/^{\circ}C$) with the YBCO superconductors. The single crystal BMT has a cubic lattice parameter a=4.0877Å. The dielectric constant increases and saturates as the bulk density approaches the theoretical density. Dielectric loss reduces with the enhancement of the ordering of the B-site. Single crystals of high temperature disordered cubic form preserve a moderate dielectric constant (26.0 at 10GHz) and low dielectric loss tanδ (2.78×10^{-4} at room temperature and 10kHz and $<10^{-5}$ at 90K) that make this material unique for microwave device applications.

The BMT lattice parameter of a=4.0877Å, represents a lattice mismatch of 5.3% to the b-axis of YBCO (b=3.883Å); this seems less ideal as a substrate for YBCO. However, there has been no clear cut-off for lattice parameter matches for "epitaxial" (or highly oriented) film deposition of YBCO. "Epitaxial" YBCO thin films on MgO single crystals (with mismatch of 8.5%) have been reported. A BMT single crystal has a twin-free cubic perovskite structure that is advantageous as a substrate compared to some of the heavily twinned substrates, e.g., LaAlO$_3$ and NdAlO$_3$. High temperature BMT single crystal grown by LHMZ is twin free, of moderate dielectric constant, low dielectric loss, and good thermal expansion matching and is therefore identified to be a potentially suitable substrate for the HTSC thin film deposition.

The application of BMT as a substrate, beside its fiber crystals' applications for microwave antenna, may be restricted by the fact that single crystals are difficult to grow. Skull melting growth techniques,[8] could presumably be used to grow BMT crystals of adequate sizes. The high melting temperature of BMT will not be a crucial issue, when the material is used as an insulating layer between the YBCO films in a multichip-module type of integrated structure, because vapor phase deposition techniques (e.g., laser ablation and metal-organic chemical vapor deposition) rather than liquid phase growth methods will be utilized.

Sr(Al$_{1/2}$Ta$_{1/2}$)O$_3$ (SAT) and Sr(Al$_{1/2}$Nb$_{1/2}$)O$_3$ (SAN)

The compounds of Sr(Al$_{1/2}$Ta$_{1/2}$)O$_3$ (SAT) and Sr(Al$_{1/2}$Nb$_{1/2}$)O$_3$ (SAN) were first prepared and tested to learn their crystallographic phases and melting behavior by the group at the AT & T Bell Labs.[9] Ceramic samples were identified to have double cell

cubic perovskite structure with a=7.795Å and melting temperatures of 1900°C and 1790° C for SAT and SAN, respectively. On the basis of our understandings of the crystal chemistry-dielectric property relation of various oxide perovskites, and the reports by the Bell Labs group that showed both the SAN and SAT melt congruently and produce a single phase of the perovskite structure after melting, we selected the SAT and SAN as primary candidates in the $A(B1_{1/2}B2_{1/2})O_3$ complex oxide perovskite family for crystal growth and to investigate their properties in relation to substrate applications.

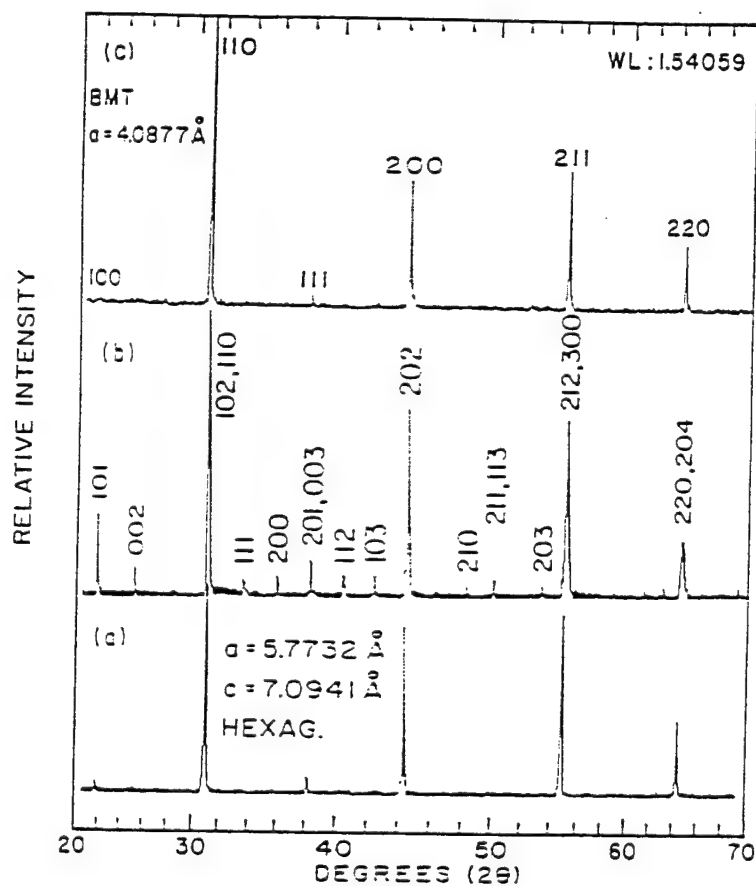Fig. 2. Typical x-ray diffraction pattern of $Ba(Mg_{1/3}Ta_{2/3})O_3$: (a) ceramic powder calcined at 1500 °C for 3 h showing weak ordering; (b) ceramic sintered at 1655 °C for 5 h showing strong B-site ordering; and (c) single crystal (powder) grown by LHMZ showing an ideal simple cubic perovskite structure with a=4.0877 Å. BMT ceramic XRD patterns are indexed as a hexagonal perovskite structure with a=5.7731(6) Å and c=7.0941(2) Å.

$Sr(Al_{1/2}Ta_{1/2})O_3$ (SAT) and $Sr(Al_{1/2}Nb_{1/2})O_3$ (SAN) are grown using the LHMZ growth technique. Their crystallographic structures are found to be simple cubic perovskite with lattice parameters a=3.8952Å (SAT) and a=3.8995Å (SAN) that are of close lattice matching to the YBCO superconductors. No structural phase transitions or twins have been found and the average coefficients of the thermal expansion are in good matching with the YBCO superconductor materials. SAT currently represents one of the best potential HTSC substrate materials for microwave applications. The unique feature of this material is that it has desired dielectric properties (dielectric $\kappa \sim 12$, loss factor $\tan\delta < 10^{-4}$) at the microwave frequencies with twin-free lattice and good thermal expansion matching along with chemical compatibility with the YBCO superconductors. Dielectric constants in RF region as measured on the dense ceramic samples of SAT and SAN at 23°C are shown in Fig.3.

Our experimental results on the SAT composition (first reported at the Office of Navel Research Workshop on Substrates for HTSC, Williamsburg, VA, 1992) along with the earlier report on the congruent melting nature of the SAT and SAN compounds, have stimulated research works in the thin film area. MOCVD-derived SAT films grown at 850 °C on $LaAlO_3$ were found to have exclusively (001) growth with in-plane orientation.[10] Using SAT polycrystalline materials as targets in a pulsed laser deposition process, Findikoglu et al.[11,12] have reported high quality epitaxial (c-axis orientation) growth of thin films of SAT and multilayers of YBCO/SAT on (001) $LaAlO_3$ and MgO substrates. Dielectric constants of the SAT films ($\sim 100-390nm$ thick), however, were reported to be $\sim 23-30$, notably higher than the value ($\kappa \sim 12$) found in bulk ceramic materials. The deviations from perfect cation stoichiometry in films may be one of the causes for the discrepancy in value of the dielectric constants as the Al/Ta ratio in SAT films was found to be ~ 0.8 rather than the stoichiometric ratio of unity.[12,13] No dielectric loss data has been reported for the SAT films therefore direct comparison between the dielectric constants of the film and that of the bulk SAT sample is not intended.

SOLID SOLUTION OF TERNARY AND COMPLEX PEROVSKITE OXIDES

Further modification of the SAN and SAT compositions has been carried out to fine tune their properties, particularly reducing their melting temperatures (SAT:

1900~(1908±25)[9], and SAN:1790~(1739±10)[9])[13] for easier fabrication of the crystals and better control of the reduction problem of the Nb^{5+} and Ta^{5+}. This modification was also an attempt to overcome the twinning problem and to stabilize the cubic phase at room temperature in $LaAlO_3$ crystals.
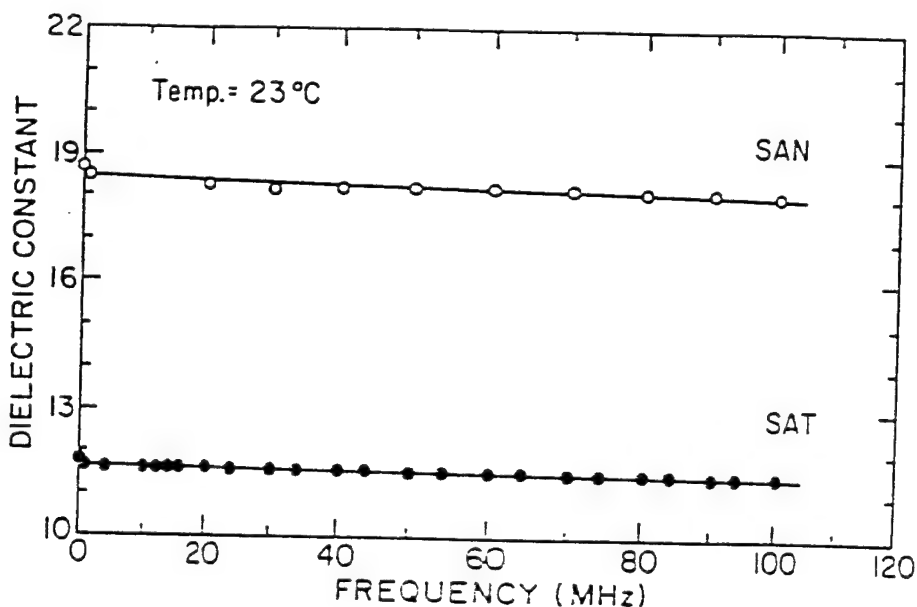

Fig. 3. Dielectric constants of SAT and SAN ceramics as functions of frequency at room temperature.

LaAlO$_3$ has a rhombohedrally distorted perovskite ($A^{3+}B^{3+}O_3$ type) structure. Although the La^{3+} ion generally prefers the 12-coordination-site, it has a tendency for 9-coordination. The distortion in the LaO_{12} polyhedron is brought about by a slight displacement of the oxygen atoms away from the ideal positions of the cubic perovskite form, that is more clearly shown in other [rear-earth]$^{3+}AlO_3$ family members when the A-site cation radii become even smaller, e.g., in the case of PrAlO$_3$.[14, 15] Fig. 4 presents a classification of [A]$^{3+}$[B]$^{3+}O_3$ type compounds according to the constituent ionic radii (8-coordination cation radii were used for A-site cations) focusing on the perovskite region. In fact, no ideal cubic perovskite structure but the rhombohedral [LaAlO$_3$] and the orthorhombic [GdFeO$_3$] structure have been reported in ternary compounds of the [A]$^{3+}$[B]$^{3+}O_3$ type.[16] For aluminate compounds, rhombohedral symmetry is found when

A-site is occupied by the largest A^{3+} cation, La^{3+}, and other $[A]^{3+}[Al]^{3+}O_3$ compounds have even lower symmetry

Our approach following this direction was to introduce "balanced" cation substitution simultaneously in the A- and B-sites to increase the average cation size at the A-site, hence to stabilize the 12-coordination of that position and consequently the cubic perovskite structure. The solid solution of ternary $LaAlO_3$ and complex oxides of $Sr(Al_{1/2}Ta_{1/2})O_3$ or $Sr(Al_{1/2}Nb_{1/2})O_3$ was chosen for investigation.

By forming crystalline solutions with compounds of low melting temperatures, it was expected that the crystalline solution would result in lower melting temperature and consequently avoid the reduction problem and permit growth in platinum crucibles. $NdGaO_3$ was found to have a melting temperature of $\sim 1484 \pm 24°C$, and it was therefore selected as an end member of the crystalline solution series with SAT and/or SAN for the present studies. $NdGaO_3$ has the $[GdFeO_3]$ structure with orthorhombic symmetry. No twinning problems are reported in this material. YBCO thin films deposited on $NdGaO_3$ were of better quality compared to those deposited on $LaAlO_3$ substrates. However, the high dielectric loss in the $NdGaO_3$ is a limiting factor for the YBCO film applications in microwave devices.

Single crystal fibers of modified strontium aluminum tantalum oxide $(1-x)Sr(Al_{1/2}Ta_{1/2})O_3{:}xLaAlO_3$ (SAT:LA) and $(1-x)Sr(Al_{1/2}Ta_{1/2})O_3{:}xNdGaO_3$ (SAT:NG), and modified strontium aluminum niobium oxide $(1-x)Sr(Al_{1/2}Nb_{1/2})O_3{:}xNdGaO_3$ (SAN:NG) and $(1-x)Sr(Al_{1/2}Nb_{1/2})O_3{:}xLaAlO_3$ (SAN:LA) were grown using a laser heated molten zone growth technique.[17] 0.7SAT:0.3LA grows congruently and remains twin free simple cubic perovskite structure (as the SAT) when cooled down to room temperature. 0.7SAT:0.3LA crystals have moderate dielectric constant ($\kappa = 21.7$) and low dielectric loss ($\tan\delta = 7.5 \times 10^{-5}$) at 10 kHz and 90K. The reduction problem of Ta^{5+} is eliminated (which is common in the case of SAT growth). 0.7SAT:0.3NG and 0.7SAN:0.3NG have lower melting temperatures and crystal growth is easier. $NdGaO_3$ addition to the SAT and SAN enhances the potential of SAT and SAN as large area substrates for HTSC growth. However, the dielectric

constants increased from κ~12 to κ~16 (0.7SAT:0.3NG) and from κ~18 to κ~23 (0.7SAN:0.3NG) as a result of NdGaO$_3$ incorporation.
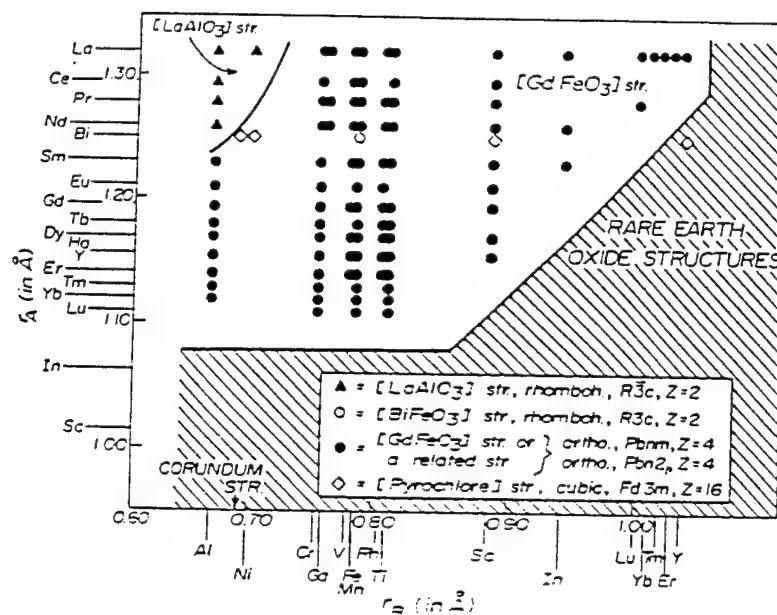

Fig. 4. Structure field map for $[A]^{3+}$-$[B]^{3+}$O$_3$ type compounds (ref. 15).

Our results further confirmed the report of Mateika et al.[13,19] that the ideal cubic phase can be formed in (La,Sr)(Al,Ta)O$_3$ compounds. It is interesting to notice that similar substitutions using [Ca,Ta] instead of [Sr,Ta] did not produce a compound with cubic structure. The average A-site cation radii of the [Ca,Ta] substitution is smaller than that of LaAlO$_3$ (ionic radii of Ca^{2+}, La^{3+}, and Sr^{2-} are 1.14, 1.185, and 1.27Å, respectively),[20] therefore, no stabilization effect on 12-coordination A-site is expected.

The cubic symmetry for the compound of SAT-NG and SAN-NG may be due to the fact that Ga^{3+} is almost of the same cation size as Ta^{5+}/Nb^{5+}. Slight reduction in the A-site cation size is accompanied by the slight increase of the B-site cation size and thus the cubic structure of SAN or SAT stays intact.

The ideal cubic perovskite structure can be stabilized in the case of ternary LaAlO$_3$ by forming a crystalline solution composition with cubic Sr(Al$_{1/2}$Ta$_{1/2}$)O$_3$ and Sr(Al$_{1/2}$Nb$_{1/2}$)O$_3$. The mechanism of this type of stabilization is through introducing the

10

compensated cation substitution in the form of $[2La^{3+}]+[Al^{3+}] \rightarrow [2A^{2+}]+[B^{5+}]$ with the A^{2+} cation having a radius larger than that of La^{3+} and therefore stabilizing the 12-coordinated A-site. Crystalline solutions of SAT-LA maintained or improved most of the dielectric and thermal properties of $LaAlO_3$ and gained the advantage of forming a twin-free simple cubic structure and improved lattice compatibility. $NdGaO_3$ is shown to be an effective end member to decrease the melting temperature of SAN and SAT without disturbing their simple cubic (twin-free) crystal structure. Dielectric constants of SAN and SAT with addition of the $NdGaO_3$ were increased; however, the dielectric loss factor still remained less than $5x10^{-4}$. The results suggesting that SAT-LA and SAN-LA are better candidates as substrate materials than $LaAlO_3$ because the latter is intrinsically twinned. The growth of SAT-NG and SAN-NG are comparatively convenient as they have relatively low melting temperatures together with the relatively lower dielectric constants and the ideal lattice constants and thermal compatibility with the YBCO superconducting materials.

Other substrate candidates such as $La(Mg_{2/3}Ta_{1/3})O_3,$[21] $La(Mg_{1/2}Ti_{1/2})O_3,$[22] $(Ca,Sr)(Ga,Nb)O_3$[23] and a family of materials of the magnetoplumbite structures[24] have also been fabricated and their dielectric properties studied. These crystals and their associated solid solutions provide several new options for ultra low loss, low permittivity, twin free oxides with low congruent melting temperature, matching thermal expansion and excellent chemical compatibility.

PREDICTION OF THE DIELECTRIC CONSTANTS OF IONIC MATERIALS

An ion polarizability additivity rule (R.D. Shannon)[25] was applied to calculate the dielectric constants of a large family of substrate materials (for HTS films) and to compare with the measured dielectric constant values.

The macroscopic dielectric constant and the molecular polarizability are connected through the Clausius-Mosotti relation:

$$\alpha_D = \frac{3}{4\pi} V_m \frac{\kappa-1}{\kappa+2}$$

(1)

where α_D is the dielectric polarizability and V_m is the molar volume in $Å^3$. Much of the effort in this field has been, rather than trying to resolve the local field of each complex

substance, to utilize the increasing pool of dielectric polarizabilities of substances with various compositions and structures. Dielectric polarizabilities and hence the dielectric constants of new materials/compounds whose dielectric constants have not been measured are potentially predictable by linear addition of the molecular polarizabilities of simpler substances (molecular polarizability additivity rule)[26,27,28] or ion polarizabilities of individual ions (ion polarizability additivity rule).[29,28] Review and comments about the application of polarizability additivity rules can be found in Shannon's paper.[25]

The calculation results using Shannon's ion polarizability data[25] (Table III, second column) and the ion polarizability additivity rule are shown in Table II. Comparison of the calculated and experimental molar polarizability and dielectric constants are tabulated. All the materials chosen for this study could be effective substrates for HTSC thin films. Some materials which appeared in Shannon's database or calculation are also included for the sake of completeness. Most of the structural data, symmetry parameters and the molar volume (V_m), are reasonably well established and the refined single crystal structure information used may be found in The Inorganic Crystal Structure Database (ICSD).[30] Crystal structures and the molar volumes of new substrate materials are determined on available single crystal samples (grown by a laser heated pedestal growth technique) by x-ray diffraction. Ceramic samples of new substrate materials are also used, only for those well sintered samples having high density and cubic or pseudocubic symmetries. The experimental value of the dielectric constants were taken from Shannon's database wherever available, otherwise were our measurement results. Dielectric constants of new substrate materials are measured using a high precision capacitance measurement system (Gen Rad 1621) in frequency range 10^3-10^5 Hz at room temperature and resonance technique or cavity perturbation techniques at the microwave frequencies (GHz). Details regarding the synthesis, preparation, and properties of new substrate materials may be found in the referred publications.
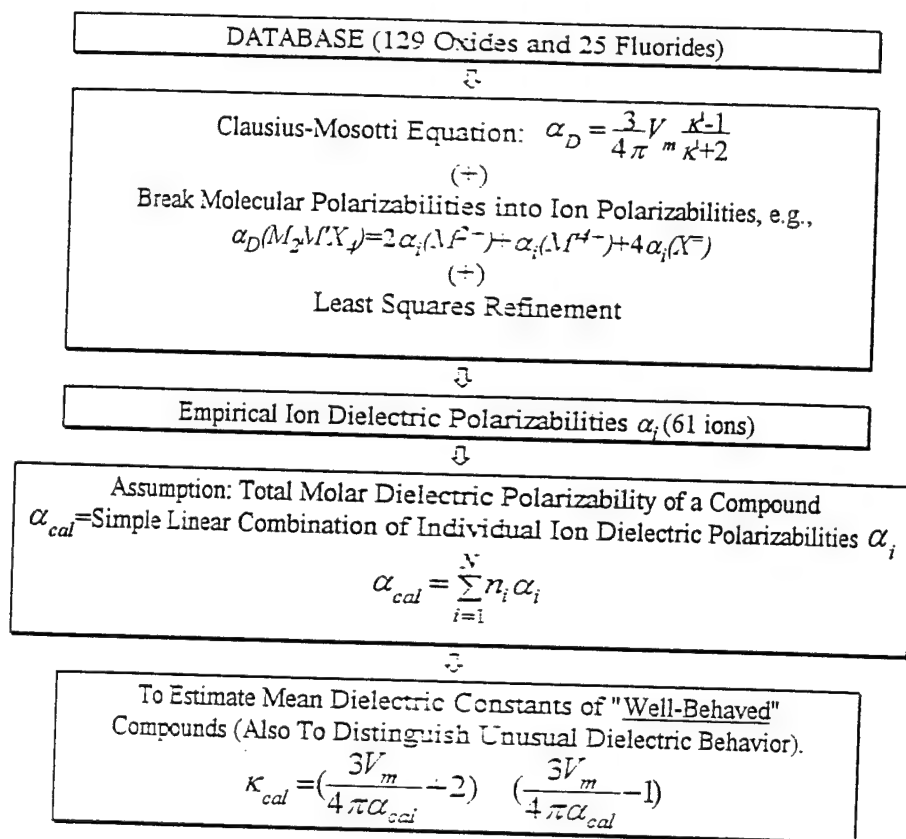
12

DATABASE (129 Oxides and 25 Fluorides)

Clausius-Mosotti Equation: $\alpha_D = \frac{3}{4\pi} V_m \frac{\kappa-1}{\kappa+2}$

($\div$)

Break Molecular Polarizabilities into Ion Polarizabilities, e.g.,

$\alpha_D(M_2MX_4) = 2\alpha_i(M^-) + \alpha_i(M^{4-}) + 4\alpha_i(X^=)$

($\div$)

Least Squares Refinement

Empirical Ion Dielectric Polarizabilities α_i (61 ions)

Assumption: Total Molar Dielectric Polarizability of a Compound α_{cal}=Simple Linear Combination of Individual Ion Dielectric Polarizabilities α_i

$$\alpha_{cal} = \sum_{i=1}^{N} n_i \alpha_i$$

To Estimate Mean Dielectric Constants of "Well-Behaved" Compounds (Also To Distinguish Unusual Dielectric Behavior).

$$\kappa_{cal} = (\frac{3V_m}{4\pi\alpha_{cal}} + 2) \quad (\frac{3V_m}{4\pi\alpha_{cal}} - 1)$$

Figure 5. Schematic approach of the ion polarizability additivity rule applied by Shannon.[1]

Several observations on the results listed in Table II are worth mentioning for further discussions. First, it is strikingly apparent that small discrepancies in molar polarizability can many times cause large discrepancies in dielectric constant prediction that indicates the V_m value in dielectric constant prediction plays a significant role. Second, good agreements are usually seen in case of substances containing cations having high valence and small sizes, while large discrepancies are common in ternary systems that involve large cations in high coordination sites. Third, poor agreements are found in materials containing Nb or Ta ions such as $Ba(Mg_{1/3}Ta_{2/3})O_3$, $Sr(Al_{0.5}Ta_{0.5})O_3$, and $Sr(Al_{0.5}Nb_{0.5})O_3$ and cations of rare-earth family such as $LaAlO_3$.

Table II. Comparison of Calculated and Experimental Dielectric Constants Using Ion Polarizability Additivity Rule.[1]

Substance	Space Gr. or Sym.	V_m	κ'_{exp}	κ'_{cal}	$\Delta\alpha\%$
Al_2O_3	R3ch	42.45	9.34, 9.34, 11.54	10.05	0.06
CaF_2	Fm3m	40.75	6.81	6.77	0.23
MgO	Fm3m	18.68	9.65	9.86	-0.61
Ba_2YSbO_6	Cubic	139.53	25.0	23.71	0.63
$Sr(Ga_{.5}Ta_{.5})O_3$	Cubic	61.58	26.9	31.54	-1.60
MgF_2	P42/mnm	32.40	5.50	5.31	1.73
$(Sr_{0.5}Ca_{0.5})(Ga_{0.5}Nb_{0.5})O_3$	Cubic	58.64	32.0	25.41	2.32
SiO_2 (quartz syn)	P6222	39.37	4.42, 4.41, 4.6	4.26	3.10
$Zr_{0.72}Y_{0.28}O_{1.862}$	Pm3m	34.35	29	21.43	3.60
$BaZrO_3$	P23	73.10	43.0	27.59	3.72
$NdGaO_3$ (NG)	Pbn21	57.68	20-25	31.66	-3.80
$CaYAlO_4$	Tetra	79.85	21.44,21.44,16.12	15.54	3.80
1/3SAN-1/3SAT-1/3NG	Cubic	63.30	22.8	17.13	4.08
$Nd_{.39}Sr_{.61}Al_{.695}Ta_{.305}O_3$		56.76	24.04	39.20	-4.79
$La(MgAl_{11})O_{19}$	Hex	296.86	13.50	10.81	5.03
$GdAlO_3$		51.87	19.50	29.17	-5.03
$LiBaF_3$	Cubic	63.40	11.71	14.98	-5.40
$0.7Sr(Al_{.5}Nb_{.5})O_3-0.3NdGaO_3$	Cubic	63.30	23.50	16.06	5.49
$0.7Sr(Al_{.5}Nb_{.5})O_3-0.3LaAlO_3$	Cubic	63.28	25.90	17.02	5.63
$SrLaAlO_4$	Tetra	38.99	16.70,16.70,20.02	23.30	-6.19
$Sr(Al_{.5}Nb_{.5})O_3$ (SAN)	Cubic	59.09	17.30	27.08	-6.19
$KMgF_3$	Pm3m	63.00	5.98	6.97	-6.66
$KZnF_3$	Pm3m	66.70	8.85	7.20	6.85
$0.7Sr(Al_{.5}Ta_{.5})O_3-0.3LaAlO_3$	Cubic	53.08	21.9	45.52	-7.08
$La(Mg_{2/3}Ta_{1/3})O_3$	Hex	74.33	24.1	14.56	7.30
$Nd(MgGaAl_{10})O_{19}$	Hex	296.50	14.9	10.60	7.37
$0.7Sr(Al_{.5}Ta_{.5})O_3-0.3LaAlO_3$	Cubic	57.89	21.9	47.94	-7.44
$PrAlO_3$	R3-mr	53.25	25.0	64.81	-7.45
$SmAlO_3$	Pbnm	52.30	19.0	38.53	-8.03
$BaSnO_3$	P23	69.40	18.0	36.06	-8.37
$LaGaO_3$	[$GdFeO_3$]	59.10	25.0	81.33	-8.45
$(Ba_{0.8}Sr_{0.2})(Mg_{1/3}Ta_{2/3})O_3$	Cubic	67.48	25.9	91.67	-8.46
$(Ba_{0.9}Sr_{0.1})(Mg_{1/3}Ta_{2/3})O_3$	Cubic	67.84	25.3	123.65	-9.66
$CaGa_{12}O_{19}$	Hex	301.48	9.70	15.12	-9.83
$Ba(Mg_{1/3}Ta_{2/3})O_3$	Hex	68.59	24.6	138.91	-10.31
$La(Mg_{.5}Ti_{.5})O_3$	Cubic	60.10	26.5	355.40	-10.83
$NdAlO_3$	R3ch	52.80	17.50	46.89	-10.93
$CaGa_6Al_6O_{19}$	Hex	302.00	18.2	10.72	11.43
$0.7Sr(Al_{.5}Ta_{.5})O_3-0.3NdGaO_3$	Cubic	57.90	16.3	42.22	-11.49
$LaAlO_3$	R3mr	54.40	23.8	406.86	-10.96
$YAlO_3$	P63/mmc	61.69	16.83,16.83,15.94	8.79	14.13
$Sr(Al_{.5}Ta_{.5})O_3$ (SAT)	Cubic	59.09	11.78	37.36	-18.09

Origin of Large Discrepancy in Predicted Dielectric Constants Values

Obviously any inaccuracy in dielectric constant measurements or structure parameter determinations are the up front cause for the discrepancies. All the data used in our calculation are believed to be the most reliable data available.

Besides experimental errors, large deviations from additivity rule using Shannon's ion polarizability data can sometimes be traced to, as pointed out by Shannon, unusual properties of the compounds such as ionic or electronic conductivity, the presence of dipolar impurities, or piezo- or ferroelectricity. However, above mentioned irregularities are presumably non existent in the substrate materials in current study.

After taking into consideration the oxygen polarizability dependence of the volume, V_{ox}, the calculation in Table II was repeated using the refined ion polarizabilities given by Shannon[25] (Table III, first column). The improvement is insignificant and discrepancy is largely non corrected.

A critical question needed to be answered after examining the ion polarizability calculation is whether the assumption is valid that cation (and fluorine) polarizability is independent of the compound in which it is found.

There seems to be enough indication that suggests the answer to the this question is no. Evidence was presented by Safford and Silverman[31] that a change of coordination of an ion alters the molar refraction contribution of the ion or more correctly of the group immediately surrounding the ion. Fajans and co-workers[32] showed that the coordination number of Zn^{2+} is related to the molar volume (of Zn^{2+}) and demonstrated a relationship between molar refraction and molar volume (of the cation). These authors showed that the Al^{3+} in fourfold coordination in glass or in certain crystals has a molar refraction contribution of 12.3 (calculated for Al_2O_3), whereas in sixfold coordination it is 10.5. Kreidl[33] first indicated that MgO may assume both "basic" and "acidic" properties in glass. Difference in molar refractions were found for Mg^{2+} in sixfold coordination such as in periclase MgO where R=4.538, and in fourfold coordination such as in spinel $MgAl_2O_4$ where R=5.18.[34] For ions preferably found only in the same coordination, the dielectric polarizability of the ion remains relatively constant and the additivity rule applies well. Molar volumes of the compounds in these cases are all one need to calculate total

15

polarizabilities of the compounds. Examples of this type would be the silicates and borates. For substances that contain cations which are found in different coordination, the difference in the dielectric polarizability is averaged when enough (unbiased) substances are used in the least square fitting process and therefore good or fair additivity application can be obtained. Examples of this type may be identified as aluminates, and gallates. However, for cations like Cu^{2+}, Ba^{2+}, RE^{3+}, Sb^{3+}, As^{3+}, Nb^{5+}, Ta^{5+}, the ion polarizability data are scarce and single crystal data are not available, the uncertainties are larger because the ratio of the number of observed molar polarizabilities to refined ion polarizabilities is rather low and the observed total polarizabilities have larger errors (as also noted by Shannon).

Modification Proposed on Current Additivity Approach

Following the above discussion, if the dielectric polarizability of a cation is dependent on individual compound, can a set of generally constant ion polarizability data be found and valid for use by the additivity rule for a broad range of compounds with various coordination combinations or crystallographic senses? Following the work of O'Keeffe[35] and Brown and Altermatt[36] on the apparent bond valences and their relations to bond lengths, we suggest reformulating of the ion polarizability additivity rule by normalizing each ion polarizability to its electrostatic valence status. In order to narrow down the differences between the calculated and measured values, we condisered several new factors in Shannon's approach. One of the new approach defines the normalized ion polarizability which is applicable for estimation of the dielectric constants with higher precision once the refined crystal structure is known. The derivation of the modified ion polarizability data and the preliminary examination on ionic materials of broad range is content of a seperare publication.

SUMMARY

Oxide crystals with the perovskite structure are major candidates for YBCO film epitaxial deposition particularly if large size cubic, twin free crystals become available. SAT has already shown promise in high quality epitaxial YBCO film growth. With

improved growth capability, the SAT and particularly its modified solid solutions may be more useful than the intrinsically twinned LaAlO$_3$. Solid solutions between the known complex perovskite oxide and ternary end members, especially gallates, will provide large number of options to tailor the material for specific device applications. The property parameters of the newly proposed substrate materials of oxide perovskite family are summarized in Table III. LaAlO$_3$ and NdGaO$_3$ are also listed for comparison.

Table III. Properties of Some Newly Proposed Oxide Perovskite Substrate Materials

Compo-sition	symmetry	Lattice Constant (Å)	κ 10kHz 90K	tanδ 10kHz 90K	α (x10^{-6}/°C) (@~300K)	Melting Point (°C) *
BMT (crystal)	Cubic	4.0877	25.9	$<10^{-5}$	9.0	(>2800)
SAT	Cubic	3.8952	11.8	4.2×10^{-5}	9.7	1908±25
SAN	Cubic	3.8995	18.7	2.2×10^{-4}	8.5	1739±10
SAT-LA	Cubic	3.8727	21.7	7.5×10^{-5}	7.7	1830±22
SAN-LA	Cubic	3.8634	25.7	2.8×10^{-4}	9.5	1705+20
SAT-NG	Cubic	3.8866	16.0	4.3×10^{-4}	8.8	1767±31
SAN-NG	Cubic	3.8790	23.0	5.2×10^{-4}	10.8	1582±20
LaAlO$_3$ (crystal)	Rhomb.	a=3.789 a=90.12°	23	7.5×10^{-5}	8.2//[1$\bar{1}$0] 6.4//[001]	2040±9
NdGaO$_3$ (crystal)	Ortho.	a=5.426 b=5.502 c=7.706	23 (77K,10G Hz)	3.2×10^{-4}		1484±24

*The melting point was determined rather simply using a strip furnace, with two operators using two separate optical pyrometers and averaging several readings per sample.

REFERENCES

1 J.S. Haggerty, W.P. Menashi and J.F. Wenckus, U.S. Patent No. 3 944 640 (16 March 1976); U.S. Patent No. 4 012 213 (15 March 1977).
2 R.S. Feigelson, *MRS Bull.* 13 47 (1988).
3 J. Yamamoto and A.S. Bhalla, *Mat. Res. Bull.* 24 761 (1989).

4   K. Wakino, *Ferroelectrics* **91** 69 (1989).

5   S. Nomura, K. Toyama, and K. Kaneta, *Jpn. J. Appl. Phys.* **21**(10) L624 (1982).

6   F. Galasso and J. Pinto, *Nature* vol. **207** No. 4992, 70 (1965).

7   e.g., T. Terashima, K. Iijima, K. Yamamoto, K. Irata, Y. Bando, and T. Takada, *Jpn. J. Appl. Phys.* **28**, L987 (1989).

8   H.R. Harrison and J.M. Honig, *Bull. Mater. Sci.* **3**(3), 247 (1981).

9   C.D. Brandle and V.J. Fratello, *J. Mater. Res.* **5**(10), 2160 (1990).

10 B. Han, D. A. Neumayer, B.H. Goodreau, T. J. Marks, H. Zhang, and V.P. Dravid, *Chem. Mater.* **6**, 18 (1994).

11 A.T. Findikoglu, C. Doughty, S. Bhattacharya, Qi Li, X.X. Xi, T. Venkatesan, R.E. Fahey, A.J. Strauss, and J. M. Phillips, *Appl. Phys. Lett.* **61** 1718 (1992).

12 A.T. Findikoglu, S. Bhattacharya, C. Doughty, M.S. Pambianchi, Qi Li, X.X. Xi, S.M. Anlage, R.E. Fahey, A.J. Strauss, J.M. Phillips, and T. Venkatesan, *IEEE Trans. Appl. Superconductivity*, **3**(1) 1425 (1993).

13 R. Guo, A.S. Bhalla, J. Sheen, F. Ainger, E.C. Subbarao, S. Erdei, and L.E. Cross, *J. Mat. Res.* **10**, 18 (1995).

14 R.D. Burbank, *J. Appl. Cryst.* **3** 112 (1970).

15 O. Muller and R. Roy, in *"The major ternary structural families"* (Springer-Verlag, Berlin, Heidelberg, New York 1974) p.215.

16 F.S. Galasso, in *"Structure, properties and preparation of perovskite-type compounds"* (Pergamon Press, Oxford, London, Edinburgh, Now York, Toronto, Sydney, Paris, Braunschweig 1969) p.10.

17 R. Guo, P. Ravindranathan, U. Selvaraj, A.S. Bhalla, L.E. Cross, and R. Roy, *J. Mater. Sci.* **29**, 5054 (1994).

18 S. Haussühl and D. Mateika, *Crystal. Res. Technol.* **26**(4) 481 (1991).

19 D. Mateika, H. Kohler, H. Laudan and E. Völkel, *J. Cryst. Growth* **109** 447 (1991).

20 R.D. Shannon and C.T. Prewitt, *Acta Cryst.* **B25** (1969) 925; *Acta Cryst.* **B26** 1046 (1970).

21 P. Ravindranathan and A.S. Bhalla *et al.* (to be published).

22 G. Harshe, A.S. Bhalla, and L.E. Cross, *Materials Letters* **18**(4), 173 (1994).

23 S. Erdei, L.E. Cross, F.W. Ainger, and A.S. Bhalla, *J. Cryst. Growth* **139**, 54 (1994).

24 R. Guo and A.S. Bhalla (to be published).

25 R.D. Shannon, *J. Appl. Phys.* **73**(1), 348 (1993).

26 A. Heydweiller, *Z. Phys.* **3**, 308 (1920).

27 D.A.A.S. Narayana Rao, *Proc. Ind. Acad. Sci.* **30A**, 317 (1949).

28 A.C. Lasaga and R.T. Cygan, *Amer. Mineral.* **67**, 328 (1982).

29 R. Roberts, *Phys. Rev.* **76**, 1215 (1949).

30 The Inorganic Crystal Structure Database (ICSD), copyrighted by Fachinformationszentrum-Karlsruhe, D-7514 Eggenstein-Leopoldshafen 2, Karlsruhe, West Germany.

31 H.W. Safford and A. Silverman, *J. Am. Ceram. Soc.*, **30**, 203 (1947).

32 K. Fajans and N.J. Kreidl, *J. Am. Ceram. Soc.*, **31**, 105 (1948); K. Fajans and G. Joos, *Z. Physik*, **23**, 1 (1923).

33 N.J. Kreidl, *Glastchn. Ber.*, **7**, 313 (1929).

34 Rustum Roy, *J. Am. Chem. Soc.*, **72**, 3307 (1950).

35 M. O'Keeffe, *Structure and Bonding*, **71** (Springer-Verlag, Berlin Heidelberg, 1989) p.163-190.

36 I.D. Brown and D. Altermatt, *Acta Cryst.* **B41**, 244 (1985).

Appendix 3.

"(Abstract) A Study on Magnetoplumbite Structure Materials as Potential Substrates for High Tc Superconducting Thin Films,"

M.S. Thesis, Pennsylvania State University (submitted, 1996)

Manwen Yao

The Pennsylvania State University

The Graduate School

Intercollege Program in Materials

A STUDY ON

MAGNETOPLUMBITE STRUCTURE MATERIALS AS POTENTIAL

SUBSTRATES FOR HIGH Tc SUPERCONDUCTING THIN FILMS

A Thesis in

Material Science

by

Manwen Yao

Submitted in Partial Fulfillment
of the Requirements
for the Degree of

Master of Science

December 1996

ABSTRACT

Compounds of magnetoplumbite structure with compositions such as $LaMgAl_{11}O_{19}$, $NdGaMgAl_{10}O_{19}$, $CaGa_6Al_6O_{19}$, and $CaGa_{12}O_{19}$ are studied in this work to identify whether they are suitable for epitaxial deposition of high T_C superconducting (HTS) yttrium barium cuprate (YBCO) thin films for microwave applications. The study is directed toward (1) to test the feasibility of single crystal fiber growth by utilizing the Laser Heated Pedestal Growth (LHPG) technique, and (2) to evaluate the various characteristics of the materials including their crystallographic structures, thermal expansion coefficients, and dielectric properties (dielectric constant and loss tangent) to judge the potential of these materials as substrates for HTS thin films.

The ceramic pulling and feeding rods for the growth of single crystal fibers are prepared by solid state reaction, using conventional mixed oxide technique. Test-growth of candidate materials in single crystal fiber form by utilizing the LHPG technique has been undertaken. Successful growth conditions have been carefully investigated.

Crystallographic structures and lattice parameters of these materials in single crystal fiber form have been determined by X-ray powder diffraction patterns. Thermal expansion coefficients have been measured as well. Measured structural and thermal property are compared to that of the YBCO superconductor and therefore provide the information on extent of matching of the lattice and thermal expansion with YBCO. Dielectric property (dielectric constant and loss tangent) is another important selecting criterion of substrate materials for depositing YBCO thin films. Dielectric property measurement shows that they have moderate dielectric constant and fairly low dielectric loss tangent ($\sim 10^{-3}$).

Appendix 4.

"Epitaxial $Sr_2(AlTa)O_6$ Films as Buffer Layers on MgO for $YBa_2Cu_3O_{7-x}$ Thin Film Growth"

J. Appl. Phys., 78(3):2138-40 (1995)

K.Y. Chen

S. Afonso

R.C. Wang

Y.Q. Tang

G. Salamo

F.T. Chan

R. Guo

A. Bhalla

Epitaxial $Sr_2(AlTa)O_6$ films as buffer layers on MgO for $YBa_2Cu_3O_{7-x}$ thin film growth

K. Y. Chen, S. Afonso, R. C. Wang,[a] Y. Q. Tang, G. Salamo, and F. T. Chan
Department of Physics/High Density Electronics Center, University of Arkansas, Fayetteville, Arkansas 72701

R. Guo and A. S. Bhalla
Material Research Laboratory, Pennsylvania State University, University Park, Pennsylvania 16802

$Sr_2(AlTa)O_6$ thin films (2000–3000 Å) have been deposited on MgO (001) substrates using pulsed laser deposition (PLD). X-ray-diffraction analysis shows that the $Sr_2(AlTa)O_6$ grows with the c axis highly oriented normal to the substrate plane and very good in-plane epitaxy. The subsequently deposited $YBa_2Cu_3O_{7-x}$ films using PLD on $Sr_2(AlTa)O_6$ buffered MgO substrates exhibit excellent epitaxial growth with a narrow rocking curve width and a small ϕ scan peak width. The critical temperature T_{c0} of 90–92 K has been achieved reproducibly and the critical current density is over 2.7×10^6 A/cm^2 at 77 K. © *1995 American Institute of Physics.*

High-T_c superconducting $YBa_2Cu_3O_{7-x}$ (YBCO) films have been successfully grown on a number of substrates, such as $SrTiO_3$, $LaAlO_3$, MgO, YSZ, and $LaGaO_3$. In many high-frequency electronic applications, such as superconducting multichip modules, one requires substrates and dielectric layer materials with a low dielectric constant and a low loss tangent. In recent years, great efforts have been made in searching for substrates and dielectric intermediate layer materials which can meet these requirements for specific electronic applications as well as the requirements for growth of superconducting films.[1–5] Several materials such as $SrTiO_3$,[2,4] MgO,[2,3] YSZ,[1] and CeO_2,[3,5] have been used as buffer layers for fabricating $YBa_2Cu_3O_{7-x}$ films on some substrates of application interest. The dielectric constant of $SrTiO_3$, however, is too high to be useful in some high-frequency devices, whereas MgO and YSZ have a relatively large lattice mismatch with superconducting materials. Another cubic perovskite material $Sr_2(AlTa)O_6$ (SAT) has recently become of interest as a buffer layer and dielectric interlayer for thin films of oxide superconductors[6,7] because it has a good lattice match with the high-T_c superconductors. Ordered SAT arises from the alternate ordered distribution of Al and Ta atoms on the octahedral site of the primitive perovskite unit cell, resulting in a doubling of the lattice constant. In disordered SAT, Al and Ta atoms randomly occupy the octahedral site. Both ordered and disordered structures are closely lattice matched to the a-b plane of YBCO. Another advantage of SAT is that it has a lower dielectric constant than that of $SrTiO_3$, YSZ, and CeO_2. Table I shows the dielectric properties of SAT ceramic samples measured at both room and liquid nitrogen temperatures. Moreover, the thermal expansion coefficient of SAT is 9.7×10^{-6} °C in the temperature range from room temperature to 600 °C, which is highly compatible with that of YBCO, and there are no structural phase transitions and twinning behavior observed.

These properties indicate that SAT is suitable as a buffer layer material for high-T_c thin films in device applications.

In this communication, we report our experimental results on fabricating SAT buffer layers on MgO substrates and YBCO/SAT/MgO multilayers. We chose MgO as a substrate material in this work because it has a relatively low dielectric constant ($\epsilon = 10$) and is inexpensive compared to other substrates such as $SrTiO_3$ and $LaAlO_3$. The main disadvantage of using MgO for making superconducting films is the large lattice mismatch between it and YBCO. As a result, the critical temperature of YBCO grown directly onto MgO is usually limited to 88 K.[4] The motivation of this study is to use SAT as a buffer layer to overcome the drawback of MgO. Furthermore, MgO has been successfully used as a first buffer layer on a few substrates such as MgF_2 and Si.[2,8] This suggests, therefore, that if SAT can be successfully deposited onto MgO, it can be used as a second buffer layer for growing YBCO films.

SAT and YBCO films were deposited using the pulsed laser deposition technique. A 193 nm laser beam generated by an excimer laser was focused to provide an energy density of ~ 1.3 J/cm^2. The laser repetition rate was 6 Hz. An oxygen pressure was maintained in the vacuum chamber at 200–250 mTorr during deposition of both the SAT and YBCO films. The quality of the SAT and YBCO films was examined by x-ray diffraction, and four-probe T_c and J_c measurements.

The SAT target used was a ceramic pellet of the ordered phase with a lattice constant $a_0 = 7.777$ Å prepared using

TABLE I. Dielectric properties of ceramic SAT with 97% theoretical density.

	Room temperature		Low temperature (77 K)	
	10 kHz	Microwave	10 kHz	Microwave
ϵ	11.8	10.7 (11.0 GHz)	11.8	...
$\tan \delta$ ($\times 10^{-4}$)	16.8	3.64 (7.64 GHz)	0.42	2.09 (7.64 GHz)

[a] Permanent address: Department of Materials Science, Fudan University, Shanghai, People's Republic of China.
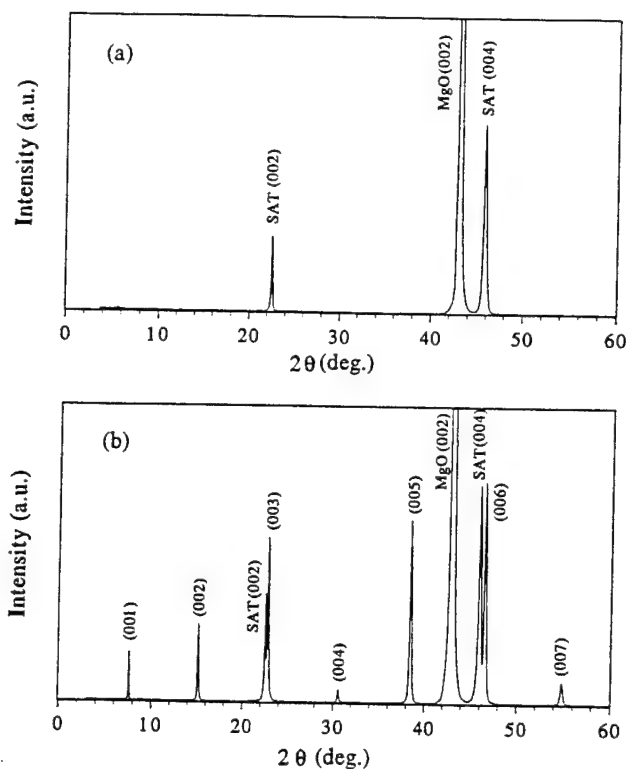
FIG. 1. θ–2θ x-ray-diffraction pattern for (a) the SAT film on a (001) MgO substrate and (b) the YBCO film on SAT/MgO.

FIG. 2. X-ray ϕ scan of {202} peaks of an SAT film on a MgO substrate.

the conventional solid-state reaction technique.[9] SAT films of 2000–3000 Å thickness were deposited on (001) MgO substrates at several different substrate temperatures. Upon completion of deposition, the sample was cooled to room temperature in ~30 min. All films deposited in the temperature range 710–810 °C exhibited c-axis oriented growth as shown in Fig. 1(a). X-ray rocking curve widths on the (004) peak versus deposition temperature are listed in Table II. In the temperature range 755–810 °C, rocking curves have a full width at half maximum (FWHM) of less than 1.0°. The film grown at 780 °C had the narrowest rocking curve, with a FWHM of 0.75°, exhibiting excellent epitaxial growth.

The in-plane epitaxy of the SAT films was examined by x-ray ϕ scan. Figure 2 shows a ϕ scan of the SAT {202} peaks. The four peaks every 90° indicate an excellent epitaxial alignment of the films. There is no in-plane misorientation. The (202) peak widths (FWHM) in ϕ are between 1.7° and 2.4° for all the films deposited in temperature range 755–810 °C. Our resolution of the ϕ scan is 0.8° as measured on the MgO substrate (202) peak. Comparison of the

SAT {202} ϕ scan and the MgO substrate {202} ϕ scan points out the in-plane expitaxial relationship: MgO[100](001)‖SAT[100](001).

YBCO films (2000–3000 Å thick) were subsequently grown on SAT/MgO with an SAT layer deposited at an optimum temperature of 780 °C. The substrate temperature for growing YBCO is 750 °C. After deposition, the films were cooled to 500 °C in 30 min in 500 Torr oxygen, and then kept at 450–500 °C for an hour.

Figure 1(b) displays an x-ray θ–2θ scan pattern for a YBCO/SAT/MgO multilayer. One observes only YBCO (00l) peaks and SAT (002), (004), and MgO (002) peaks, revealing a high degree of c-axis orientation of the YBCO film. The rocking curve measurements of the YBCO (005) peak showed a FWHM $\leq 0.17°$. The minimum FWHM of 0.07° was observed for a couple of samples, which is just the resolution of our x-ray ω scan measured on Si (333) peak. X-ray ϕ scans were performed on YBCO {102} peaks to examine the in-plane epitaxial alignment. Figure 3 shows a ϕ scan of the YBCO {102} peaks for a typical sample. Peak widths in ϕ are 1.5° FWHM. The θ–2θ scan and ϕ scan analysis revealed the following "cube on cube" epitaxial relationship: YBCO[100](001) ‖SAT[100](001)‖MgO[100](001).

TABLE II. Rocking curve widths (FWHM) of SAT (004) peaks for samples grown at different temperatures.

Temperature (°C)	725	755	780	810
Rocking curve FWHM (deg)	1.20	0.94	0.75	0.86
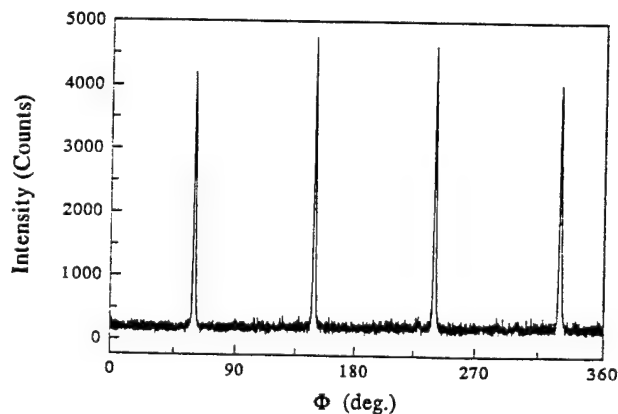
FIG. 3. X-ray ϕ scan of YBCO {102} peaks for a YBCO film grown on SAT/MgO.
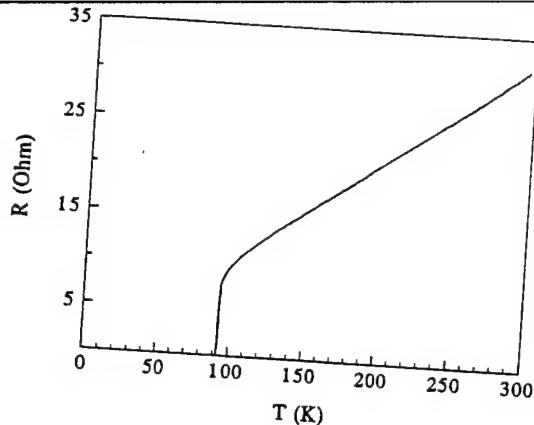
FIG. 4. Resistance vs temperature for a 3000 Å YBCO film on SAT/MgO.

perature T_{c0} achieved was 92 K and critical current density was in excess of 2.7×10^6 A/cm^2 at 77 K. This work not only demonstrates that high quality YBCO films can be grown on an MgO substrate with an SAT buffer layer, but also shows that SAT may be a promising buffer layer material for making multilayer structures. Therefore, examining the potential of SAT as an interlayer on other multilayer structures will be of interest for electronics applications. Further study toward this direction is now in progress.

The critical temperatures (T_{c0}) of the YBCO films fabricated on SAT/MgO were found to be 90–92 K with good reproducibility. Figure 4 shows the resistance versus temperature for a YBCO film. The zero resistance temperature T_{c0} is 92 K with a transition width less than 1 K. The critical current density was measured to be higher than 2.7×10^6 A/cm^2 at 77 K in zero field.

In conclusion, epitaxial SAT films have been successfully deposited on MgO substrates using pulsed laser deposition. The YBCO films deposited on SAT buffered MgO substrates exhibit a small rocking curve width and good in-plane epitaxy. X-ray analysis indicates the cube on cube in-plane epitaxial relationships among the YBCO films, the SAT buffer layer, and the MgO substrate. The critical tem-

[1] D. K. Fork, D. B. Fenner, R. W. Barton, J. M. Phillips, G. A. N. Connell, J. B. Boyce, and T. H. Geballe, Appl. Phys. Lett. **57**, 1161 (1990).
[2] K. S. Harshavardhan, A. Pique, S. M. Green, K. Patel, J. R. Zhang, E. Belohoubek, R. Edwards, T. Venkatesan, E. J. Denlinger, V. Pendrick, D. Kalokitis, A. Fathy, X. D. Wu, M. Rajeswari, and A. Smith, Appl. Phys. **64**, 1570 (1994).
[3] B. F. Cole, G.-C. Liang, N. Newman, K. Char, G. Zaharchuk, and J. S. Martens, Appl. Phys. Lett. **61**, 1727 (1992).
[4] F. C. Wellstood, J. J. Kingston, and John Clarke, J. Appl. Phys. **75**, 683 (1994).
[5] X. D. Wu, R. C. Dye, R. E. Muenchausen, S. R. Foltyn, M. Maley, A. D. Rollett, A. R. Garcia, and N. S. Nogar, Appl. Phys. Lett. **58**, 2165 (1991).
[6] A. T. Findikoglu, C. Doughty, S. Bhattacharya, Qi Li, X. X. Xi, T. Venkatesan, R. E. Fahey, A. J. Strauss, and J. M. Phillips, Appl. Phys. Lett. **61**, 1718 (1992).
[7] C. D. Brandle and V. J. Fratello, J. Mater. Res. **5**, 2160 (1990).
[8] D. K. Fork, F. A. Ponce, J. C. Tramontana, and T. H. Geballe, Appl. Phys. Lett. **58**, 2294 (1991).
[9] Ruyan Guo, A. S. Bhalla, Jyh Sheen, F. W. Ainger, S. Erdei, E. C. Subbarao, and L. E. Cross, J. Mater. Res. **10**, 18 (1995).

Chen *et al.*

Appendix 5.

"Epitaxial $Tl_2Ba_2CaCu_2O_8$ Superconducting Thin Film on $Sr_2(AlTa)O_6$ Buffer Layer"

J. Appl. Phys, 78(11):6846-6848 (1995)

Y.Q. Tang

K.Y. Chen

S. Afonso

X.L. Xu

Q. Xiong

G. Salamo

F.T. Chan

R. Guo

A. Bhalla

COMMUNICATIONS

Epitaxial $Tl_2Ba_2CaCu_2O_8$ superconducting thin film on $Sr_2(AlTa)O_6$ buffer layer

Y. Q. Tang, K. Y. Chen, S. Afonso, X. L. Xu,[a] Q. Xiong, G. Salamo, and F. T. Chan
Department of Physics/High Density Electronic Center, University of Arkansas, Fayetteville, Arkansas 72701

R. Guo and A. Bhalla
Materials Research Laboratory, Pennsylvania State University, University Park, Pennsylvania 16802

Epitaxial $Tl_2Ba_2CaCu_2O_8$ superconducting films have been successfully grown on the dielectric $Sr_2(AlTa)O_6$ (SAT) buffer layers. X-ray diffraction data showed that the films were highly c-axis oriented with a rocking curve full width half maximum as narrow as 0.3°. The films also had an excellent in-plane epitaxy with $Tl_2Ba_2CaCu_2O_8$[100] aligned with SAT[100] and MgO[100] of the substrate. The zero resistance temperature T_c of the superconducting films ranged from 95 to 103 K and the transport critical current density J_c in zero field was 3×10^5 A/cm² at 77 K. © *1995 American Institute of Physics.*

In the study of high-temperature superconducting films, buffer layers have been extensively used[1-6] because being interposed between the substrate and the film of interest, these layers can alleviate a variety of problems such as chemical incompatibility, thermal or lattice mismatch.[7] As a new dielectric compound, $Sr_2(AlTa)O_6$ (SAT) was synthesized to be one of the potential substrate materials for the growth of high T_c superconducting films.[8] Because of its relatively low dielectric constant[9,10] and good thermal expansion coefficient and lattice match with YBCO,[8-11] SAT was successfully used as a buffer layer material for the growth of YBCO thin films.[10,11] Recent studies have shown that by depositing an epitaxial SAT buffer layer on MgO, the lattice mismatch problem between a MgO substrate and a YBCO superconducting film was reduced, leading to an improvement of superconducting properties.[10]

$Tl_2Ba_2CaCu_2O_8$ superconducting films, while exhibiting higher T_c and lower surface resistance than YBCO,[12] are much more difficult to prepare with good qualities due to the high volatility and chemical reactivity of thallium and the high reaction temperature. Although best films with transport J_c of $1.06-5.3\times10^6$ A/cm² were obtained by carefully optimizing the thallination procedure and using suitable substrates such as $LaAlO_3$[13-15] or $SrTiO_3$,[16] the high cost and high dielectric constants of such substrates can limit further applications of $Tl_2Ba_2CaCu_2O_8$ films in microelectronics. Some other substrates of low cost and low dielectric constants such as sapphire, silica, and MgO suffer from the chemical incompatibility or large lattice mismatch with $Tl_2Ba_2CaCu_2O_8$ and consequently yield poor film quality and low J_c. To resolve these problems, a suitable buffer layer compatible both with the $Tl_2Ba_2CaCu_2O_8$ film and with the substrate should be used. By choosing CeO_2 as buffer layers,

Holstein *et al.* were able to avoid the chemical reaction of the $Tl_2Ba_2CaCu_2O_8$ films with the sapphire substrates and produced epitaxial $Tl_2Ba_2CaCu_2O_8$ films with T_c of 97–98 K and transport J_c of 2.8×10^5 A/cm² at 75 K.[3]

The crystallographic phase of ordered SAT has a double cell cubic perovskite structure with a lattice constant $a_0=7.777$ Å[10] or $a_0/2=3.888$ Å, while $a_0=3.895$ Å in the disordered cubic perovskite.[9] These lattice constants are close to those of Tl-based superconductors ($a_0=3.85-3.86$ Å). In fact, SAT has better lattice match to the TlBaCaCuO superconductors than many other substrates such as MgO ($a_0=4.213$ Å), YSZ ($a_0/\sqrt{2}=3.639$ Å), $LaAlO_3$ ($a_0=3.792$ Å), and even $SrTiO_3$ ($a_0=3.905$ Å). Moreover, SAT is similar to $SrTiO_3$ in structure and was tested to be chemically stable at high temperature.[8,9] Therefore, it should also be a good candidate to act as a buffer layer in the fabrication of Tl-based superconducting films. In this communication, we report for the first time the preparation of epitaxial
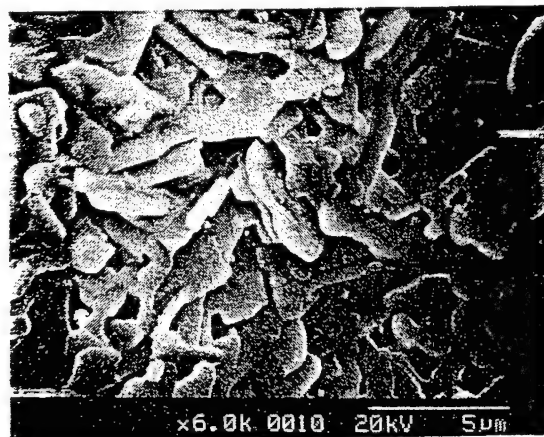

FIG. 1. SEM photograph of a $Tl_2Ba_2CaCu_2O_8$ superconducting film on SAT/MgO.

[a] Permanent address: Ion Beam Laboratory, Shanghai Institute of Metallurgy, Chinese Academy of Sciences, Shanghai 200050, China.
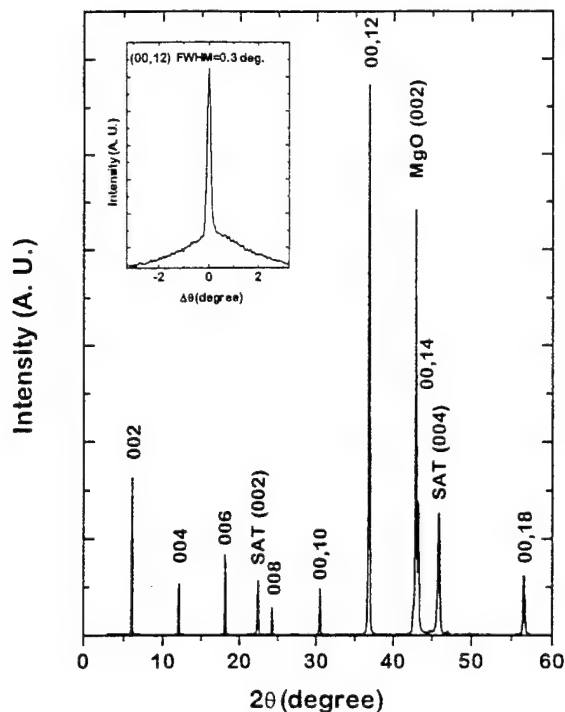
FIG. 2. X-ray diffraction θ-2θ scan of a $Tl_2Ba_2CaCu_2O_8$ superconducting film on SAT/MgO. The inset is the rocking curve of the $Tl_2Ba_2CaCu_2O_8$ (00.12) peak.
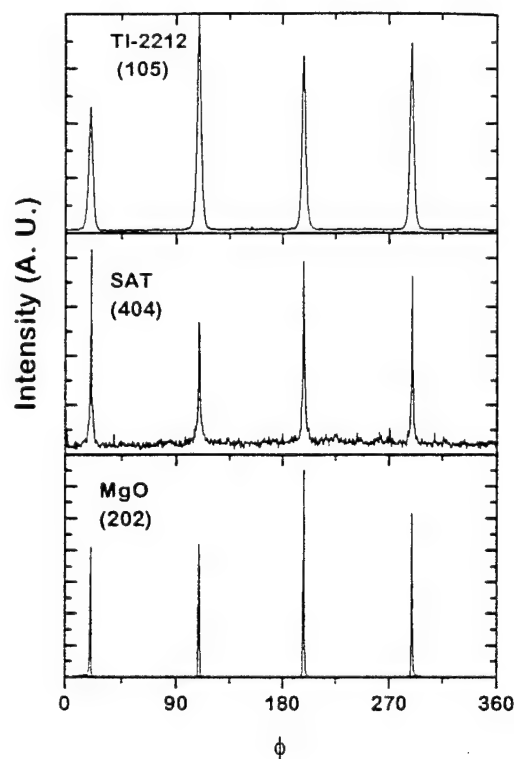

FIG. 3. X-ray diffraction ϕ scans of the $Tl_2Ba_2CaCu_2O_8$ (105) reflection and the underlying SAT (404) and MgO (202) reflections for the film showing XRD data in Fig. 2.

$Tl_2Ba_2CaCu_2O_8$ superconducting thin films on SAT buffer layers. Laser ablation technique was used for both the growth of epitaxial SAT(100) buffer layers on MgO(100) substrates and the subsequent deposition of precursor $Ba_2CaCu_2O_x$ films. The resulting $Tl_2Ba_2CaCu_2O_8$ superconducting films were obtained via an off-line Tl-diffusion procedure. These films were highly epitaxial with a T_c of 95–103 K and a transport J_c of 3×10^5 A/cm^2 at 77 K in zero field.

The laser used for the deposition of both the SAT buffer layers and the precursor $Ba_2CaCu_2O_x$ films was a ArF excimer laser with an oscillating wavelength at 193 nm. It operated at a repetition rate of 6 Hz with an output energy density of about 1.5 J/cm^2. An oxygen pressure of 200 mTorr was maintained during the growth of both the SAT and the precursor films. The SAT buffer layer with a thickness of 2000–2500 Å was deposited on a polished MgO(100) substrate at a temperature of 780 °C. At this temperature, the SAT buffer layer was epitaxially grown on the substrate with excellent c-axis orientation and in-plane alignment.[10] The precursor $Ba_2CaCu_2O_x$ film was then deposited on the SAT buffer layer at about 350 °C followed by a short time off-line annealing in air at 820 °C. The film was then treated in a thallination process. Raw pellets with a composition of $Tl_2Ba_2CaCu_2O_x$ were used as the Tl source. The superconducting $Tl_2Ba_2CaCu_2O_8$ films were then formed by annealing the precursor films with the Tl source at 800 °C in air for a period of 8 h.[17] For comparison, precursor films were also directly deposited on MgO(100) substrates and were treated with the same procedures. In both cases, the $Tl_2Ba_2CaCu_2O_8$ films generally had a thickness of 0.9–1 μm.

The surface morphology of the $Tl_2Ba_2CaCu_2O_8$ super-conducting films were observed using an atomic force microscope (AFM) and a scanning electron microscope (SEM). The images showed no significant difference between the films on SAT/MgO and those on MgO. Although the microstructure of the films varied with the thallination conditions, the best films had layered structure with micron size platelets (Fig. 1). Most of the platelets were parallel to the surface of the substrate and only a few showed small angles. The mean roughness of the $Tl_2Ba_2CaCu_2O_8$ films on SAT/MgO was around 400 Å.

X-ray diffraction θ-2θ scan of a typical $Tl_2Ba_2CaCu_2O_8$ film on SAT/MgO (Fig. 2) revealed only (00l) peaks of $Tl_2Ba_2CaCu_2O_8$, SAT, and MgO, indicating that the film had a pure 2212 phase and was c-axis oriented. As a further investigation of the film orientation, we measured the rocking curve of the (00, 12) peak (inset in Fig. 2). The curve had a full width half maximum (FWHM) as narrow as 0.3°, indicating an excellent c-axis alignment. Figure 3 shows a group of x-ray diffraction ϕ scans for the film as well as the underlying SAT buffer layer and the MgO substrate. The reflection of $Tl_2Ba_2CaCu_2O_8$ (105) yielded peaks at 90° intervals and the FWHM of the peak in ϕ is 3.5°, giving an evidence of good in-plane epitaxy. The overlaps of the $Tl_2Ba_2CaCu_2O_8$ (105), SAT (404), and MgO (202) peaks further indicated that the $Tl_2Ba_2CaCu_2O_8$[100] was epitaxial with respect to the SAT [100] which was in turn epitaxial to MgO [100], thus forming a cube-on-cube epitaxial relationship.[4,18]

The critical temperature T_c and the transport critical current density J_c of the $Tl_2Ba_2CaCu_2O_8$ films were measured

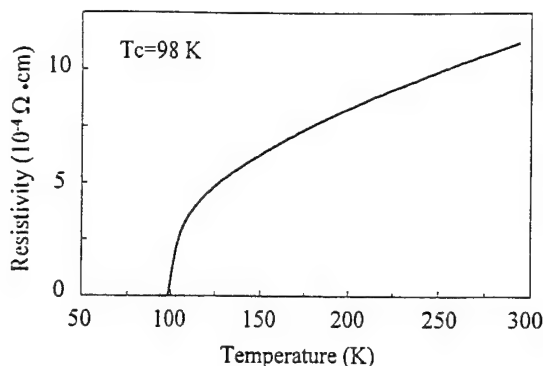J. Appl. Phys., Vol. 78, No. 11, 1 December 1995

Tang *et al.* 6847

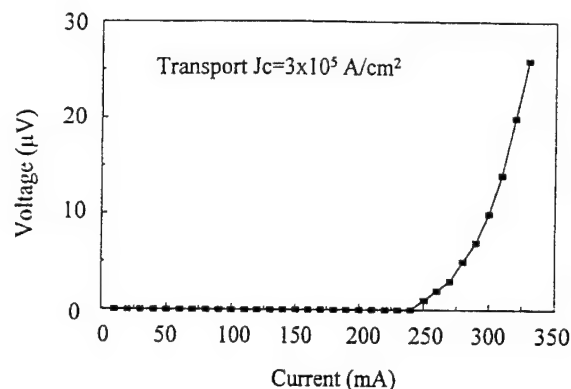FIG. 4. Resistivity vs temperature for the $Tl_2Ba_2CaCu_2O_8$ film on SAT/MgO.

FIG. 5. I-V curve for measuring the transport J_c of the $Tl_2Ba_2CaCu_2O_8$ film on SAT/MgO.

by the four-probe method. The T_c ranged from 95 to 103 K. Figure 4 is the resistivity versus temperature curve of the film. The zero resistance temperature was 98 K. Before the J_c measurements, the films were patterned into microbridges of 70–80 μm wide and about 200 μm long by photolithography and wet etching. A Dektak surface profilometer was used to measure the width and length as well as the thickness of each microbridge. The measurements were carried out in liquid nitrogen at 77 K and zero field. A voltage criterion of 1 μV/cm was used to determine the J_c value. Figure 5 shows the I-V curve for the same $Tl_2Ba_2CaCu_2O_8$ film on SAT/MgO. The J_c calculated from the curve was 3×10^5 A/cm^2. As comparison, while the $Tl_2Ba_2CaCu_2O_8$ films directly deposited on MgO showed a similar room-temperature resistivity and also had T_c around 100 K, the corresponding transport J_c were only 2–3×10^4 A/cm^2, about 10 times lower.

We have also briefly examined some SAT/MgO and MgO substrates after removing the $Tl_2Ba_2CaCu_2O_8$ films. Under a microscope, the MgO substrate covered by the SAT buffer layer was still shiny and smooth, showing no sign of chemical reaction between SAT and the $Tl_2Ba_2CaCu_2O_8$ film. On the bare MgO substrate some shallow tiny pits were observed, indicating that chemical reaction had occurred at the interface during the film formation. As a matter of fact, despite its good dielectric characteristics, MgO is susceptible to quite a few chemical reactions. It is even not very stable in an ambient environment. The moisture in air can easily corrode the substrate surface and affect the quality of film deposited on it. Thus, the SAT buffer layer on MgO substrate has not only resolved the lattice mismatch but also avoided the unwanted chemical interaction between the superconducting $Tl_2Ba_2CaCu_2O_8$ film and the MgO substrate.

In summary, epitaxial $Tl_2Ba_2CaCu_2O_8$ superconducting films have been grown on the $Sr_2(AlTa)O_6$ (SAT) dielectric buffer layers. X-ray diffraction data of the $Tl_2Ba_2CaCu_2O_8$ films on SAT/MgO showed that the films were epitaxially oriented with the c axis normal to the substrate surface and the $Tl_2Ba_2CaCu_2O_8$[100] aligned with SAT[100] and MgO[100]. The T_c of the superconducting films ranged from 95 to 103 K and the transport J_c at 77 K in zero field was at least 3×10^5 A/cm^2. This study shows that SAT is a suitable buffer layer material for the growth of superconducting

$Tl_2Ba_2CaCu_2O_8$ films due to their good lattice match and chemical compatibility. We are now extending the use of SAT buffer layer to the preparation of other Tl-based superconducting phases with higher T_c such as $Tl_2Ba_2Ca_2Cu_3O_{10}$ and $TlBa_2Ca_2Cu_3O_9$ films. The applications of SAT buffer layer on other low cost and/or low dielectric constant substrates for the fabrication of Tl-based superconducting thin films are also under investigation.

[1] X. D. Wu, R. E. Muenchausen, N. S. Nogar. A. Pique, R. Edwards, B. Wilkens, T. S. Ravi, D. M. Hwang, and C. Y. Chen, Appl. Phys. Lett. **58**, 304 (1991).

[2] K. Char, N. Newman, S. M. Garrison, R. W. Barton, R. C. Taber, S. S. Laderman, and R. D. Jacowitz, Appl. Phys. Lett. **57**, 409 (1990).

[3] W. L. Holstein, L. A. Parisi, D. W. Face, X. D. Wu, S. R. Foltyn, and R. E. Muenchausen, Appl. Phys. Lett. **61**, 982 (1992).

[4] K. S. Harshavardhan, A. Pique, S. M. Green, K. Patel, J. R. Zhang, E. Belohoubek, R. Edwards, T. Venkatesan, E. J. Denlinger, V. Pendrick, D. Kalokitis, A. Fathy, X. D. Wu, M. Rajeswari, and A. Smith, Appl. Phys. Lett. **64**, 1570 (1994).

[5] R. P. Reade, P. Berdahl, R. E. Russo, and S. M. Garrison, Appl. Phys. Lett. **61**, 2231 (1992).

[6] R. P. Reade, P. Berdahl, R. E. Russo, and L. W. Schaper, Appl. Phys. Lett. **66**, 2001 (1994).

[7] J. M. Phillips, MRS Bulletin **XX(4)**, 35 (1995).

[8] C. D. Brandle and V. J. Fratello, J. Mater. Res. **5**, 2160 (1990).

[9] R. Guo, A. S. Bhalla, J. Sheen, F. W. Ainger, S. Erdei, E. C. Subbarao, and L. E. Cross, J. Mater. Res. **10**, 18 (1995).

[10] K. Y. Chen, S. Afonso, R. C. Wang, Y. Q. Tang, G. Salamo, F. T. Chan, R. Guo, and A. Bhalla, J. Appl. Phys. **78**, 2138 (1995).

[11] A. T. Findikoglu, C. Doughty, S. Bhattacharya, Q. Li, X. X. Xi, T. Venkatesan, R. E. Fahey, A. J. Strauss, and J. M. Phillips, Appl. Phys. Lett. **61**, 1718 (1992).

[12] W. L. Holstein, L. A. Parisi, C. Wilker, and R. B. Flippen, Appl. Phys. Lett. **60**, 2014 (1992).

[13] R. B. Hammond, G. V. Negrete, L. C. Bourne, D. D. Strother, A. H. Cardona, and M. M. Eddy, Appl. Phys. Lett. **57**, 825 (1990).

[14] W. L. Hostein, C. Wilker, D. B. Laubacher, D. W. Face, P. Pang, M. S. Warrington, C. F. Carter, and L. A. Parisi, J. Appl. Phys. **74**, 1426 (1993).

[15] S. L. Yan, L. Fang, Q. X. Song, J. Yan, Y. P. Zhu, J. H. Chen, and S. B. Zhang, Appl. Phys. Lett. **63**, 1845 (1993).

[16] A. H. Cardona, H. Suzuki, T. Yamashita, K. H. Young, and L. C. Bourne, Appl. Phys. Lett. **62**, 411 (1993).

[17] Y. Q. Tang, Z. Z. Sheng, W. A. Lou, I. N. Chan, Z. Y. Chen, Y. F. Li, and D. O. Pederson, Physica C **214**, 190 (1993).

[18] W. Y. Lee, S. M. Garrison, M. Kawasaki, E. L. Venturini, B. T. Ahn, R. Boyers, J. Salem, R. Savoy, and J. Vazquez, Appl. Phys. Lett. **60**, 772 (1992).

Appendix 6.

"Sol-Gel Synthesis of $Ba(Mg_{1/3}Ta_{2/3})O_3$: Phase Pure Powder and Thin Films"

Mat. Res. Bull., 31(7), 817-825 (1996)

D. Ravichandran

R. Meyer, Jr.

R. Guo

A.S. Bhalla

L.E. Cross

and R. Roy

Pergamon

PII S0025-5408(96)00073-6

SOL-GEL SYNTHESIS OF Ba(Mg$_{1/3}$Ta$_{2/3}$)O$_3$:
PHASE PURE POWDER AND THIN FILMS

D. Ravichandran*, R. Meyer Jr., R. Roy, R. Guo, A.S. Bhalla and L.E. Cross
Materials Research Laboratory, The Pennsylvania State University
University Park, PA 16802, USA

ABSTRACT

Phase pure Ba(Mg$_{1/3}$Ta$_{2/3}$)O$_3$ (BMT) powders were prepared using Ba metal, Mg(OC$_2$H$_5$)$_2$, and Ta(OC$_2$H$_5$)$_5$ as metal-organic precursors. Thin films of BMT were spin coated onto Pt-coated Si (100) substrates using the prepared solution and then fired at various temperatures. The X-ray diffraction patterns show that the films crystallize to a single disordered perovskite phase on Si (100) at ~600°C. Scanning electron microscopy reveals that the films 0.3 μm in thickness and approximately 0.1 μm in grain size were essentially crack-free.

KEYWORDS: A. thin-films, A. electronic materials, B. sol-gel chemistry, C. thermogravimetric analysis (TGA), C. X-ray diffraction

INTRODUCTION

The requirements for dielectric materials used in microwave applications usually include (i) a high unloaded Q, (ii) a moderate dielectric constant, and (iii) small temperature coefficient of the resonant frequency. Additionally, good sinterablity and high reproducibility are desirable processing features for these dielectric materials. Ba(Mg$_{1/3}$Ta$_{2/3}$)O$_3$ (1-4), Ba(Zn$_{1/3}$Ta$_{2/3}$)O$_3$ (5), (Zr,Sn)TiO$_3$ (6), Ba(Mn$_{1/3}$Ta$_{2/3}$)O$_3$ (7), and other complex oxides have been reported as promising microwave materials. However,
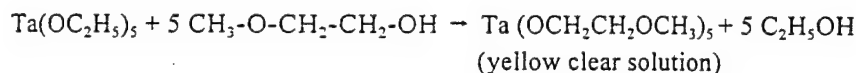
---

* To whom correspondence should be addressed.

very high processing temperatures and poor sinterability are known obstacles for production, particularly for BMT. BMT has a melting point of ~3000°C (4) and is difficult to make in the form of high density ceramics and large area crystals. Additives such as Sn or Mn have been used in the synthesis of BMT to reduce the sintering temperatures or prolonged sintering time at high tempratures. Many materials for microwave applications have cations such as Mg, Sn, and Mn that easily form compounds with tantalum during the conventional solid state reactions and possibly resulting in undesirable phases. Sol-gel processing has been used for preparing phase pure bulk ceramics and thin films. Sol-gel techniques ensure homogeneous mixing of cations and low crystallization temperatures.

In this paper, we report the synthesis for the first time of phase pure BMT powders, ceramics, and thin films by the sol-gel process, using Ba metal, $Mg(OC_2H_5)_2$, and Ta $(OC_2H_5)_5$ as metal-organic precursors. The densification of ceramics as a function of sintering temperature without the use of any sintering aids commonly used in solid-state reaction routes is also reported.

EXPERIMENTAL

A schematic reaction sequence for the formation of BMT gels and thin films is shown in Figure 1. Initially, $Ta(OC_2H_5)_5$ (Aldrich Chemicals, 99.99% purity) in stoichiometric amount was dissolved in 20 ml of 2-methoxyethanol in a three-neck flask and refluxed at 125°C for 6 hours in an argon atmosphere.

$$Ta(OC_2H_5)_5 + 5\ CH_3\text{-}O\text{-}CH_2\text{-}CH_2\text{-}OH \rightarrow Ta\ (OCH_2CH_2OCH_3)_5 + 5\ C_2H_5OH$$
(yellow clear solution)

The required amount of $Mg(OC_2H_5)_5$ (Aldrich Chemicals, 99.99% purity) was dissolved in 15 ml of 2-methoxyethanol along with 3-5 ml of CH_3COOH needed to dissolve the
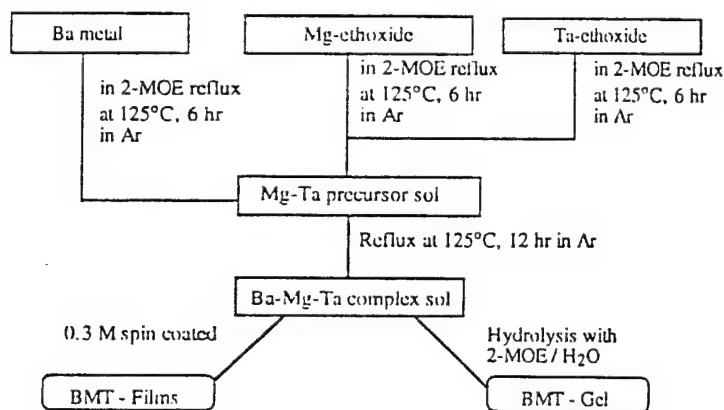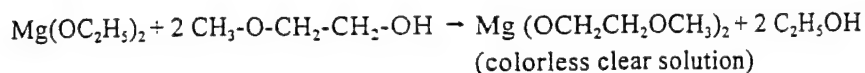

FIG. 1
Schematic reaction sequence for the formation of BMT xero-gel.

$Mg(OC_2H_5)_5$ completely. The mixture was refluxed for 6 hours in an inert atmosphere (e.g., Argon/N_2 gas).

$$Mg(OC_2H_5)_2 + 2\ CH_3\text{-}O\text{-}CH_2\text{-}CH_2\text{-}OH \rightarrow Mg\ (OCH_2CH_2OCH_3)_2 + 2\ C_2H_5OH$$
(colorless clear solution)

A double alkoxide (6) can be formed by mixing $Mg(OCH_2CH_2OCH_3)_2$ and $Ta(OCH_2CH_2OCH_3)_5$ under inert gas atmosphere. Finally, $Ba(OCH_2CH_2OCH_3)_2$ was formed following the reaction

$$Ba + 2\ CH_3\text{-}O\text{-}CH_2\text{-}CH_2\text{-}OH \rightarrow Ba(OCH_2CH_2OCH_3)_2 + H_2$$
(golden yellow solution)
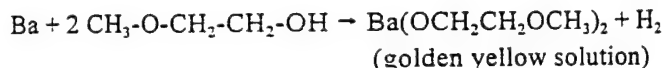
The Ba-methoxyethoxide was cooled to room temperature and then added to the double alkoxide solution. The clear homogeneous solution obtained was further refluxed at 125°C for 12 hours in argon atmosphere. This process forms the barium-magnesium-tantalum precursor solution. In order to form the BMT gel, a part of the solution was hydrolyzed by adding a theoretical amount of deionized water diluted with 2-methoxyethanol in the volume ratio 1:5. The clear solution was put in a 60°C oven for 3-4 hours to form the gel. The transparent BMT xero-gel thus formed after drying was crushed with a mortar and pestle.

The powder was analyzed using a Perkin-Elmer PC-series thermogravimetric (TGA) analyzer to determine the drying and organic burnout behavior of the gel. Differential thermal analysis (DTA) was done in a Perkin-Elmer PC-7 series differential thermal analyzer interfaced with a computer for determination of crystallization temperature. Phase identification was carried out using a Scintag powder X-ray diffraction (model DMC-15) with Ni-filtered Cu K_{a1} radiation.

BMT thin films were made by spin coating onto Si substrates, using the sol-gel prepared solution. The BMT solution concentration was diluted to 0.3 M and hydrolyzed with water (1:2 ratio with deionized water). In order to prepare crack-free films, 4% (by volume) formamide was added to the solution. Prior to the spin coating, the Pt-coated Si substrates were thoroughly washed with isopropanol. Thin films were spun at 3000 rpm for 20 seconds using an Integrated Technologies P-6000 spincoater.

The deposited films were pyrolyzed on a hot plate at 400-450°C to remove the volatile organics and then held in a furnace set at 600°C for 3 hours. The films were characterized by thin-film Scintag X-ray diffractometer (model DMICRO8) with a pair of divergence solvo silts ahead of the scintillation detector. A scanning electron microscope (SEM) (model ISI-DS 130, Akashi Beam Tech, Japan) was used to study the microstructures and also to measure film thickness. In order to measure dielectric constant and loss, a pellet of BMT powder was pressed, sintered, and gold sputtered on both sides. The density of the pellet as a function of sintering temperature was determined using the Archimedes method.

RESULTS AND DISCUSSION

The TGA results for the gel dried at 70°C from 30°C to 850°C with a heating rate of 10°C/min in an air atmosphere are shown in Figure 2. The TGA thermograms show a maximum weight loss at 240°C, indicating the decomposition of volatile organics from the
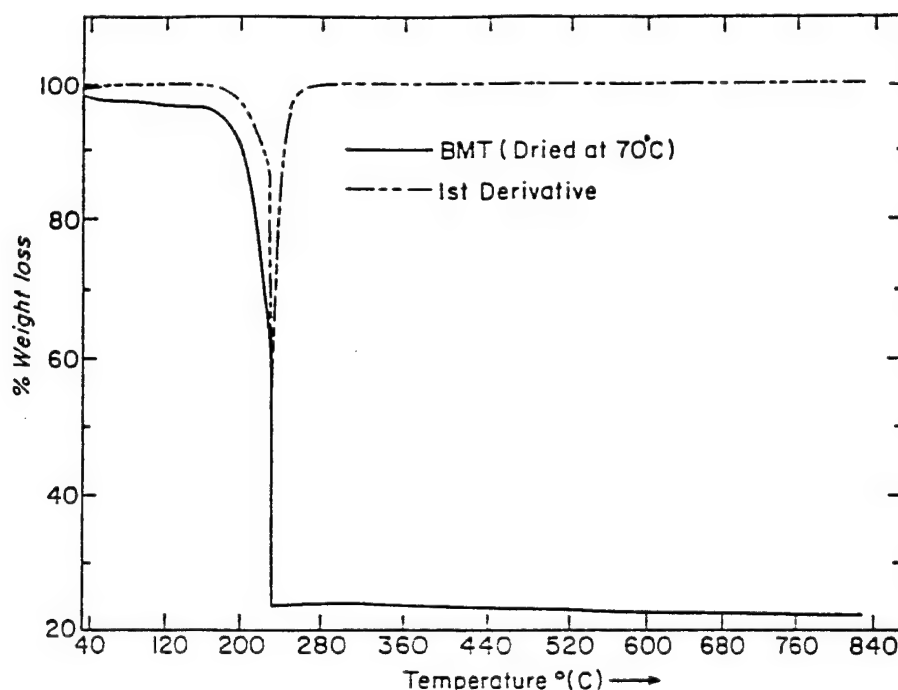
FIG. 2
TGA trace of BMT gel dried at 70°C in an air atmosphere.

gel. To determine the calcination, sintering, and crystallization temperatures of the gel, DTA analysis was done from 100°C to 1000°C with a heating rate of 10°C/min in an air atmosphere. The DTA thermograms show a sharp exotherm with an onset temperature of 278°C and a broad endotherm with an onset temperature of 570°C, as shown in Figure 3. The sharp exotherm at 278°C shows the organic burnout to form the inorganic BMT phase, and the broad endotherm at 570°C is due to the compound formation, which corroborates the X-ray analysis. The gel dried at 60°C was crushed and analyzed by powder X-ray diffraction. It was found to be amorphous with no well-defined diffraction lines. DTA thermograms show a sharp crystallization temperature at 278°C. A powder X-ray diffraction of the amorphous powder heated at 300°C for 6 hours is shown in Figure 4. Most of the diffracted lines could be indexed for the BMT. In addition, a few impurity lines were detected at the low angles. TGA analysis of the BMT powder heated at 300°C for 6 hours (Fig. 5) shows an additional weight loss from organics of 1.64% at 500°C. Reheating the gel powder at a 650°C for 7 hours gave rise to X-ray diffraction patterns in which all the diffraction lines could be indexed in terms of a disordered perovskite structure of BMT. The lattice parameters were calculated using the least-square fitting program with a pseudo cubic perovskite structure $a = 4.0905$ Å.

The values obtained are in accordance with the data reported earlier (4,8) for BMT synthesized by solid-state reaction. The structure of BMT (4) is similar to that of $Ba(Sr_{1/3}Ta_{2/3})O_3$, based on the P3m1 space group. The perovskite structure has close-packed
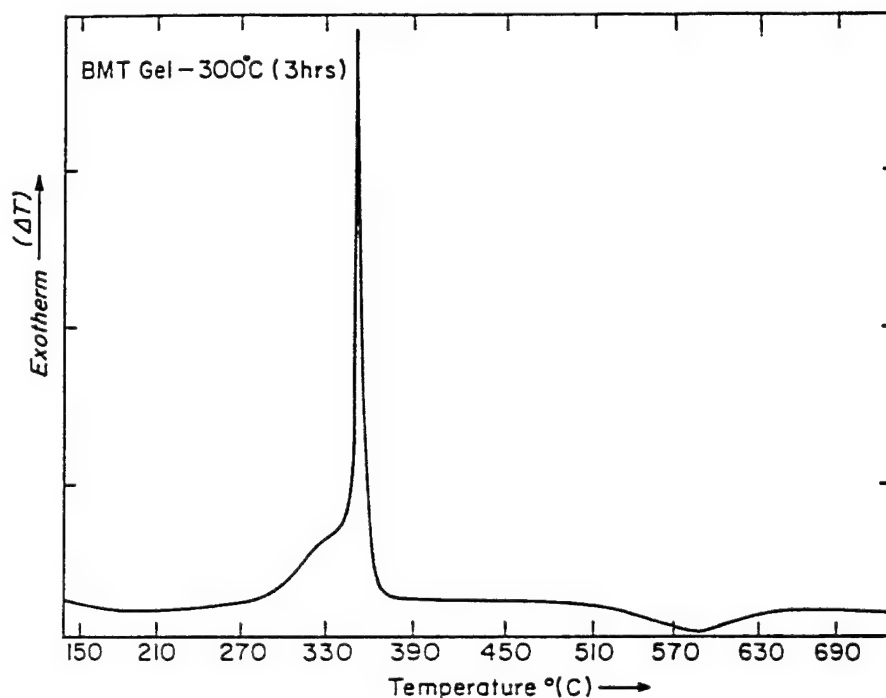
FIG. 3

DTA trace of BMT powders calcined at 300°C for 6 hours in an air atmosphere.

layers of barium and oxygen ions perpendicular to <111>, with Mg and Ta cations occupying the octahedral sites between the layers.

In the case of solid-state reaction, the phase pure BMT phase is obtained at high temperatures ~1600°C (4) or at ~1300°C when precipitated via oxine (2). In contrast, the sol-gel synthesis route produced phase pure BMT powders at 600°C, as shown in Figure 4. The density of sintered pellets as a function of sintering temperature (1300, 1400, and 1500°C) was measured by the Archimedes method. The pellets sintered at 1500°C had high relative density of 98.4% kg/m³.

Sintering Temperature (°C)	Duration (hours)	Measured Relative Density
1300	24	97.3
1400	24	97.9
1500	24	98.4

X-ray diffraction patterns for the spin-coated thin films on the Pt-coated silicon substrates are shown in Figure 6. The BMT films were transparent with a smooth mirror-like surface after pyrolysis at 600°C for 3 hours. The thickness of the films was measured using SEM. Typical films 0.3 μm in thickness were formed free from cracks.
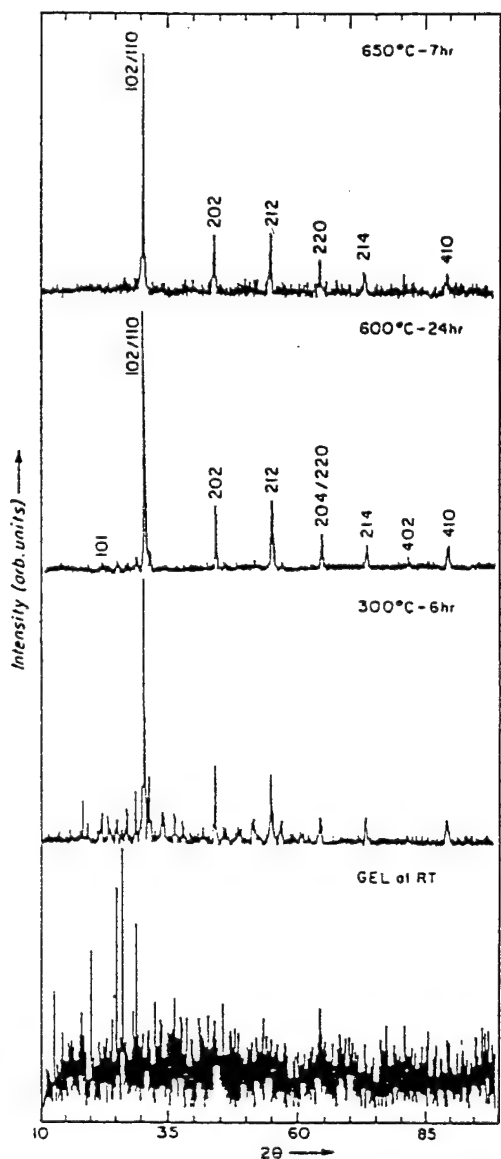
FIG. 4
Powder X-ray diffraction patterns of the BMT powders heated at various temperatures.

CONCLUSIONS

We have synthesized phase pure BMT powder by the sol-gel technique and thin films at a very low temperature (~600°C) instead of by the solid-state reactions usually done at
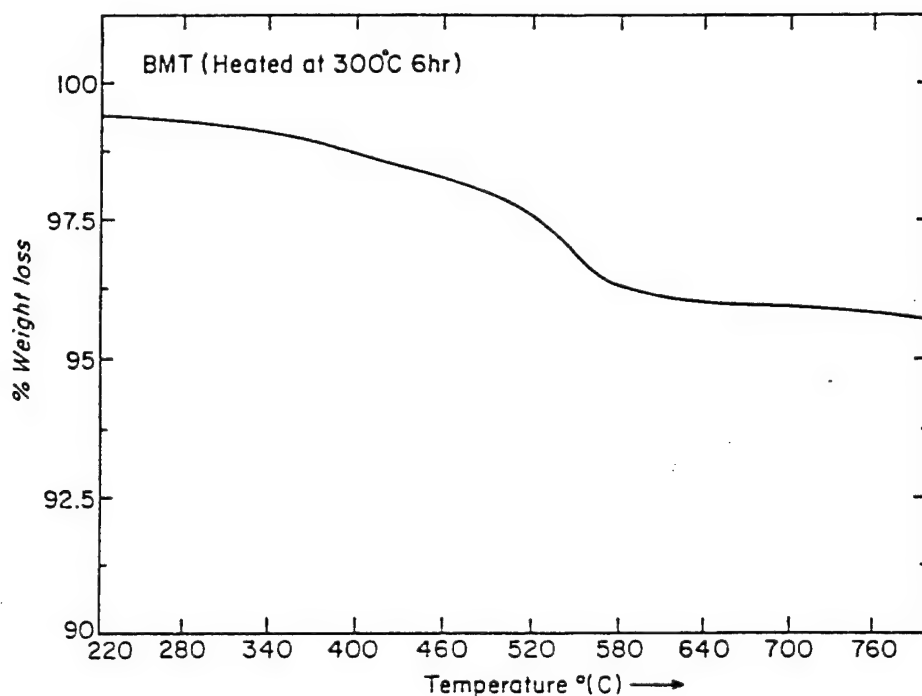
FIG. 5

TGA trace of BMT powders heated at 300°C for 6 hours in an air atmosphere.

high temperature (~1400°C) with very long heating schedules. High quality, crack-free BMT films were prepared on Pt-coated Si substrates for the first time. The relative density of pellets made with sol-gel BMT powder increased with increasing sintering temperature. High relative density (98.4%) kg/m³ BMT ceramics were formed at 1500°C in 24 hours without the addition of any sintering aid. SEM analysis showed that the films of 0.3 μm in thickness were essentially crack-free.

ACKNOWLEDGMENT
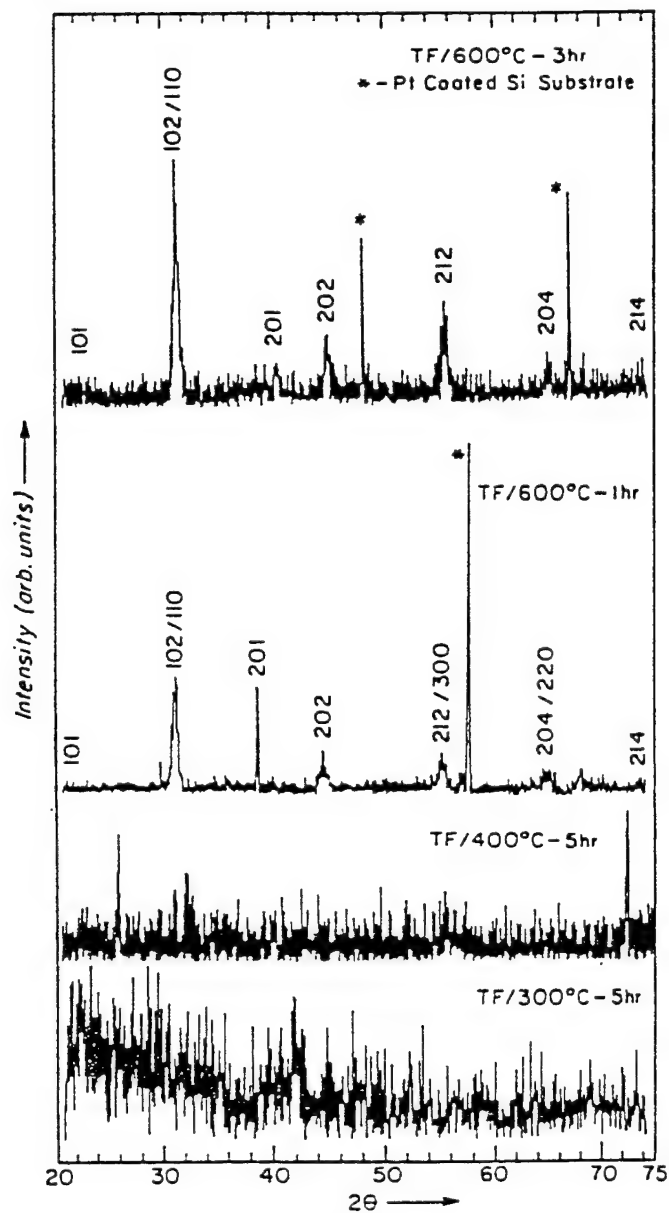
FIG. 6

X-ray patterns of BMT films spin-coated onto a Pt-coated Si substrate.

REFERENCES

1. S. Nomura, K. Toyama and K. Kaneta, *Jpn. J. Appl. Phys.* **21**, L624 (1982).
2. S. Kakegewa, T. Wakabayashi and Y. Sasaki, *J. Am. Ceram.* **69**, C-82 (1986).
3. S. Katayama and M. Sekine, *J. Mater. Chem.* **2**, 889 (1992).
4. R. Guo, A.S. Bhalla and L.E. Cross, *J. Appl. Phys.* **75**, 4704 (1994).
5. S. Kawashima, M. Nishida, I. Ueda, and H. Ouchi, *J. Amer. Ceram.* **66**, 421 (1983).
6. D.C. Bradley, R.C. Mehrotra and D.D. Gaur, *Metal Alkoxides*, p. 308, Academic Press, London (1978).
7. S. Nomura and K. Kaneta, *Jpn. J. App. Phys.* **23**, 507 (1984).
8. F. Galasso and J. Pinto. *J. Inorg. Chem.* **2**, 482 (1963).

Appendix 7.

"A Study of Sol-Gel Derived $Sr_2(AlTa)O_6$ by Raman Spectroscopy"

J. Materials Science Letters 15, 805-806 (1996)

D. Ravichandran

R. Roy

B. Jin

A.S. Bhalla

A study of sol–gel derived $Sr_2(AlTa)O_6$ by Raman spectroscopy

D. RAVICHANDRAN, R. ROY, B. JIN, A. S. BHALLA
Materials Research Laboratory, The Pennsylvania State University, University Park, PA 16802, USA

Among the dielectric materials of current interest the cubic ternary system $Sr_2(AlTa)O_6$ (SAT) is particularly attractive since it exhibits an excellent lattice and thermal expansion match with Y-123, Y-124, Bi-2212, Bi-2223 and Tl-1223 superconductors. Its low dielectric constant and low $\tan\delta$ favours its use in microwave device applications. Thin films of high T_c oxides deposited on SAT ceramics are chemically non-reactive at the interface between the films and the ceramic material. SAT ceramic samples were identified to have double cell cubic perovskite structure with lattice parameter $a = 0.77805$ nm and melting temperature 1900 °C [1]. Thin films of SAT and multilayers of SAT/YBCO (YBa_2Cu_3O-) were grown on (001) $LaAlO_3$ and (001) MgO substrates by pulsed laser deposition [2]. SAT was first prepared by Brandle and Fratello [3] in a study of potential substrate materials for the growth of high temperature superconductor films.

The growth of bulk single crystals has not yet been reported. In our recent work we grew single crystal fibres by a laser beam pedestal growth technique [4]. In comparison to other binary perovskite dielectrics the crystal structure of SAT is cubic. As a result, fibres having potential deleterious multiple growth orientations [1, 5, 6] are unlikely.

Phase-pure $Sr_2(AlTa)O_6$ (SAT) was prepared by the sol–gel route including Sr metal, Al (tri-sec-butoxide) and $Ta(OC_2H_5)_5$ as the starting organic precursors. Sol–gel processing of SAT can lead to highly phase-pure homogeneous powders, and these powders can offer significant advantages over conventionally processed powders. The SAT phase was formed at 1400 °C from a transparent xero-gel. Scanning electron microscope (SEM) analysis showed the particle size to be sub-micrometre ~0.1 μm. Raman analysis of SAT exhibited a sharp band at 791 cm^{-1} due to well-defined molecular vibration.

Complex alkoxides were prepared by reacting Sr metal, Al (tri-sec-butoxide) and $Ta_2(OC_2H_5)_{10}$ organic precursors. First, B-site was formed by refluxing Al(tri-sec-butoxide) and $Ta(OC_2H_5)_5$ organic precursors with 2-methoxyethanol (MOE; $C_3H_8O_2$) at 125 °C for 6 h. Finally, the Sr metal was refluxed with $C_3H_8O_2$ and later reacted with the double alkoxide mixture of Al–Ta precursor complex sol at 125 °C for 12 h. The solution was cooled to room temperature and the pH was found to be ~4.0. Later the solution was hydrolysed with H_2O and C_3H_8O in the ratio 1:4.

The solution was placed in a 60 °C oven for 4–5 h

the formation of xero-gels is shown in Fig. 1. Transparent xero-gel formed after 4–5 h was analysed by thermogravimetric analysis (TGA) and differential thermal analysis (DTA) to determine the drying and crystallization temperatures of the gel.

The gel powder was crushed and fired in air at various temperatures to study the crystallization behaviour. The microstructure was obtained by SEM (model ISI-DS 130, Akashi Beam Technology, Japan). Raman spectroscopy was also done to study the modes of vibration in SAT ceramics. Argon ion laser radiation (514.5 nm) passes through the microscope and is reflected downwards by the beam splitter to the sample mounted on a x-y stage. Focusing was controlled by adjusting the focal length of the objective, and monitored by a CCD camera. The reflected beam was passed through the beam splitter and double monochromator to the photo detector [7].

Fig. 2 shows the powder X-ray diffraction (XRD) pattern of SAT heated at 1400 °C for 7 h. All diffracted peaks could be indexed in terms of the cubic perovskite structure without any impurity phase. The lattice parameter was estimated using a least square fit program to be $a = 0.77904$ nm, which is in good aggrement with reported values [1]. A SEM micrograph (Fig. 3) of the SAT powder formed at 1400 °C for 7 h shows that the particles are reasonably well crystallized with sub-micrometre particle size (<0.1 μm). Fig. 4 shows the microprobe Raman spectrum of SAT ceramics sintered at 1440 °C. The Raman spectrum indicates well-defined molecular vibration. As shown in the spectrum, both the internal and the external vibrations have sharp peaks, indicating that each vibration is well char-
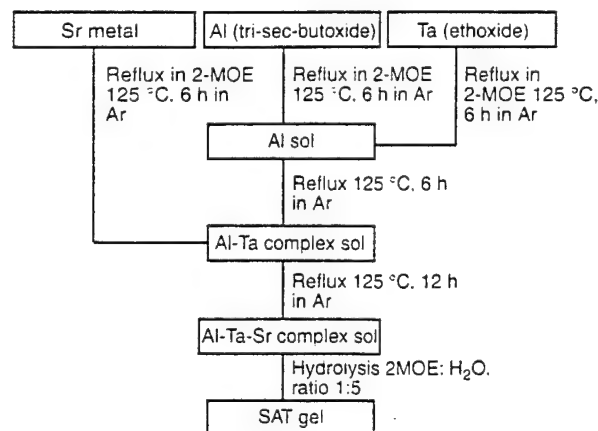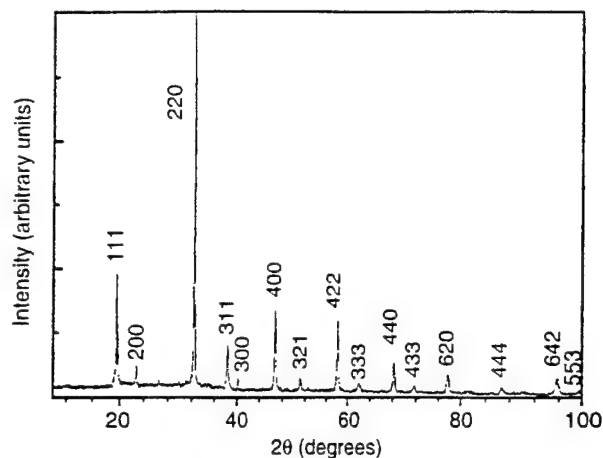
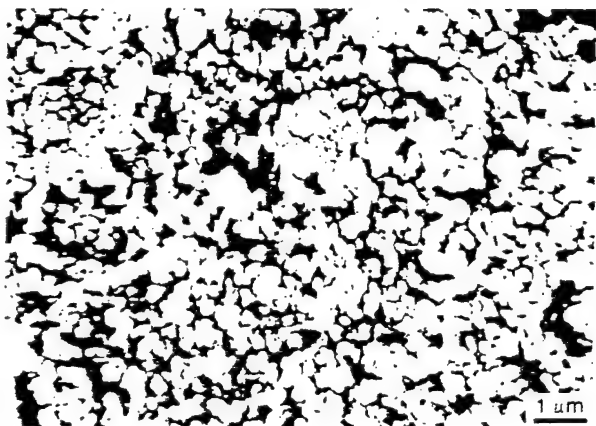Figure 2 Powder XRD pattern of SAT powders at 1400 °C for 7 h.

Figure 4 Micro-probe Raman spectrum of SAT sintered at 1400 °C for 7 h.

Figure 3 SEM micrograph of SAT powders formed at 1400 °C for 7 h.

acterized except for a few bands around 100 cm^{-1} and 200 cm^{-1}. Well-defined prominent bands appear at 60. 123 and 839 cm^{-1}.

The sharp band at 60 cm^{-1} appears to be a single crystal peak. indicating well-formed internal vibration. Detailed specification of mode assignment is in progress. Several coupled peaks are found around 290. 442. and 839 cm^{-1}. Low temperature Raman measurements will make a confirmation of these peaks. and show if they originate from high temperature vibration causing coupling modes or from the diffusivity of the structural disordering during material fabrication. The results will be presented elsewhere. Among the sharp bands. relatively broad bands are found at 252, 356 and 839 cm^{-1}. These peaks have a well-defined Lorentzian shape. indicating that they contain only one
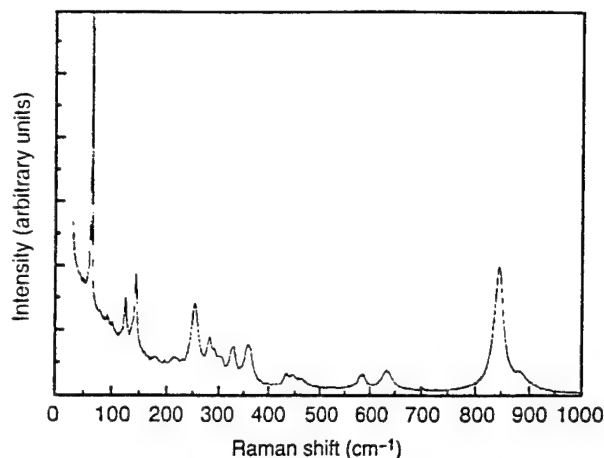
possible vibration. However, because of structural stress due to cation vacancies, it has wide full width at half maximum (FWHM). Like the X-ray pattern. FWHM of Raman bands also indicates the degree of disorder or stress due to cation vacancies or non-stoichiometry in the compound.

Acknowledgement

References

1. R. GUO. A. S. BHALLA. JYH. SHEEN. F. W. AINGER. S. ERDEI. E. C. SUBBARAO and L. E. CROSS. *J. Mater. Res.* **10** (1995) 18.
2. D. DIJIKAMP. T. VENKATESAN. X. D. WU. S. A. SHAHEEN. N. JISRAWI. Y. H. MIN-LEE. W. L. McLEAN and M. CROFT. *Appl. Phys. Lett.* **51** (1987) 619.
3. C. D. BRANDLE and R. J. FRATELLO, *J. Mater. Res.* **5** (1990) 2160.
4. L. E. CROSS and R. ROY, in 3rd Annual Defense Advanced Research Projects Agency Workshop on High Temperature Superconductors. Seattle. WA. 30 September–2 October 1991.
5. J. KOBAYASHI. Y. TAZOH. M. MUKAIDA. M. SASAURA and S. MIYAZAWA. in "Advances in superconductivity" (Springer-Verlag. Tokyo. 1993) p. 865.
6. B. HAN. D. A. NEUMAYER. D. L. SCHULZ. B. J. HINDS. T. J. MARKS. H. ZHANG and V. P. DRAVID. *J. Chem. Mater.* **5** (1993) 14.
7. D. RAVICHANDRAN. B. JIN. R. ROY and A. S. BHALLA. *J. Mater. Letts.*. in press.

Appendix 8.

"Temperature Dependent Raman Spectroscopic Studies on Microwave Dielectrics Sr(Al$_{1/2}$Ta$_{1/2}$)O$_3$ and Sr(Al$_{1/2}$Nb$_{1/2}$)O$_3$"

R. Tao

A.R. Guo

C.-S. Tu

I. Siny

R.S. Katiyar

Ruyan Guo

and A.S. Bhalla

TEMPERATURE DEPENDENT RAMAN SPECTROSCOPIC STUDIES ON MICROWAVE DIELECTRICS $Sr(Al_{1/2}Ta_{1/2})O_3$ AND $Sr(Al_{1/2}Nb_{1/2})O_3$

Ruiwu Tao, A.R. Guo, C.-S. Tu, I. Siny and R.S. Katiyar,
Department of Physics, University of Puerto Rico, Rio Piedras, PR 00931-3343;
Ruyan Guo and A.S. Bhalla,
Materials Research Laboratory, Penn. State University, University Park, PA 16802

Complex oxide perovskites, namely strontium aluminum tantalum oxide (SAT) and strontium aluminum niobium oxide (SAN) were recently investigated to be potential substrate materials for HTSC films in microwave applications. Single crystals (disordered phase) were prepared by laser heated pedestal growth technique (LHPG) and ordered ceramics samples were prepared by conventional sintering technique. We report Raman vibrational spectrum studies on them for the first time. Order-disorder effects of (Al,Ta) and (Al, Nb) sites were studied by comparing Raman spectra of single-crystal samples with ceramic samples. Influences of B sites (Ta and Nb) on O-O modes are discussed in relation to their dielectric properties.

I. Introduction

High temperature oxide superconducting (HTSC) materials have drawn much interest from scientists in various fields. The suitable substrate material for HTSC thin film devices is also an important subject to many researchers. Strontium aluminum tantalum oxide (SAT) and strontium aluminum niobium oxide (SAN) have been identified as potential microwave dielectric substrate materials for thin film of HTSC devices[1]. It is believed that both SAT and SAN belong to the mixed perovskite family. It is also known that they do not belong to the class of ferroelectric materials. One of the critical requirements of HTSC substrate is that the material should have a low dielectric constant and loss at microwave frequencies ($\sim$ 10 GHz). In perovskite materials, the B-site order-disorder behavior is believed to have influence on the dielectric properties and especially on the dielectric loss. It is possible that some low frequency modes may have characteristics which may be useful to understand the dielectric loss mechanism in these materials and in general in other microwave dielectric materials of mixed oxide family.

SAT and SAN samples in ceramic form are known to have a 1:1 ordered cubic structure with a doubled perovskite unit cell[1]. On the other hand, their LHPG grown crystals are best described as disordered, but twin-free, simple cubic perovskite structures. The ordered ceramic samples have Fm3m space group symmetry and typical ordering takes place along crystallographic [111] direction. Factor groups of each site are $Sr(T_d)$, $B'(O_h)$, $B''(O_h)$, and $O(C_{4v})$. The normal vibrational modes are given by

$$\Gamma_{total} = A_{1g} + E_g + T_{1g} + 5T_{1u} + 2T_{2g} + F_{2u} .$$

The Raman active modes are,

$$\Gamma_{Raman} = A_{1g}(O\text{-}O) + E_g(O\text{-}O) + 2T_{2g}(Sr\text{-}O) ,$$

where the atoms that participate in the motion of particular symmetry are shown in the parenthesis.

The crystal structure and some normal modes of vibrations are shown in Figs. 1 and 2 respectively. From the mode classification, it is evident that the atoms at B sites are not involved in any Raman active normal vibrational motions.
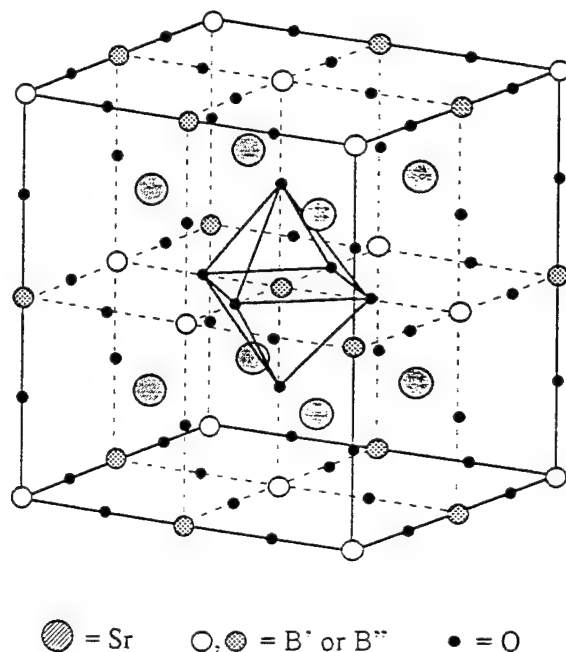

$\bigcirc\!\!\!\!\!/ = Sr$ $\bigcirc, \bigcirc\!\!\!\!\!\circ = B' \text{ or } B''$ $\bullet = O$

Fig. 1 The unit cell of SAN and SAT with Fm3m symmetry.

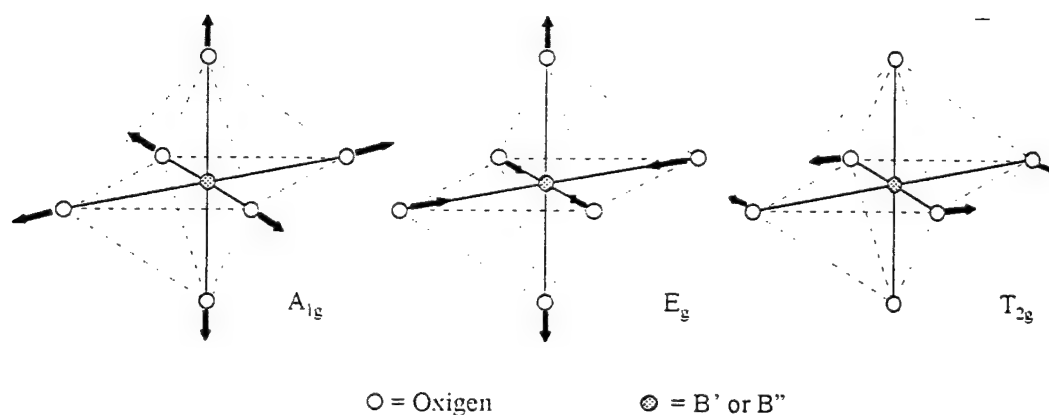$\bigcirc = Oxigen$ $\bigcirc\!\!\!\!\!\circ = B' \text{ or } B''$

Fig. 2 The Raman active normal vibrational modes of a free oxygen octahedron around the B ion in the center (only motion of oxygen atoms is show here).

II. Experiment

For the Raman experiments, both ceramic and single crystal samples of SAN and SAT were used. The ordered ceramic samples of SAN and SAT were prepared by using

the conventional sintering process. The disordered single crystals of SAN and SAT were prepared in fiber shape through the LHPG technique[1]. LHPG has been used as a powerful method for rapidly growing small diameter single crystals, particularly oxides of high melting temperature, for both property studies and fiber devices. The LHPG equipment used in the preparation of the samples consisted of a power source (water-cooled, tunable flowing gas CO_2 55 W laser), an optical layout, and a growth section.[1]

Differential thermal analysis (DTA) was used to determine the minimum calcination temperature to achieve the desired phases and to select sintering temperature[1]. To characterize the crystallographic phases and to adjust the processing conditions of the ceramic samples, X-ray diffraction technique was used. Radio frequency dielectric constants and the loss tangent were measured.

Here we report Raman experiments including the room temperature measurements on ceramics and single crystals SAN and SAT samples and the low temperature measurements on ceramic samples. The experiments at room temperature were carried out by using a Micro Raman Triple Spectrometer (ISA Model T64000), and the experiments below room temperature were done on a Double-grating Micro Raman Spectrometer (ISA Model S3000). Both spectrometers were equipped with liquid nitrogen cooled CCD detectors. A modified Cryogenic Tech. closed-cycle refrigerator, Model 20 with a LakeShore DRC-84C temperature controller was used to cool down the system. The spot of the focused laser through the microscope was around 1 μm.

III. Results and Discussion

The polarized Raman spectra were recorded for all orientations, but no significant influence of the polarization tensor component was observed. A possible explanation for this phenomenon could be that the ordered regions in the samples of either ceramic or single crystal fiber are much less than 1 μm in size. In other words, all of the samples are apparently disordered on a 1 μm scale.

For both ceramics and single crystals, the four expected Raman modes were observed at room temperature, shown in Fig. 3. No Raman peaks were found beyond
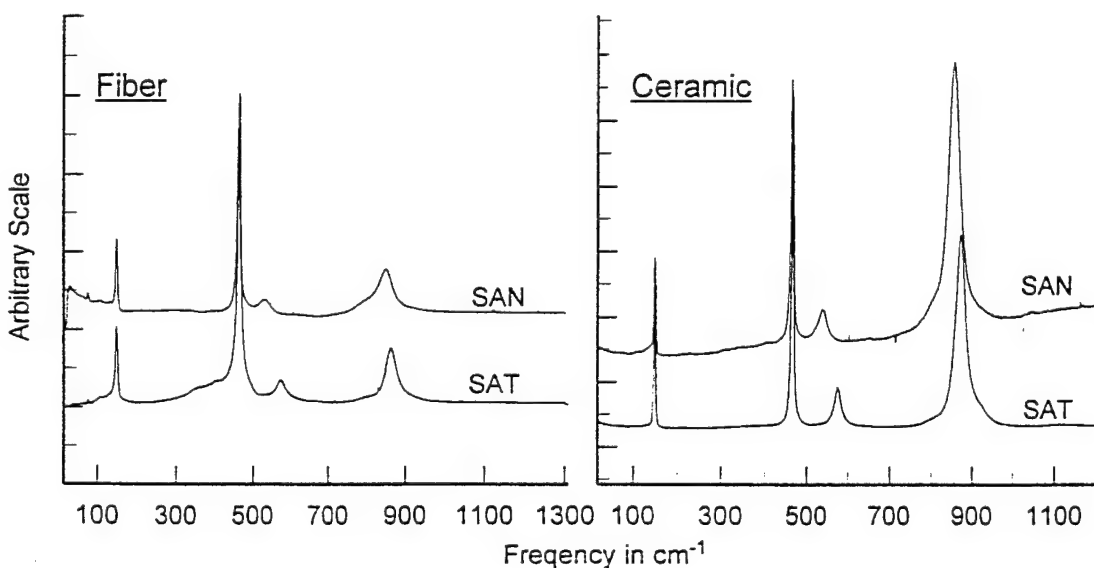

Fig. 3 Room temperature Raman spectra of SAN and SAT in ceramic and fiber forms.

1000 cm^{-1}. In order to determine the peak positions and half-widths of vibrational modes, the damped harmonic oscillator model with spectral distribution function (for Stokes scattering)[3], i.e.

$$S(\omega) = \frac{\chi_o \Gamma \omega \omega_o^2}{\left(\omega^2 - \omega_o^2\right)^2 + \Gamma^2 \omega^2} \cdot \frac{1}{1 - e^{-\hbar\omega/kT}} , \qquad (1)$$

was used, where ω_o and Γ correspond to the mode frequency and half-width, respectively. χ_o is the susceptibility constant (in arbitrary units), k is Boltzmann's constant and T is absolute temperature. The frequencies of the Raman modes are listed in Table 1 in which Raman results from structurally similar materials, PST and BYT[4],[5],[6] are also listed. From the view of lattice dynamics, the two T_{2g} modes (Sr-O bonds) are independent of other bonds in the cell. Fig. 4 shows that the relation between the vibrational frequencies and reduced mass of these modes in different materials follows adequately an isolated anharmonic oscillator described as,

$$\omega_0 = \omega_{anh} + \omega_e v' \qquad (2)$$
$$\omega_e = 2\pi(\kappa/\mu)^{1/2} \qquad (3)$$

where ω_{anh} is the anharmonic and ω_e is the harmonic term, v' is the vibrational quantum number, κ is the force constant, and μ is the reduced mass.

Table 1. Raman mode frequencies in cm^{-1}

	SAN	SAT	PST[1]	BYT[2]
A_{1g}	856.3	871.9	830	838
E_g	540.3	577.7	240	765
T_{2g}	150.0	150.0	61	105
T_{2g}	464.7	466.8	370	388

[1] PST = Pb(Sc$_{0.5}$Ta$_{0.5}$)O$_3$
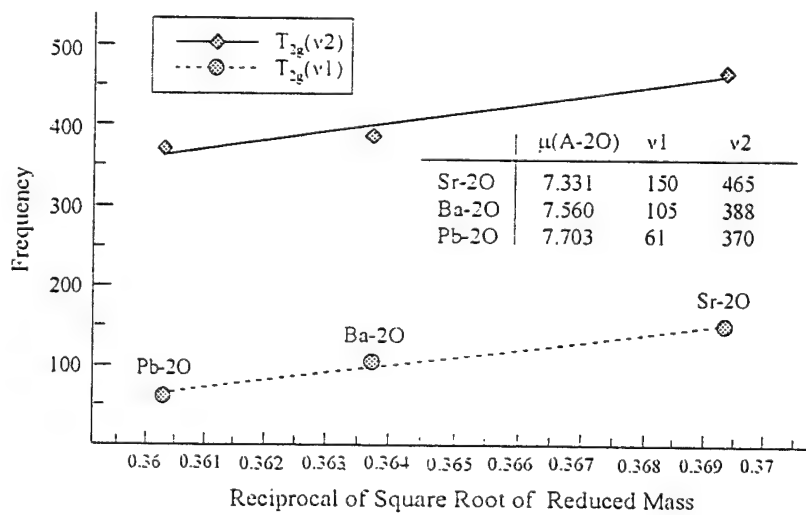[2] BYT = Ba(Y$_{0.5}$Ta$_{0.5}$)O$_3$

Fig. 4 Linear relationship between frequencies of T_{2g} modes
and reduced masses of A-O bonds.

The E_g and A_{1g} modes are entirely due to the motion of oxygen ions. However, the presence of B ions at the center of the oxygen octahedron influences their frequencies (see Fig. 2), and that could be the reason for the two peaks in SAN, namely E_g at 540.28 cm^{-1} and A_{1g} at 856.3 cm^{-1} shifting to 577.7 cm^{-1} and 871.9 cm^{-1} in SAT when the Nb at B" cation was replaced by Ta. This is an indication of the short range interaction constant of O-Ta-O being greater than that of O-Nb-O. This explanation is in agreement with SAT having smaller dielectric constant and loss than those of SAN[1].

Comparing the spectra of ceramics and single crystal fibers, the disorder behavior of the samples in the latter form is obvious, (Table 2). All of the peaks of the disordered samples (in single crystal form) are shifted to the lower frequencies and exhibit broadening. One may assume that for disordered samples the Raman selection rule is broken and the phonon momentum in the lattice is not conserved any more, so that the contribution to the phonon spectrum comes from the entire Brillouin zone thus broadening and shifting the peaks.

Table 2, Frequencies and halfwidths (in cm^{-1}) of Raman modes

	SAN				SAT			
	Frequency		Width		Frequency		Width	
Mode	Ceramic	Fiber	Ceramic	Fiber	Ceramic	Fiber	Ceramic	Fiber
A_{1g}	856.3	851.4	34.01	41.04	871.9	864.5	28.79	34.25
E_g	540.3	532.6	26.82	37.19	577.7	573.9	19.40	27.71
$T_{2g}(1)$	150.0	148.3	5.948	6.116	150.0	148.4	5.597	7.176
$T_{2g}(2)$	464.7	462.2	7.175	9.232	466.8	464.8	6.704	9.305

* Ceramic = Ordered sample;   Fiber (Single crystal) = Disordered sample

Table 3 gives the result of low temperature Raman spectra of SAN and SAT in ceramic form. It can be seen that all modes are shifted towards lower frequencies and become broader when temperature increases, which are expected for the normal anharmonic oscillators. An interesting exception is observed for the $T_{2g}(1)$ mode. When

Table 3. Low temperature Raman frequencies and halfwidths for SAN and SAT ceramics

Mode		SAN				SAT			
		31K	100K	200K	290K	31K	100K	200K	290K
A_{1g}	Freq.	859.2	858.6	857.2	855.3	875.0	874.5	873.1	871.1
	Width	27.69	27.87	30.63	34.64	20.69	21.30	24.48	28.90
E_g	Freq.	547.6	546.9	544.1	539.8	584.9	583.9	581.0	576.8
	Width	14.45	16.06	20.00	27.23	10.88	11.76	14.97	19.11
$T_{2g}(1)$	Freq.	149.0	149.3	149.9	150.0	149.3	149.4	150.0	150.2
	Width	4.222	4.413	4.546	4.534	3.370	3.565	3.943	3.968
$T_{2g}(2)$	Freq.	464.8	464.8	464.8	464.3	466.9	466.9	466.9	466.4
	Width	5.026	5.306	5.968	6.970	4.270	4.694	5.136	6.174

temperature increases, $T_{2g}(1)$ mode shifts to higher frequencies, (see Fig. 5 and Fig. 6). This mode possesses soft mode characteristics, its behavior is consistent with what is expected for materials in a paraelectric phase above any phase transition. However, no phase transition is evident from Raman scattering studies in SAN and SAT ceramics down to 31K which is in agreement with other workers [1],[2].
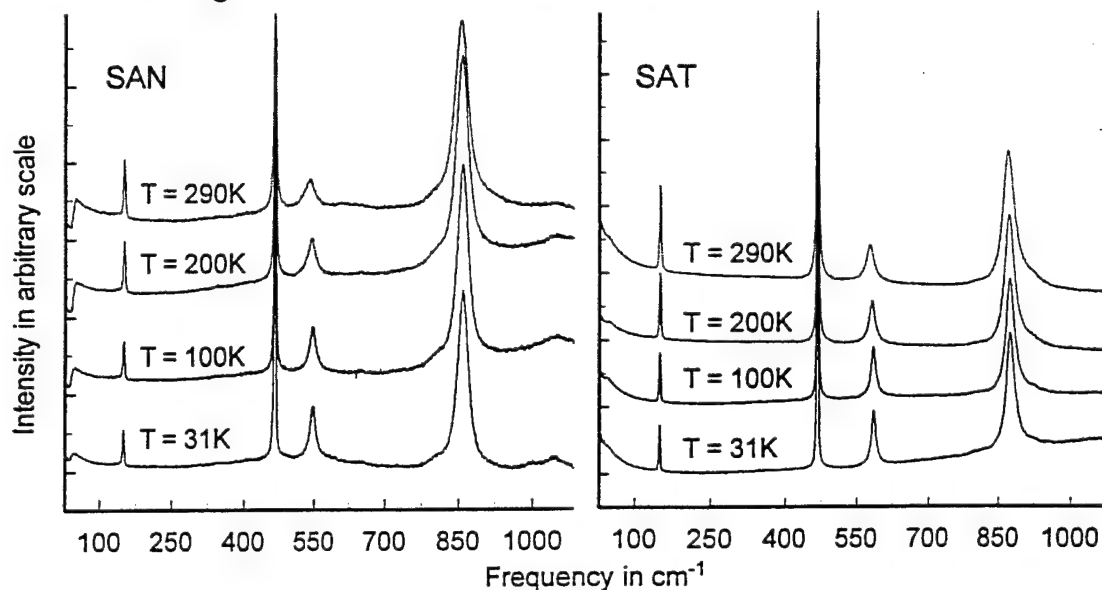

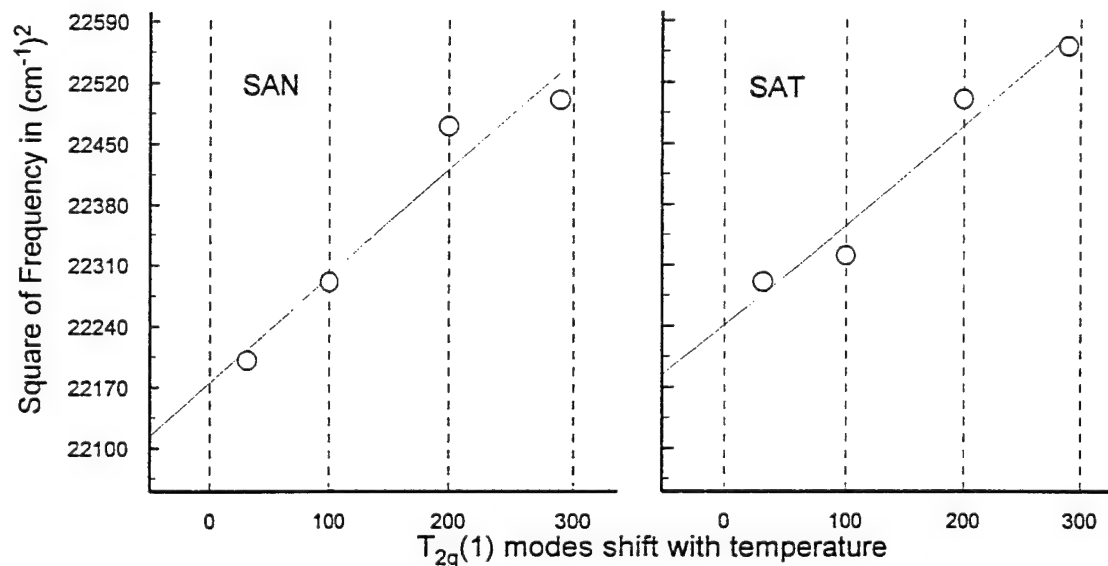Fig. 5   Low temperature Raman spectra of SAN and SAT ceramics.

Fig. 6 $T_{2g}(1)$ mode shift with temperature change

IV. Conclusions

Temperature dependent Raman studies were made on SAN and SAT in both ceramic and single crystal forms. From the Raman spectra, it is evident that both of them belong to Fm3m group symmetry. Effect of order-disorder in the samples was observed in

Raman studies. Our results suggest that ceramic samples are ordered, and single crystals are relatively disordered. From our studies, it was also concluded that both SAN and SAT single crystals possess disordered regions probably of much less than 1 μm in size.

Low temperature Raman studies on SAN and SAT ceramics did not reveal any phase transition down to 31K, which is in agreement with the experiments on temperature dependent dielectric constant reported by Guo et al[1].

V. Acknowledgment

VI. References

1) R.Guo, A.S.Bhalla, Jyh Sheen, F.W. Ainger, S.Erdei, E.C. Subbarao, and L.E. Cross, J. Mater. Res., 10, 1, (1995).
2) A.T. Findikoglu, C.Doughty, S. Bhattacharya, Qi Li, X.X.Xi, and T. Venkatesan, Appl. Phys. Lett 61(14), (1992).
3) J.F Ryan, R.S. Katiyar and W. Taylor, Effet Raman Et Théorie, C2-49 .
4) I. Gregora, J. Petzelt, J. Pokorny, V. Vorlicek, and Z. Zikmund, Solid State Comm., vol. 94, 11, 899, (1995).
5) I.G.Siny, and T.A. Smirnova, Ferroelectrics, 90, 191, (1989)
6) U. Bismayer, V. Devarajan and P. Groves, J. Phys. Condens. Matter 1, 6977, (1989).

Appendix 9.

"Raman Spectroscopy of Sol-Gel Derived $BaMg_{1/3}Ta_{2/3}O_3$ Perovskites"

Materials Letters, 25, 257-259 (1995)

D. Ravichandran

B. Jin

R. Roy

A.S. Bhalla

MATERIALS LETTERS

ELSEVIER

Raman spectroscopy of sol–gel derived BaMg$_{1/3}$Ta$_{2/3}$ perovskites

D. Ravichandran *, B. Jin, R. Roy, A.S. Bhalla

Materials Research Laboratory, The Pennsylvania State University, University Park, PA-16802, USA

Abstract

Barium magnesium tantalate (BMT) perovskite was prepared from organic precursors including Ba metal, Mg(OC$_2$H$_5$)$_5$ and Ta(OC$_2$H$_5$)$_5$. Crystallization and phase formation were studied for the sol–gel derived BMT powders. Microstructure of BMT shows particle sizes less than 0.1 μm. Raman spectroscopy was done to study the modes of vibration in the BMT ceramics.

1. Introduction

Complex perovskites with general formula A(B$_{1/3}$B'$_{2/3}$)O$_3$, where A = Ba ion, B = Mg, Zn and B' = Ta, Nb have been reported earlier to possess excellent microwave properties [1–5]. These perovskite compounds have poor sinterability. In order to obtain dense ceramics with good microwave properties, sintering additives like MnO$_2$, La$_2$O$_3$ or rapid sintering methods were used.

These perovskite compounds have an ordered hexagonal structure and ordering of the B sites affects the Q value of these compounds. In the case of BMT ceramics, the influence of density and ordering on the dielectric Q values has not been studied because variations in density and ordering can occur together in these ceramics. BMT is considered to be one of the most refractory oxides, as a result single crystal growth is quite difficult [5]. It was found that BMT single crystal grown using BaF$_2$ flux resulted in higher dielectric constant; this was attributed to flux contamination.

In the recent times, the metal alkoxide method has been used to synthesize perovskite ceramics such as BaTiO$_3$, SrTiO$_3$ and other electro ceramics. The main advantage is that this alkoxide route can yield phase formation at very low temperatures in comparison to conventional preparation methods.

In this Letter, we present the synthesis of BMT powder via organic precursors including Ba metal, Mg(ethoxide) and Ta(ethoxide). Scanning electron microscopic analysis was done to study the microstructure of BMT powders. Raman spectroscopy was done to study the different modes of vibration in the BMT phase.

2. Experimental

Initially Mg(ethoxide) was weighed and reacted stoichiometrically with 5–10 ml of CH$_3$COOH. To dissolve Mg(ethoxide) completely 10–15 ml of 2-methoxyethanol (CH$_3$OCH$_2$CH$_2$OH) was added and refluxed at 125°C for 6 h under inert gas atmosphere (Ar gas). In a similar manner Ta(ethoxide) was refluxed with 20–25 ml of 2-methoxyethanol at 125°C for 6 h in argon atmosphere. This solution was cooled to room temperature and mixed with Mg(OCH$_2$CH$_2$OCH$_3$)$_2$ solution.

The mixture of Mg–Ta solution was refluxed at 125°C for 12 h in argon atmosphere. Finally, the Ba
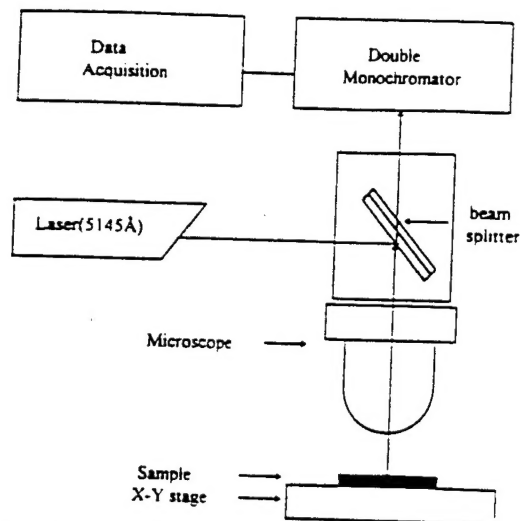
* Corresponding author.

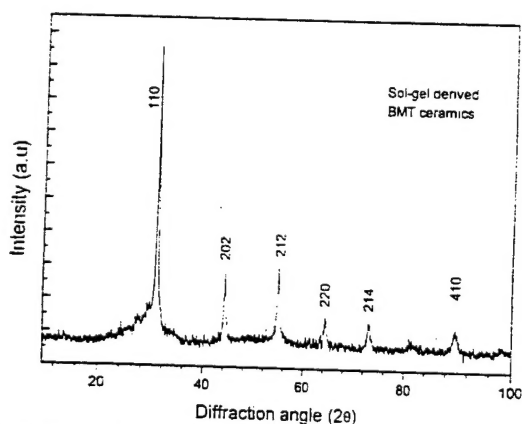Fig. 1. Micro-probe Raman spectroscopy – experimental configuration.

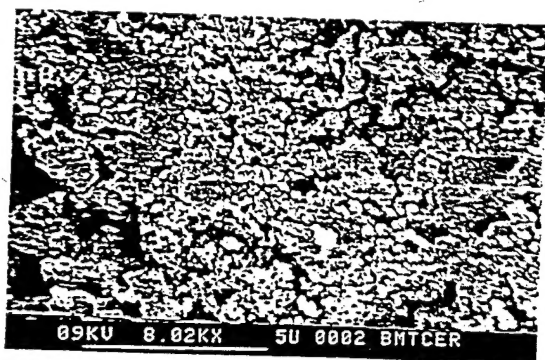Fig. 2. Powder X-ray diffraction pattern of BMT powder calcined at 650°C–7 h.

Fig. 3. SEM micrograph of BMT powder calcined at 650°C–7 h.

metal was dissolved with few drops of CH_3COOH and 15–20 ml of 2-methoxyethanol at 125°C for 6 h.

The double alkoxide mixture of Mg–Ta complex sol was reacted with $Ba(OCH_2CH_2OCH_3)_2$ solution for 12 h with continuous stirring under inert gas atmosphere. Later, the solution was cooled to room temperature and hydrolyzed to form the gel with 2-methoxyethanol and H_2O in the ratio 1 : 4. A clear yellow solution was formed and the pH of the solution was found to be ≈ 4. This solution was placed in a 60°C oven for 5–6 h to form the gel. The transparent xerogel formed was fired in an air atmosphere at different temperatures to crystallize the BMT phase. TGA and DTA analyses were done for the gel to determine the weight loss of the gel due to organic burnout and the crystallization temperatures.

Room-temperature micro-probe Raman spectroscopy was done to study in-plane modes of vibration in BMT ceramics. Argon-ion laser radiation (5145 Å) passed the microscope and got reflected downward by the beam splitter to the sample mounted on an X–Y stage (Fig. 1). Focusing was controlled by adjusting the focal length of the objective, and monitored by a CCD camera. The reflected beam was passed through the beam splitter and double monochromator to the photo detector. The spectrum was scanned from 30 to 1000 cm^{-1} with a resolution of 0.5 cm^{-1}.

3. Results and discussion

Fig. 2 shows powder X-ray diffraction patterns of the BMT phase formed at 650°C–7 h. All the diffracted peaks could be indexed in terms of the cubic perovskite structure without any impurity phase. The structure of BMT [5] is similar to that of $Ba(Sr_{1/3}Ta_{2/3})O_3$ based on the P3m1 space group. The perovskite structure has closed packed layers of Ba and oxygen perpendicular to the (111) plane with Mg and Ta cations occupying the octahedral sites between the layers.

Literature reports show that BMT ceramics prepared by the conventional powder process were obtained at very high temperature and longer heating schedules (≈ 1600°C) [4] and (≈ 1300°C) precipitated via oxine [6]. In contrast, the sol–gel process which is a low temperature route can produce phase pure BMT at 650°C as shown in Fig. 2. The SEM microstructure of the BMT powder is shown in Fig. 3. A particle size of
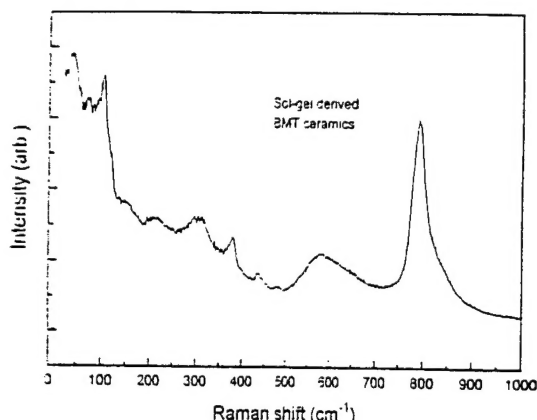
Fig. 4. Micro-probe Raman spectrum of BMT powder sintered at 1000°C–6 h.

0.1 μm was observed with reasonably well crystallized particles.

Fig. 4 shows the micro-probe room-temperature Raman spectrum of BMT ceramics sintered at 1000°C for 6 h. Overall spectrum shows a little unstable state, especially in the internal vibration region. Prominent vibration frequencies measured are 72, 581 and 791 cm^{-1}. The mode at 581 cm^{-1} has a very wide full width at half maximum (fwhm). This indicates it may contain several coupled modes or may be because of diffuse characteristics of complex perovskite materials. This fact will be confirmed by measuring the low temperature Raman data.

In case it is caused by the coupling of several independent modes of vibration, it should be observed as distinct peaks at low temperature measurement. Another possibility is that if this material still contains organic components which are used as the precursor starting materials, the effect of these organic components could contribute to this broad band. Very feeble broad bands are observed below 400 cm^{-1}. This fre-quency region is usually attributed to the internal vibration of BO_3 octahedron in ABO_3 perovskites. The instability of these peaks may be caused by: BO_3 octahedron might not have well formed or due to the vacant B-site or oxygen deficiency in the compound.

4. Conclusions

Phase pure BMT was formed at very low temperature by the sol–gel route for the first time. SEM micrographs show that particles are reasonably well crystallized with a particle size of ≈ 0.1 μm. Feeble broad bands at low frequencies below 400 cm^{-1} indicate the internal modes of vibration of the BO_3 octahedron in ABO_3 type perovskite.

Acknowledgements

References

[1] S. Nomura, K. Toyama and K. Kaneta, Jpn. J. Appl. Phys. 21 (1982) L624.

[2] M. Onada, J. Kuwata, K. Kaneta and K. Toyama and S. Nomura, Jpn. J. Appl. Phys. 21 (1982) 1707.

[3] S. Nomura, Ferroelectrics 49 (1983) 61.

[4] S. Nomura, T. Konoike, Y. Sakabe and K. Wakino, J. Am. Ceram. Soc. C 59–61 (1984).

[5] R. Guo, A.S. Bhalla and L.E. Cross J. Appl. Phys. 75 (1994) 4704.

[6] S. Kakegawa, T. Wakabayashi and Y. Sasaki, J. Am. Ceram. Soc. C-82, 69 (1986).